Skeletal muscle alternative splicing of *TBC1D1* gene encoding a Rab GTPase activating protein: A functional insight

Inaugural – Dissertation

zur Erlangung des Doktorgrades
an der Mathematisch-Naturwissenschaftlichen Fakultät
der Heinrich-Heine-Universität Düsseldorf

vorgelegt von
Awovi Didi Tolo Humpert (geb. Bedou)
aus Frankreich

Düsseldorf, January 2025

aus dem Institut für Klinische Biochemie und Pathobiochemie
des Deutschen Diabetes-Zentrums,
Leibniz-Zentrum für Diabetesforschung
an der Heinrich-Heine-Universität Düsseldorf

Gedruckt mit der Genehmigung der
Mathematisch-Naturwissenschaftlichen Fakultät der
Heinrich-Heine-Universität Düsseldorf

Berichterstatter:

1. **Prof. Dr. Hadi Al-Hasani**
2. **Prof. Dr. Axel Gödecke**

Tag der mündlichen Prüfung: 16.05.2025

Table of Contents

Summary

Maintaining the body's energy balance and physiological functions is a delicate and complex process that relies heavily on the efficient metabolism of glucose in cells. Glucose metabolism encompasses a series of intricate processes, including the uptake, breakdown, and utilisation of glucose to produce energy for cellular activities. The glucose transporter 4 (GLUT4) is at the heart of this process. It is a crucial player in glucose metabolism, as it facilitates glucose uptake into the cells in insulin-sensitive tissues like skeletal muscle. Disruptions in regulating GLUT4 function in skeletal muscle consequently lead to impaired glucose metabolism, which is associated with insulin resistance, a hallmark of type 2 *diabetes mellitus* (T2DM). The latter is an indicator of the critical role of GLUT4 in metabolic health and disease prevention. A distal regulator of GLUT4 translocation, and consequently glucose uptake, is the protein TBC1D1, a Rab GTPase activating protein (RabGAP). Early studies in mouse models have demonstrated that the absence of *TBC1D1* is associated with impaired glucose metabolism.

During mRNA maturation of a gene, the alternative splicing (AS) process produces different forms of mRNA transcripts from the same gene through various combinations of exons included or excluded.

The current dissertation aims to elucidate the role of different *TBC1D1* splice variants in GLUT4-mediated glucose uptake in skeletal muscle, particularly under the control of the two significant kinases, AKT2 and AMPK.

Three annotated and validated splice variants of the human ***TBC1D1*** gene were identified: ***TBC1D1-LONG***, ***TBC1D1-SHORT***, and ***TBC1D1-LONG-GAPdel***. *TBC1D1-LONG* and *TBC1D1-SHORT*, are characterised by the presence or absence of two exons in a region of unknown regulatory function, while *TBC1D1-LONG-GAPdel* lacks part of the exon 20 in the functional GTPase-activating (GAP) domain. This deletion in *TBC1D1-LONG-GAPdel* results in a truncated protein demonstrating a loss of GTP hydrolysis activity, regardless of the Rab GTPase substrates: Rab8a and Rab10. *TBC1D1-LONG* and *TBC1D1-LONG-GAPdel* are expressed exclusively in myotubes, whereas *TBC1D1-SHORT* is expressed in both myoblasts and myotubes.

The variants TBC1D1-LONG and TBC1D1-LONG-GAPdel serve as substrates for AKT2 and AMPK, which phosphorylate them at different sites, suggesting distinct regulatory functions. The dissertation also reveals that these two isoforms interact with the cytoplasmic tail of insulin-regulated aminopeptidase (cIRAP), a co-resident protein involved in intracellular GLUT4-containing vesicles (GSVs) translocation to the plasma membrane of the cells. Although the truncation of TBC1D1-LONG-GAPdel does not impair its ability to interact with cIRAP, it compromised its GTP hydrolysis activity. Furthermore, TBC1D1-LONG-GAPdel can form oligomers with TBC1D1-LONG, altering the overall activity of these proteins. This oligomerization is regulated by AKT2 and AMPK kinases and may influence the protein activity.

In conclusion, this dissertation emphasises the critical role of AS in modulating the functions of TBC1D1 and, by extension, in regulating glucose metabolism in skeletal muscle. The AS of *TBC1D1* allows for generating different protein isoforms with specific regulatory roles in glucose uptake. This plays a vital role in maintaining glucose homeostasis and providing energy for cellular functions.

The findings suggest that a deeper understanding of the molecular functions of TBC1D1 isoforms on glucose homeostasis could lead to improved therapeutic strategies for T2DM, with research focusing on **in vivo** and **in vitro investigations** on TBC1D1 splice variants in T2DM patients to guide the development of corresponding treatments.

Zusammenfassung

Die Aufrechterhaltung des Energiegleichgewichts und der physiologischen Funktionen des Körpers ist ein komplexer und fein abgestimmter Prozess, der maßgeblich vom effizienten Glukosestoffwechsel in den Zellen abhängt. Dieser Stoffwechsel umfasst eine Reihe ineinandergreifender Schritte, darunter die Aufnahme, den Abbau und die Verwertung von Glukose zur Energiegewinnung für zelluläre Aktivitäten. Eine zentrale Rolle spielt dabei der Glukosetransporter 4 (GLUT4), der essenziell für die Glukoseaufnahme in insulinempfindlichen Geweben wie dem Skelettmuskel ist. Störungen in der Regulierung der GLUT4-Funktion im Skelettmuskel können den Glukosestoffwechsel erheblich beeinträchtigen und Insulinresistenz fördern, ein charakteristisches Merkmal von Typ-2-Diabetes mellitus (T2DM). Dies unterstreicht die Schlüsselrolle von GLUT4 für die Stoffwechselgesundheit und die Prävention von Krankheiten. Ein entscheidender distaler Regulator der GLUT4-Translokation und damit der Glukoseaufnahme ist das Protein TBC1D1, ein Rab-GTPase-aktivierendes Protein (RabGAP). Frühe Studien an Mausmodellen zeigten, dass das Fehlen von TBC1D1 mit einem gestörten Glukosestoffwechsel einhergeht.

Während der mRNA-Reifung eines Gens entstehen durch den alternativen Spleißprozess (AS) verschiedene mRNA-Transkriptvarianten desselben Gens, die sich durch unterschiedliche Kombinationen eingeschlossener oder ausgeschlossener Exons auszeichnen.

Ziel der vorliegenden Dissertation ist es, die Rolle der verschiedenen TBC1D1-Spleißvarianten bei der GLUT4-vermittelten Glukoseaufnahme im Skelettmuskel zu untersuchen, insbesondere im Kontext der Regulation durch die beiden zentralen Kinasen AKT2 und AMPK.

Im Rahmen dieser Studie wurden drei annotierte und validierte Spleißvarianten des menschlichen ***TBC1D1*** Gens identifiziert: ***TBC1D1-LONG***, ***TBC1D1-SHORT*** und ***TBC1D1-LONG-GAPdel***. TBC1D1-LONG und TBC1D1-SHORT unterscheiden sich durch das Vorhandensein beziehungsweise Fehlen von zwei Exons in einer Region mit bislang unbekannter regulatorischer Funktion. TBC1D1-LONG-GAPdel hingegen weist eine Deletion eines Teils des Exons 20 in der funktionellen GTPase-aktivierenden (GAP) Domäne auf. Diese Deletion führt zu einem verkürzten Protein, das keine GTP-Hydrolyseaktivität mehr zeigt, unabhängig von den Substraten der Rab-GTPasen Rab8a und Rab10. Die Expressionsmuster der Varianten zeigen zudem eine unterschiedliche zelluläre Verteilung: Während TBC1D1-LONG und TBC1D1-LONG-GAPdel ausschließlich in Myotuben exprimiert werden, findet sich TBC1D1-SHORT sowohl in Myoblasten als auch in Myotuben.

Die Varianten TBC1D1-LONG und TBC1D1-LONG-GAPdel dienen als Substrate für die Kinasen AKT2 und AMPK, die sie an unterschiedlichen Stellen phosphorylieren. Diese spezifischen Phosphorylierungsstellen deuten auf unterschiedliche regulatorische Funktionen der beiden Isoformen hin. Zudem zeigt die Dissertation, dass beide Isoformen mit dem zytoplasmatischen Schwanz der insulinregulierten Aminopeptidase (cIRAP) interagieren, einem Co-residenten Protein, das wesentlich zur Translokation intrazellulärer, GLUT4-haltiger Vesikel (GSVs) zur Plasmamembran beiträgt. Trotz der Trunkierung bei TBC1D1-LONG-GAPdel bleibt die Fähigkeit zur Interaktion mit cIRAP erhalten, jedoch ist seine GTPase-Aktivität beeinträchtigt. Zusätzlich kann TBC1D1-LONG-GAPdel Oligomere mit TBC1D1-LONG bilden, was die Gesamtaktivität der Proteine moduliert. Diese Oligomerisierung wird durch die Kinasen AKT2 und AMPK reguliert und beeinflusst die Funktion der Proteine maßgeblich.

Zusammenfassend unterstreicht diese Dissertation die zentrale Rolle des alternativen Spleißens (AS) bei der funktionellen Modulation von TBC1D1 und dessen Bedeutung für die Regulierung des Glukosestoffwechsels im Skelettmuskel. Durch alternatives Spleißen entstehen spezifische Proteinisoformen, die gezielte regulatorische Funktionen bei der Glukoseaufnahme ausüben. Dies trägt entscheidend zur Aufrechterhaltung der Glukosehomöostase und zur Sicherstellung der Energieversorgung für zelluläre Prozesse bei.

Die Ergebnisse legen nahe, dass ein vertieftes Verständnis der molekularen Funktionen der TBC1D1-Isoformen und ihrer Auswirkungen auf die Glukosehomöostase die Entwicklung verbesserter therapeutischer Ansätze für Typ-2-Diabetes mellitus (T2DM) erheblich voranbringen könnte. Zukünftige Forschungsarbeiten sollten sich dabei auf umfassende **In-vivo-** und **In-vitro-Studien** der TBC1D1-Spleißvarianten bei T2DM-Patienten konzentrieren, um gezielte Behandlungsstrategien zu entwickeln und deren klinische Anwendung zu fördern.

1. Introduction

1.1 Diabetes mellitus

Diabetes mellitus is a metabolic disorder primarily characterised by chronic hyperglycemia, or elevated levels of blood glucose, resulting from impaired insulin secretion, insulin action, or a simultaneous occurrence of these two factors (Kerner et al., 2014). This metabolic disorder affects more than 530 million adults aged 20-79 years globally, and projections by the International Diabetes Federation (IDF) indicate a further rise to 783 million by the year 2045, underscoring the growing global burden of this disease. In Europe, approximately 6,14 million adults (20-79 years) live with diabetes as of 2021, with an alarming 35.7% of cases remaining undiagnosed, according to the recent estimates from IDF (IDF Diabetes Atlas, 10th edn. Brussels, Belgium). This lack of diagnosis is a significant concern, as unmanaged diabetes can lead to a range of debilitating complications, including cardiovascular disease, kidney failure, blindness, and nerve damage, significantly affecting the quality of life for those affected. Therefore, diabetes has significant and wide-ranging impacts on both public health and the economic stability of communities (Aguayo-Mazzucato & Bonner-Weir, 2018; Ali et al., 2022; ElSayed et al., 2023; Tomic et al., 2022). Diabetes mellitus is classified into two main types: type 1 and type 2. Both types are marked by various genetic and environmental factors, resulting in the progressive loss of the pancreatic islets of Langerhans (β-cells) mass and /or function, which manifests clinically as hyperglycemia.

i. Type 1 diabetes mellitus (T1DM)

T1DM is a chronic autoimmune disorder characterised by the selective destruction of insulin-producing β-cells in the pancreas. This autoimmune process targets the β-cells' mass, reducing their insulin secretory capacity and leading to islet-directed autoimmunity. As insulin is critical for maintaining normal blood glucose levels, the loss of these cells severely impairs glucose regulation, which is a hallmark trait in the pathology of T1DM. This dysregulation of glucose homeostasis contributes to dysglycemia, an inability to properly regulate blood sugar, which can progress to hyperglycemia. Consequently, individuals with T1DM are prone to diabetes-related complications, namely ketoacidosis and long-term vascular complications, such as diabetic retinopathy, nephropathy, neuropathy, cardiovascular disease, and peripheral artery disease. These complications can severely affect the quality of life and lifespan of individuals living with T1DM, underscoring the critical need for effective management and treatment strategies (Leney & Tavare, 2009; Powers, 2021).

ii. Type 2 diabetes mellitus (T2DM)

T2DM, on the other hand, has emerged as a global health concern with increasing prevalence and significance. According to the IDF, the number of people living with T2DM is projected to rise from 643 million (11,3%) by 2030 to 783 million (12.2%) by 2045, highlighting the growing burden of this chronic metabolic disorder. (IDF Diabetes Atlas, 10th edn. Brussels, Belgium) (ElSayed et al., 2023; Hossain et al., 2024).

T2DM manifests progressively via a combination of impaired insulin production and insulin resistance, leading to elevated blood glucose levels and an increased risk of various diseases, particularly cardiovascular diseases, renal failure, and neuropathy. The pathogenesis of T2DM is multifactorial, with a wide range of risk factors contributing to its development, such as age, ethnicity, and family history, as well as modifiable risk factors, such as low socioeconomic status, obesity, metabolic syndrome, and unhealthy lifestyle behaviour (Galicia-Garcia et al., 2020). If left untreated, T2DM significantly raises the risk of severe complications, leading to increased morbidity and mortality. A comprehensive research approach is essential to address the complexity of T2DM. By examining both the pathogenesis and genetic factors of this condition, researchers can gain a deeper understanding of the underlying mechanisms and identify potential targets for intervention. This focus will improve care and management strategies for individuals living with T2DM condition (Kyrou et al., 2020).

1.2 Insulin resistance and type 2 diabetes

Insulin resistance (IR) is a complex metabolic condition characterised by a diminished response to insulin at both the cellular and systemic levels in the body. This condition arises when insulin-sensitive tissues fail to respond adequately to normal circulating insulin levels. Therefore, critical metabolic processes such as glucose uptake and glycogen synthesis are compromised. To compensate, the pancreas increases insulin secretion to maintain normal blood glucose levels.

This increased insulin secretion, a hallmark of insulin resistance, enhances glycemic regulation by facilitating more efficient glucose uptake by the body's cells, helping temporarily maintain blood glucose within a healthy range. However, this compensatory mechanism becomes less effective over time, leading to pancreatic β-cells dysfunction and defects in insulin's target tissues. These combined defects accelerate the progression toward T2DM.

This highlights the complex interplay between insulin sensitivity, insulin secretion, and glucose uptake as a key factor in the development of T2DM. Additionally, insulin resistance is also closely associated with obesity, which amplifies metabolic disruptions and increases the risk of developing T2DM (Czech, 2017; Esser et al., 2020; Ferrari et al., 2019).

1.2.1 Insulin-regulated glucose homeostasis

The regulation of blood glucose levels in the body is governed by the coordinated action of hormones, primarily insulin and glucagon, together with various organs. Unlike insulin, which facilitates glucose uptake from the bloodstream into cells, glucagon acts as a counter-regulatory hormone, promoting the breakdown of glycogen, fatty acids, and glycerol. This dynamic interplay between insulin and glucagon maintains energy balance under different physiological conditions, particularly in three main insulin-sensitive tissues: the liver, adipose tissue, and skeletal muscle (Bano, 2013; Galicia-Garcia et al., 2020; Petersen & Shulman, 2018).

Insulin, produced by the β-cells of the pancreatic islets of Langerhans, acts as a critical anabolic hormone. It enables the uptake, storage, and synthesis of nutrients such as glucose, fatty acids, and amino acids in cells while inhibiting their breakdown and release. When insulin binds to its receptor, it initiates a signaling cascade of events that activate multiple pathways. These pathways include protein and lipid phosphorylation, activation of small G protein molecular switches, control of trafficking events, and regulation of a network of enzymes and transcriptional factors. Together, these processes enable insulin to maintain metabolic balance and energy homeostasis in the body (Saltiel, 2021; Taniguchi et al., 2006; White & Kahn, 2021).

Insulin is essential in glucose homeostasis. It facilitates the storage of excess glucose as glycogen in skeletal muscle and the liver and prevents the endogenous production and release of excessive glucose by the liver. Elevated insulin levels in the bloodstream lead to a suppression of glycogen breakdown, gluconeogenesis, and glucose release by the liver while simultaneously promoting glucose uptake in adipose tissue and skeletal muscle (Evans et al., 2019; Kowalski & Bruce, 2014).

1.2.2 Glucose transporter dynamics

Glucose is a hydrophilic molecule that requires specific transporter proteins to enter the cells. There are two main types: the glucose transporter “GLUT” and the sodium-glucose linked transporter “SGLT” (Bano, 2013). These transporters are characterised by their Michaelis constant (K_m), which reflects their affinity for glucose. This affinity indicates the binding strength between the transporter and its substrate, glucose, and is quantitatively represented by the K_m value. A lower K_m suggests higher affinity, indicating that the transporter can efficiently carry glucose even at low concentrations. Conversely, a higher K_m suggests lower affinity, indicating that the transporter requires higher glucose concentrations for effective transport (Ismail & Tanasova, 2022; Wang et al., 2020).

GLUT transporters are a family of high-affinity transporters that facilitate glucose transport across cell membranes. The GLUT consists of 14 different isoforms, among which 5 are considered to play essential roles in the body, namely GLUT1, GLUT2, GLUT3, GLUT4, and GLUT5 (Deng & Yan, 2016; Scheepers et al., 2004). GLUT1, GLUT2, GLUT3 and GLUT5 are considered insulin-independent. GLUT1, GLUT3, and GLUT4 facilitate glucose uptake in various tissues under basal conditions. GLUT1 is abundantly expressed in the endothelial cells that constitute the blood-brain barrier. GLUT3 is the principal glucose transporter in neurons, and GLUT4 is the predominant glucose transporter in skeletal muscle, cardiac muscle, and adipose tissue in response to insulin and physical activity (Holman, 2020).

In addition to insulin, exercise has also been shown to enhance the expression of GLUT3 on the surface of neuron cells. In contrast, the low-affinity transporter GLUT2 is found in β-cells and tissues subjected to significant glucose fluxes, such as the intestine, liver, and kidney.

The translocation of GLUT4 to the plasma membrane is a tightly regulated process involving multiple steps. GLUT4-containing vesicles move from the intracellular compartments to the cell membrane, downstream from the activation of the insulin-signaling cascade (van Gerwen et al., 2023; Zhang et al., 2022). This insulin-signaling cascade of events, as mentioned in section 1.2.1, is regulated by multiple proteins, such as the two Rab GTPase-activating proteins, the AKT substrate TBC1D4 also known as AS160 (Tre-2 bub2 cdc16, 1 domain family member) and TBC1D1 (Tre-2 bub2 cdc16, 1 domain family member 1), as well as other Rab GTPases, which play essential roles in controlling the mobilisation and fusion of GLUT4 vesicles (Mohan et al., 2010; Pfeffer, 2017; Zhang et al., 2022).

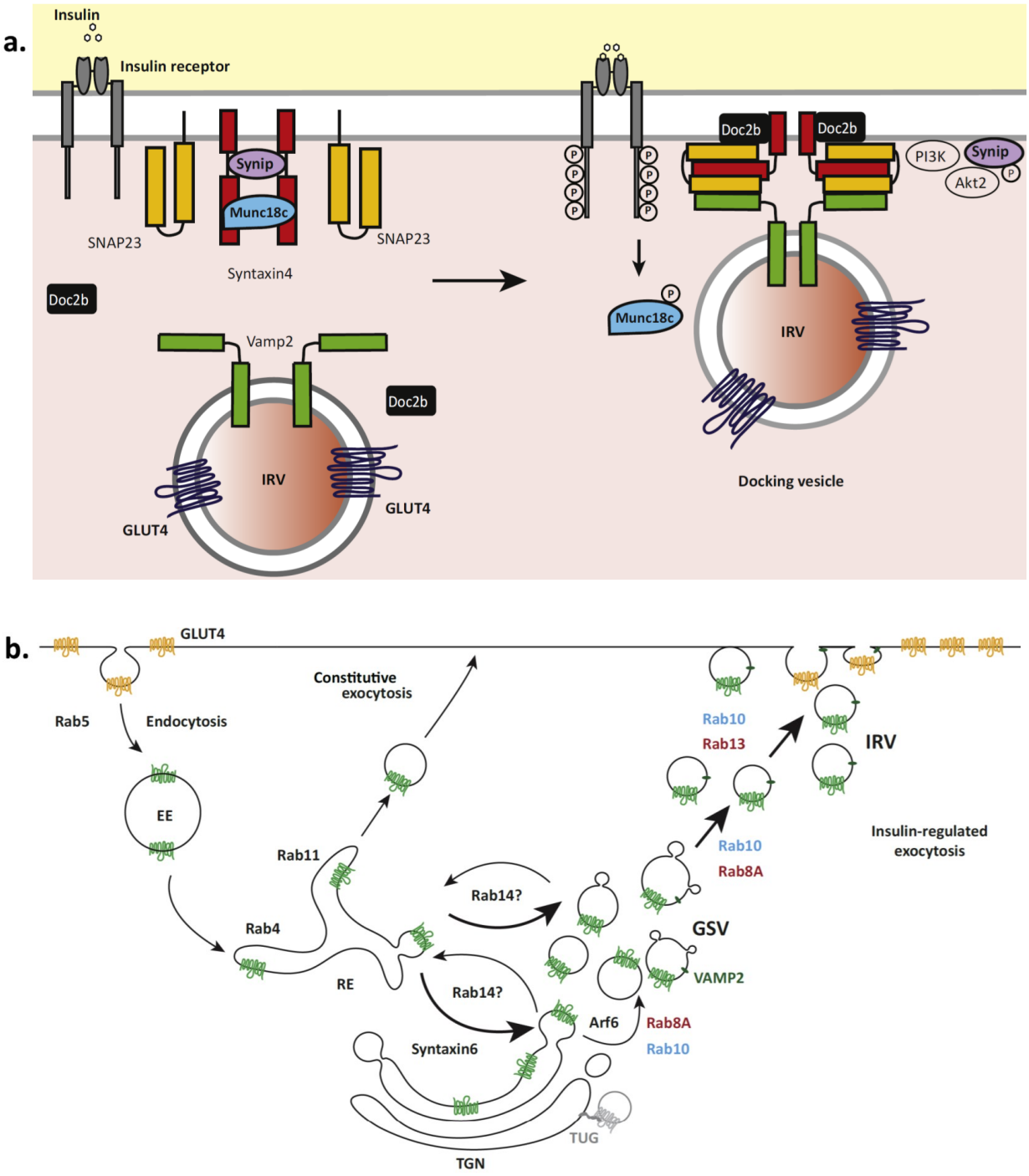

<u>Figure 1</u>: GLUT4 vesicle mobilisation and cycling (Jaldin-Fincati et al., 2017)

GLUT4 vesicle fusion is regulated by Munc18c, Synip, the calcium sensor Doc2b, and the SNARE complex of VAMP2, syntaxin4, and SNAP23. Insulin phosphorylates Munc18 and Synip, allowing SNARE complex assembly and GLUT4 vesicle fusion (a). Various Rab GTPases mediate the endosomal traffic of GLUT4 through endocytosis and exocytosis (b).

Moreover, GLUT4 vesicle mobilisation and docking are tightly regulated by SNARE proteins such as syntaxin4, Snap-23, VAMP2, and several regulatory factors such as Munc18c, Synip and the calcium sensor Doc2b (Bryant & Gould, 2011; Fukuda et al., 2009; Hoffman & Elmendorf, 2011; Jewell et al., 2011; Kioumourtzoglou et al., 2014; Leto & Saltiel, 2012; Ramalingam et al., 2012; Yu et al., 2013) (Figure 1a). Post glucose uptake, GLUT4 undergoes endocytosis and is recycled back to the intracellular storage compartments for further mobilisation upon subsequent insulin stimulation (Foley et al., 2011; Jaldin-Fincati et al., 2017) (Figure 1b).

1.3 Skeletal muscle in metabolism and energy homeostasis

1.3.1 Muscle tissue and its metabolic function

Muscle tissue is categorised into three types: smooth, cardiac, and skeletal muscle, each with a primary contraction function. Skeletal muscle is defined by its structure, which is composed of long, cylindrical muscle fibers, also known as myofibers or muscle cells. These fibers contain contractile proteins, facilitating body movement and maintaining body posture. Beyond its role in movement, skeletal muscle is an essential site for insulin-mediated glucose uptake, glycogen storage, and glucose utilisation for energy, notably during physical activity. This places skeletal muscle at the center of metabolic regulation, alongside other key tissues such as liver, adipose tissue, and cardiac muscle (Cartee, 2015; Frontera & Ochala, 2015; Howlett et al., 2007; Larsen et al., 2022; Mukund & Subramaniam, 2020; Sylow et al., 2021).

A hallmark of skeletal muscle is its capacity for regeneration, driven by satellite cells (SCs). This highly orchestrated regeneration process involves the activation, proliferation, and differentiation of SCs into muscle fibers at the injury site. Under normal conditions, quiescent SCs remain dormant. Still, they can be rapidly activated in response to muscle injury driven by environmental cues and chemical signals (Collins et al., 2009; Francetic & Li, 2011; Hernandez-Hernandez et al., 2017; Yin et al., 2013; Zammit, 2017). Upon activation, SCs express paired box (Pax) family transcription factors such as *Pax3* and *Pax7* and myogenic regulatory factors (MRFs) such as the myoblast determination protein 1 (*MyoD*), myogenic factor 5 (*Myf5*), and myogenin (*MyoG*), which regulate their proliferation and differentiation. As SCs progress through myogenesis, the expression of *MyoD* and *Myf5* decreases. At the same time, *MyoG* and *Mrf4* promote the fusion of myoblasts into mature myotubes. This finely-tuned process is critical for muscle repair (Akizawa et al., 2013; Iberite et al., 2022) (see details supplementary Figure 1).

The metabolic function of skeletal muscle is centred on generating Adenosine triphosphate (ATP), the essential energy source for muscle contraction (Sahlin et al., 1998; Sargeant, 2007). Due to limited ATP storage, skeletal muscle relies on anaerobic and aerobic metabolic pathways to meet energy demands during physical activity. During short, intense activities, anaerobic pathways dominate, rapidly generating ATP by breaking down phosphocreatine (PCr) and muscle glycogen. In contrast, prolonged, moderate-intensity exercise primarily involves aerobic pathways, where oxidative phosphorylation becomes dominant, relying on carbohydrates and fatty acids/lipids as fuel. Thus, glycolysis and oxidative metabolism maintain ATP supply, with carbohydrate metabolism being particularly crucial during higher-intensity efforts.

Skeletal muscle also plays a significant role in glucose homeostasis, absorbing glucose from the bloodstream, especially during exercise. The muscle's oxidative capacity, linked to its mitochondrial content, ensures sustained energy production, making skeletal muscle vital for energy provision and overall metabolic balance (Hargreaves & Spriet, 2020; Parolin et al., 1999; Romijn et al., 1993; Smith et al., 2023; Thyfault & Bergouignan, 2020; van Loon et al., 2001).

1.3.2 Role of skeletal muscle in systemic glucose regulation

Skeletal muscle is pivotal in maintaining systemic glucose regulation, serving as the primary site for insulin- and exercise-stimulated glucose uptake (DeFronzo & Tripathy, 2009; Mizgier et al., 2014; Sylow et al., 2017). Following the postprandial state, skeletal muscle is responsible for approximately 30-35% of the total glucose disposal, a critical process in preventing hyperglycemia and maintaining glucose homeostasis. During high insulin levels, notably in a hyperinsulinemic state, skeletal muscle’s contribution to glucose disposal can increase up to 80% (DeFronzo & Tripathy, 2009; He et al., 2022). The insulin signaling pathway primarily mediates this process by activating protein kinase B (Akt), facilitating glucose uptake into muscle cells (Jaiswal et al., 2019; Whiteman et al., 2002). In individuals with insulin resistance or T2DM, insulin-stimulated glucose uptake in skeletal muscle is significantly reduced, leading to impaired glucose regulation and systemic hyperglycemia. Therefore, improving insulin sensitivity in skeletal muscle is a primary target for preventing and managing insulin resistance or T2DM.

1.3.3 Impact of exercise on glucose homeostasis in skeletal muscle

Exercise intensely impacts glucose homeostasis in skeletal muscle by significantly enhancing glucose uptake and improving insulin sensitivity (Sylow et al., 2017). During exercise, muscle contractions trigger the translocation of GLTU4 glucose transporters to the muscle cell membrane, a process that occurs independently of insulin. This increase in GLUT4 at the membrane allows efficient glucose absorption to meet the heightened energy demands of the contracting muscles. In addition to this immediate effect, exercise induces a long-lasting enhancement of insulin sensitivity. These long-term benefits are partly due to increased expression of GLUT4 and improved insulin signaling.

As a result, skeletal muscle becomes more efficient at glucose uptake and utilisation, which aids in the resynthesis of muscle glycogen stores (Cartee, 2015; Kjobsted et al., 2019). Exercise-induced adaptations are crucial for maintaining glucose homeostasis, particularly in individuals with insulin resistance or T2DM. Consequently, regular physical activity is a key strategy in managing and preventing these conditions (Knudsen et al., 2020; Petersen & Shulman, 2018; Spaulding & Yan, 2022).

1.3.4 Pathophysiology of insulin resistance and T2DM in skeletal muscle

Insulin is crucial for the regulation of blood glucose levels by promoting the uptake of glucose into muscle and adipose tissues and is essential for maintaining whole-body glucose homeostasis (Leney & Tavare, 2009). However, in the condition of insulin resistance (IR), the body’s normal response to insulin is impaired. IR disrupts glucose uptake, glycogen synthesis, and lipolysis regulation, leading to elevated blood glucose levels. As a result, the body attempts to compensate by enhancing the insulin production from the β-cells, increasing fasting plasma insulin levels (DeFronzo & Tripathy, 2009; Kowalski & Bruce, 2014). The impaired action of insulin at the cellular level is a central problem in IR. Notably, the capacity of the GLUT4 transporter to mediate glucose uptake into the cells is affected (Petersen & Shulman, 2018). As a primary indicator of T2DM, IR necessitates the development of effective treatments and early detection techniques (Belfiore et al., 2017; Mesinovic et al., 2023; Szukiewicz, 2023).

Skeletal muscle, being one of the body's largest tissues, is the principal site for postprandial glucose absorption, meaning that IR in muscle tissue can have a profound effect on overall glucose regulation. IR in skeletal muscle significantly undermines glucose homeostasis, increasing the risk of obesity and T2DM (Balakrishnan & Thurmond, 2022; DeFronzo & Tripathy, 2009).

1.4 Molecular mechanisms of insulin signaling

The molecular signaling cascade of insulin is initiated when insulin binds to its receptor on the cell surface membrane. The binding induces a conformational change in the insulin receptor, activating its intrinsic kinase. This activation leads to the autophosphorylation of tyrosine residues. It extends its kinase activity towards other substrates such as Src Homology 2 Domain Containing (SHC), GRB2-associated binding protein 1 (Gab1) (Figure 2a), Forkhead box proteins (FOXOs) (Figure 2b), and Casitas B-lineage Lymphoma (Cbl) (Figure 2c), including Insulin Receptor Substrate (IRS).

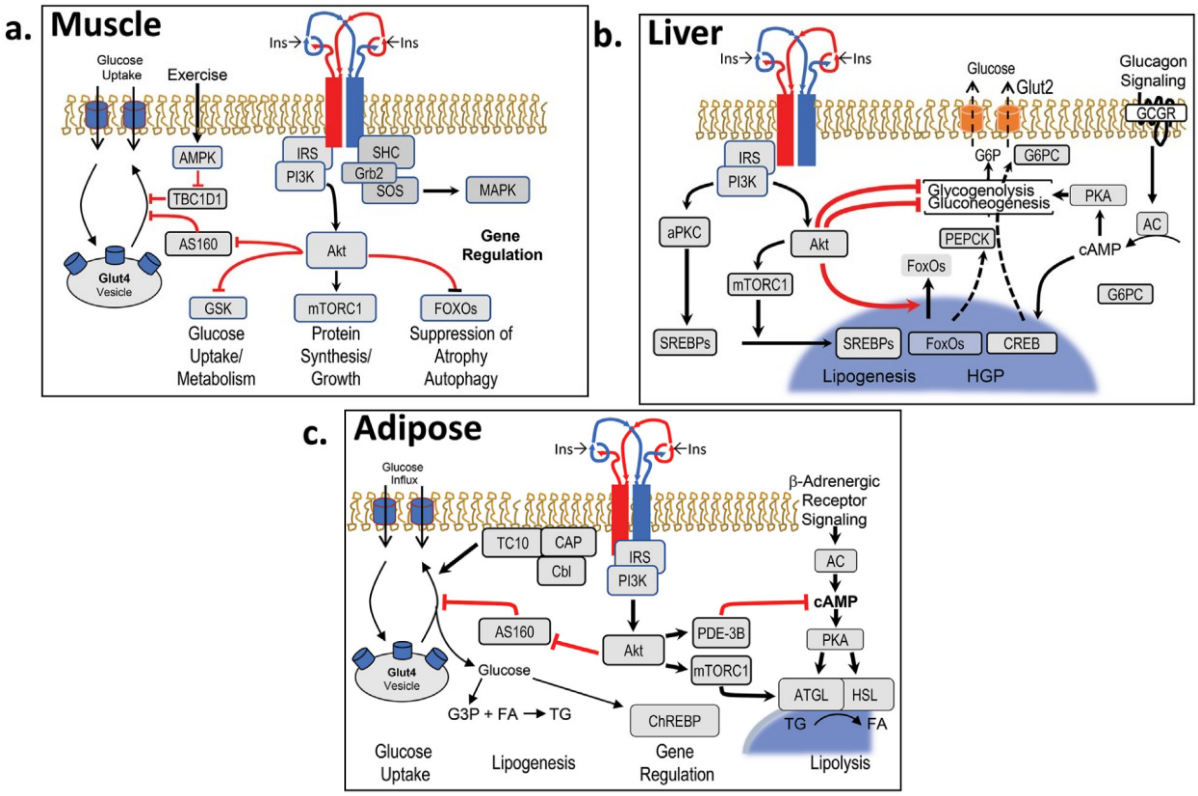

Figure 2: Tissue-specific insulin signaling (White & Kahn, 2021)

The insulin receptor is auto-phosphorylated on multiple tyrosine residues, allowing the docking and activation of numerous signaling molecules, most notably insulin receptor substrate (IRS) proteins. This, in turn, activates phosphatidylinositol-3-kinase (PI3K) and AKT to mediate glucose uptake and further metabolic changes in protein and lipid metabolism. While the general pathway is similar in all tissues, the final biological effects are specialized to the roles of insulin in muscle (a), liver (b), and adipose tissue (c).

The insulin receptor activates its substrates through tyrosine phosphorylation. Once phosphorylated, the insulin receptor substrate recruits phosphoinositide 3-kinase (PI3K) to the plasma membrane where its substrates, including Phosphatidylinositol 4,5-bisphosphate (PIP2), are located. PI3K catalyses the phosphorylation of PIP2, converting PIP2 into Phosphatidylinositol 3,4,5-triphosphate (PIP3). The latter acts as a docking site at the plasma membrane, facilitating the activation of pathways involving kinases such as Protein kinase B (AKT). AKT activation regulates a broad range of cellular processes, including vesicle trafficking, glucose uptake, glycogen synthesis, lipid metabolism, glycogenolysis, gluconeogenesis, protein synthesis, cell growth and differentiation and survival (Figure 2).

Moreover, AKT is central to insulin metabolic actions promoting the translocation of GLUT4 vesicles to the cell membrane (Haeusler et al., 2018; Nolan et al., 2015; Petersen & Shulman, 2018; van Gerwen et al., 2023). The intricate coordination of these cellular processes ensures the efficient storage, production, and utilisation of energy to meet the body's metabolic needs.

1.4.1 Regulation of GLUT4 exocytosis by Rab GTPases and Rab GAPs

The final step in glucose uptake is the fusion of GLUT4-containing vesicles with the cell's plasma membrane. This process results after several stages of its trafficking, including intracellular sorting, vesicular transport along the cytoskeletal elements, and finally, docking and fusion with the cell membrane, allowing glucose uptake from the extracellular environment (Hoffman & Elmendorf, 2011) (see Figure 1b). This translocation process involves a network of various molecules, such as Rab proteins (Ras-related in brain) and Rab GTP-activating proteins (Rab GAPs). The Rab GTPases regulate the different steps in the vesicle trafficking, while Rab GAPs ensure the well-orchestrated process by tightly regulating Rab GTPases' active and inactive states (Homma et al., 2021; Hutagalung & Novick, 2011; Stenmark, 2009). Any alterations of these parameters can disrupt normal metabolic processes, contributing to conditions such as T2DM (Benninghoff et al., 2020; Binsch et al., 2023; Zhang et al., 2022; Zhou et al., 2017).

GLUT4-containing vesicles (GSVs) undergo sorting and recycling, which is essential for efficient glucose uptake into the cells. This efficiency is quantified by the Michaelis constant (K_m), a kinetic parameter that describes the rate of enzymatic reactions as a function of substrate concentration.

While Michaelis-Menten kinetics apply to enzyme-catalysed reactions, the parameter K_m can similarly define the affinity of GLUT4 for glucose. Thus, K_m determines the rate and efficiency of glucose uptake into the cells essential for maintaining energy balance and blood glucose levels. GLUT4 exhibits a moderate K_m value, suggesting a balanced glucose concentration for effective functioning. Its moderate affinity for glucose suggests that while it effectively binds and transports glucose, it does so within an optimal range of glucose concentrations (Chew et al., 2009; Holman, 2020; Karlsson et al., 2009).

In mammalian cells, the exocytosis of GLUT4 and its regulation by insulin are central to glucose homeostasis. Under basal conditions, GLUT4 transporters are primarily located in intracellular compartments within muscle and fat cells, while only a minor fraction is present on the cell surface. Notably, insulin-regulated aminopeptidase (IRAP) is co-localized with intracellular GSVs in the basal state.

Studies showed that IRAP and GLUT4 share common trafficking pathways within the cell, underscoring their close functional relationship (Jordens et al., 2010; Keller et al., 1995; Larance et al., 2005; Mafakheri, Florke, et al., 2018; Ross et al., 1996).

Upon insulin stimulation, proteins like Rab GTPases and their regulatory RabGAPs facilitate vesicular trafficking, leading to the translocation and fusion of IRAP and GLUT4-containing vesicles with the plasma membrane, which induces glucose uptake into the cell. Thereby, IRAP and GLUT4 are continuously recycled between the cell surface and intracellular compartments, maintaining a reservoir for rapid response that shifts towards increased surface localisation in response to insulin (Descamps et al., 2020; Foley et al., 2011; Jaldin-Fincati et al., 2017; Sylow et al., 2021; Waters et al., 1997; Williams et al., 2006). The interplay between IRAP and GLUT4 exocytosis underscores the complex molecular mechanisms governing glucose uptake regulation.

1.4.2 Glucose transport by the protein kinases AKT and AMPK

As mentioned in section 1.2.1, cellular metabolism regulation relies on insulin, which initiates a protein phosphorylation cascade with AKT as a proximal central kinase node in this cascade. In skeletal muscle, this insulin-mediated cascade begins when insulin binds to and activates its cell surface receptor, leading to the autophosphorylation of the insulin receptor on tyrosine residues. The activated insulin receptor phosphorylates insulin receptor substrate proteins, such as IRS1 and IRS2, on their tyrosine residues.

These interactions on the IRS proteins lead to the activation of signaling pathways by acting on the enzyme phosphoinositide 3-kinase (PI3K). PI3K is then able to translocate to the plasma membrane, where its substrates, including phosphatidylinositol 4,5-bisphosphate (PIP2), are located. At the membrane, PI3K catalyses PIP2 phosphorylation, converting it to phosphatidylinositol 3,4,5-triphosphate (PIP3). The latter acts as a docking site at the plasma membrane for additional kinases like PDK1 and mTORC2. AKT is then fully activated through sequential phosphorylation by PDK1 and mTORC2 at specific sites (Figure 3). Once activated, AKT phosphorylates multiple proteins in the distal node of insulin signaling, leading to significant changes within the cells. An essential function of insulin-activated AKT in skeletal muscle and adipose tissue is to promote the translocation of GLUT4-containing vesicles to the cell membrane, enabling glucose uptake.

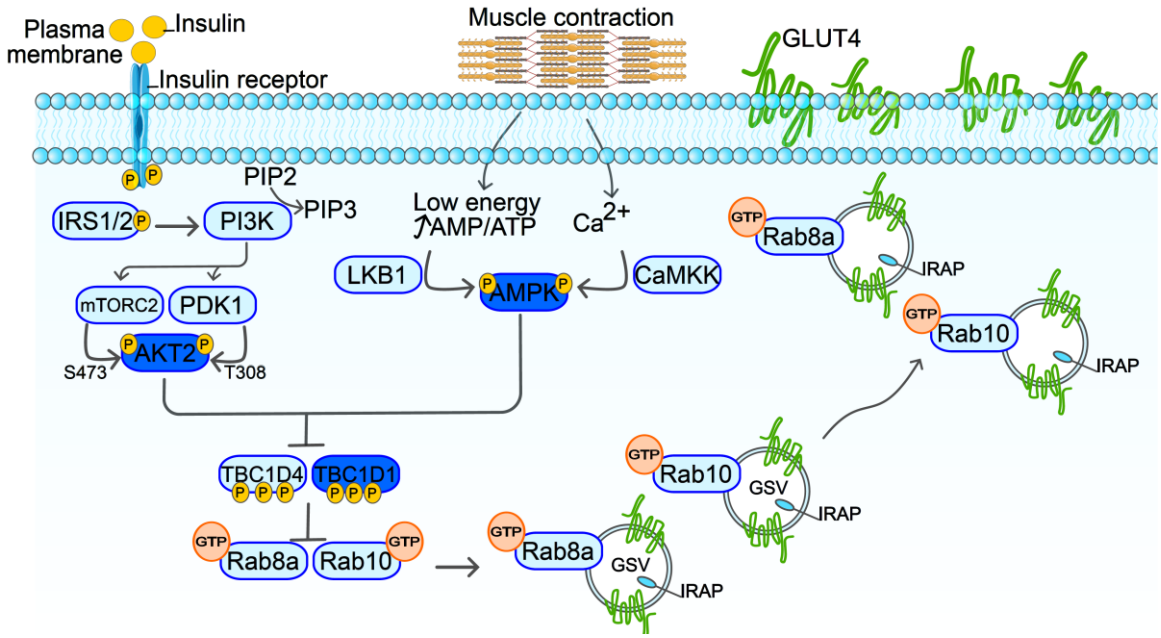

Figure 3: **Glucose transport under AMPK and AKT2 cues**

When insulin binds to its receptors at the skeletal muscle cell surface, it induces the receptor's auto-phosphorylation, leading to the recruitment and subsequent phosphorylation of insulin-responsive substrates 1, 2 (IRS1/2), which in turn leads to phosphatidylinositol 3-kinase (PI3K) activation. PI3K activation triggers signalling cascades essential for GLUT4 translocation and is dominated by the serine-threonine kinase AKT2 – the first node. The second node, AMPK signaling, is described as an energy sensor regulation that is activated by AMP-mediated phosphorylation during energy depletion in the muscle cells. Downstream signaling of both nodes, AKT2 and AMPK, involve molecules responsible for vesicle sorting and mobilisation, such as the Rab GTPase-activating proteins (RabGAPs). Phosphorylation of AKT2 and AMPK inhibits the GAP function of the two related RabGAPs, TBC1D1 and TBC1D4, towards the Rab (Ras-related in brain) GTPase proteins, Rab8a and Rab10. Consequently, Rab8a and Rab10 bind to GTP and trigger GLUT4 translocation to the plasma membrane and GLUT4-mediated glucose uptake into the skeletal muscle cells. IRAP: insulin-regulated aminopeptidase is a GLUT4 storage vesicles (GSVs) resident protein.

This process is regulated through AKT substrate TBC1D4, also known as AS160 and its close orthologue TBC1D1, both downstream effectors and members of the Rab GTPase activating proteins (RabGAPs), regulatory proteins of the Rab GTPases proteins involved in the intracellular trafficking of GLUT4-containing vesicles (Gonzalez & McGraw, 2006; Manning & Toker, 2017; Sakamoto & Holman, 2008; Szukiewicz, 2023; van Gerwen et al., 2023).

Likewise, glucose uptake in skeletal muscle significantly increases during exercise and muscle contraction to meet the higher energy demand. AMPK (AMP-activated protein kinase) becomes activated through phosphorylation at Thr172, primarily by liver kinase B1 (LKB1) and calcium/calmodulin-dependent protein kinase (CaMKK) (Figure 3). Once activated, AMPK phosphorylates various downstream effectors and substrates, such as TBC1D1 and TBC1D4, thereby regulating glucose uptake in muscle during contraction (Carling, 2017; de Wendt et al., 2021; Flores-Opazo et al., 2020; Kjobsted et al., 2019; Spaulding & Yan, 2022; Sylow et al., 2021; Winder & Thomson, 2007).

1.5 Molecular mechanisms of glucose uptake in skeletal muscle

Skeletal muscle constitutes around 40% of total body mass, making it one of the most significant tissues in terms of glucose metabolism (Frontera & Ochala, 2015; He et al., 2022). This tissue plays a pivotal role in maintaining glucose homeostasis, as it is highly responsive to the two primary physiological stimuli, insulin and muscle contraction, both of which are key drivers of glucose uptake (DeFronzo & Tripathy, 2009; He et al., 2022). Through different signaling pathways, insulin and muscle contraction converge on the critical step of translocating the GSVs at the plasma membrane, increasing GLUT4 transporters on the muscle cell membrane. GLUT4 is a critical component in regulating glucose uptake into peripheral tissues and is predominantly found in insulin-sensitive tissues such as adipose tissue, the heart, and skeletal muscle.

Under normal conditions, GLUT4 resides within the intracellular membranes in the cells. Upon stimulation by insulin or exercise, it is translocated to the cell surface, facilitating glucose uptake, as shown in Figure 3 (He et al., 2022; Jaldin-Fincati et al., 2017). The regulation of blood glucose homeostasis, a fundamental aspect of metabolic health, is mediated by the uptake and utilisation of glucose by skeletal muscle through the action of GLUT4 (Jaldin-Fincati et al., 2017; Sakamoto & Holman, 2008). Consequently, an increase in GLUT4 expression enhances the muscle's capacity to absorb glucose, playing a pivotal role in metabolic regulation (Hayashi et al., 1997; Richter et al., 2001).

1.5.1 The role of Rab GTPases proteins in glucose uptake

Rab GTPase proteins ensure the proper interaction between vesicles and their target membranes while also regulating membrane traffic within the cell (Homma et al., 2021; Lamber et al., 2019). These proteins alternate between an active state when loaded with guanosine triphosphate (GTP) and an inactive state when bound to guanosine diphosphate (GDP) (Figure 4). Two proteins are responsible for the cycling between these states: guanine nucleotide exchange factors (GEFs) and GTPase-activating proteins (GAPs). Different Rab GTPases are specialised for different cellular locations (Miinea et al., 2005; Roach et al., 2007; Stenmark, 2009; Zhou et al., 2017). When activated, Rab GTPases recruit a range of effector proteins essential for the various phases of membrane trafficking, including vesicle transport, docking, and fusion.

Interestingly, Rab GTPases' activity and interactions and their associated regulatory proteins are fine-tuned through various post-translational modifications (PTMs), such as phosphorylation and AS. These PTMs can control the cycling and interaction of RabGAPs with these effector proteins, directing them to specific organelles or vesicles throughout the membrane trafficking pathway (Zhou et al., 2017).

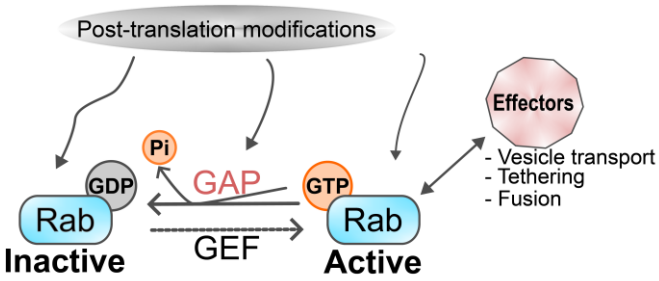

Figure 4: Rab family small GTPases cycle

Rab proteins cycle between two states facilitated by the following proteins: the guanine nucleotide exchange factors (GEFs) and the GTPases-activating proteins (GAPs). Active Rabs recruit various effector proteins within the intracellular membranes that regulate different membrane trafficking steps. The interaction between the Rabs with the proteins GEFs, GAPs, and the effectors occurs under post-translational modifications, such as phosphorylation.

1.5.2 TBC1D1 regulatory protein of Rab GTPase proteins

TBC1D1 and its close orthologue, TBC1D4 are the key members of the TBC1 family of RabGAP proteins and share about 50% of identity across their entire sequence. However, within the RabGAP protein domain, their identity increases to 79% (An et al., 2010; Sakamoto & Holman, 2008).

Both TBC1D1 and TBC1D4 proteins share a similar protein domain structure, including two phosphotyrosine-binding domains (PTB) that are involved in the binding to downstream interaction partners such as IRAP, as well as a calmodulin-binding domain (CBD) and the Rab GAP-TBC domain, which is responsible for catalysing the GTP hydrolysis (Cartee, 2015; Frosig et al., 2010; Jordens et al., 2010; Mafakheri, Florke, et al., 2018; Pehmoller et al., 2009) (Figure 5). The RabGAP domain of TBC1D1 achieves full functionality when two key catalytic residues, named "arginine-finger" (Arg^{948} in human TBC1D1, Arg^{941} in mouse Tbc1d1) and the "glutamine finger" (Gln^{985} in human TBC1D1, Gln^{978} in mouse Tbc1d1) are present. These residues are crucial for the catalytic process of GTP hydrolysis, and their absence results in the loss of RabGAP activity, underscoring their essential role in the protein's function (Majumdar et al., 2017; Pan et al., 2006; Park et al., 2011; Roach et al., 2007).

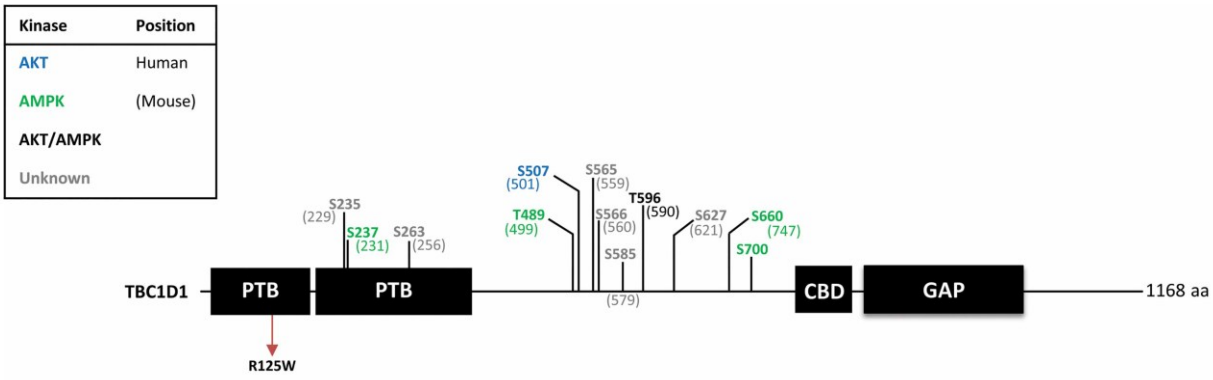

Figure 5: Structure of murine Tbc1d1 and position of phosphorylation sites (Mafakheri, Chadt, et al., 2018)

Arrows indicate R125W mutation of TBC1D1 associated with human obesity (Meyre et al., 2008; Stone et al., 2006; Volckmar et al., 2016). AKT phosphorylates TBC1D1 at Ser507 and Thr596 (An et al., 2010). Exercise stimuli induce Ser237, Thr489, Ser660 and Ser700 phosphorylation in TBC1D1 (Treebak et al., 2014). The figure displays human phosphorylation sites, with mouse phosphorylation sites indicated in parentheses. Sites targeted by AKT and AMPK are coloured blue and green, respectively. Sites phosphorylated by both are marked in black.

As illustrated in Figure 4, TBC1D1 as a RabGAP protein maintains the inactive form of Rab proteins and regulates glucose transport in the skeletal muscle and adipose tissue, whereby *TBC1D1* expression levels are higher in skeletal muscle compared to adipose tissue (Albers et al., 2015; Chavez et al., 2008; Szekeres et al., 2012; Taylor et al., 2008).

Previous studies have analysed the activity of the GAP domain of mammalian TBC1D1 against a list of Rab GTPase proteins: Rab 2, Rab8a, Rab8b, Rab10, Rab14 (Chua & Tang, 2015; Roach et al., 2007), see Table 1. These investigations concluded that the TBC1D1 GAP domain has a strong affinity for the Rab GTPase proteins Rab2, Rab8a, Rab8b, Rab10, and Rab14. Moreover, TBC1D1 was found to be highly expressed in muscle tissue in mice and rats. *In vitro* studies further demonstrated that TBC1D1 engages specifically with the Rab GTPases proteins Rab8a and Rab10 (Ishikura & Klip, 2008; Szekeres et al., 2012; Zhou et al., 2017). Several studies on TBC1D1 also emphasized the significant role of TBC1D1 in the regulation of glucose uptake, utilisation, and storage in various tissues. TBC1D1 also coordinates the overall homeostasis of glucose within different tissues and organs (An et al., 2010; Hatakeyama & Kanzaki, 2013; Hatakeyama et al., 2019).

Table 1: List of Rab GTPases substrates identified for the GAP activity of TBC1D1

Rab	Known role in vesicle trafficking	*in vitro* experiments	Reference(s)
Rab2A	GLUT4 protein translocation	*in vitro*	(Roach et al., 2007)
Rab8A		L6 myotubes	(Ishikura & Klip, 2008)
Rab8B		*in vitro*	(Roach et al., 2007)
Rab10		adipocytes	(Sano et al., 2011)
Rab14		L6 myotubes	(Ishikura & Klip, 2008)
Rab28		adipose tissue; rat tibialis anterior muscle	(Zhou et al., 2017)

The expression of *TBC1D1* and *TBC1D4* varies significantly across different tissues. While *TBC1D4* is expressed at similar levels irrespective of the tissue, *TBC1D1* shows much higher expression in skeletal muscle, particularly in glycolytic skeletal muscle, compared to other tissues (Taylor et al., 2008; Zhou et al., 2017). In addition, TBC1D1 possesses multiple phosphorylation sites targeted by Ser/Thr kinases, including AKT and AMPK. Early studies using mutational analysis and mass spectrometry highlight the phosphorylation of Thr^{596}, Ser^{237}, Ser^{660} and Ser^{700} as essential for enabling the translocation of GLUT4, see Figure 5 (Jessen et al., 2011; Roach et al., 2007; Taylor et al., 2008; Treebak et al., 2014).

In addition to these phosphorylation sites, the murine Tbc1d1 has been reported to assemble into an oligomeric complex with a molecular weight of approximately 600 kDa. Based on the predicted mass of a Tbc1d1 monomer, this complex fits into a tetramer (Mafakheri, Florke, et al., 2018). Moreover, a mutation in the *Tbc1d1* gene in Swiss Jim Lambert (SJL) mice led to the production of a truncated protein that lacks a complete GAP protein domain, as observed in cell-free experimental systems (Chadt et al., 2008). Additionally, a mutation in the arginine residue (R125W) in the first PTB domain of *TBC1D1* has been linked to obesity traits in humans (Meyre et al., 2008; Stone et al., 2006; Volckmar et al., 2016). These findings raise the possibility that the TBC1D1 protein RNA complex and protein-protein interactions in human skeletal muscle may lead to the production of variants with different functions and susceptibilities to disease development.

Bioinformatic analysis of *TBC1D1* expression has identified a total of 20 transcript variants, including protein-coding sequences undefined protein-coding CDS, and alternatively spliced transcript with retained intron. Among these, 9 variants encode distinct protein isoforms. However, only 3 transcripts: ENST00000698857.1, ENST00000508802.5, and ENST00000261439.9, contain nucleotide sequences that directly correspond to the protein-coding regions of TBC1D1 (Ensembl release 111-January 2024). This variability in splicing may contribute to the functional diversity of TBC1D1 and its involvement in disease mechanisms.

1.6 Alternative splicing and glucose homeostasis

The TBC1 RabGAP family of proteins are critical regulators of Rab GTPases proteins, interacting through post-translational modifications, like phosphorylation and alternative splicing (AS), to glucose homeostasis in skeletal muscle (see Figure 3 and Figure 4). AS is achieved by a macromolecular machine called spliceosome, which is located in the nucleus of eukaryotic cells and is responsible for removing noncoding introns from precursor messenger RNA (pre-mRNA) (Love et al., 2023; Wahl et al., 2009). During post-transcriptional regulation of gene expression, pre-mRNA AS takes place and is responsible for proteomic diversity (Juan-Mateu et al., 2016). Thus, pre-mRNA AS enables a single gene to generate multiple mRNA and structurally different protein isoforms by converting alternative exons into mature mRNA. These various isoforms can possess distinct biological properties, thus enhancing the functional diversity of genes and proteins in cellular functions (Chen & Manley, 2009; Goldtzvik et al., 2023; Nilsen & Graveley, 2010).

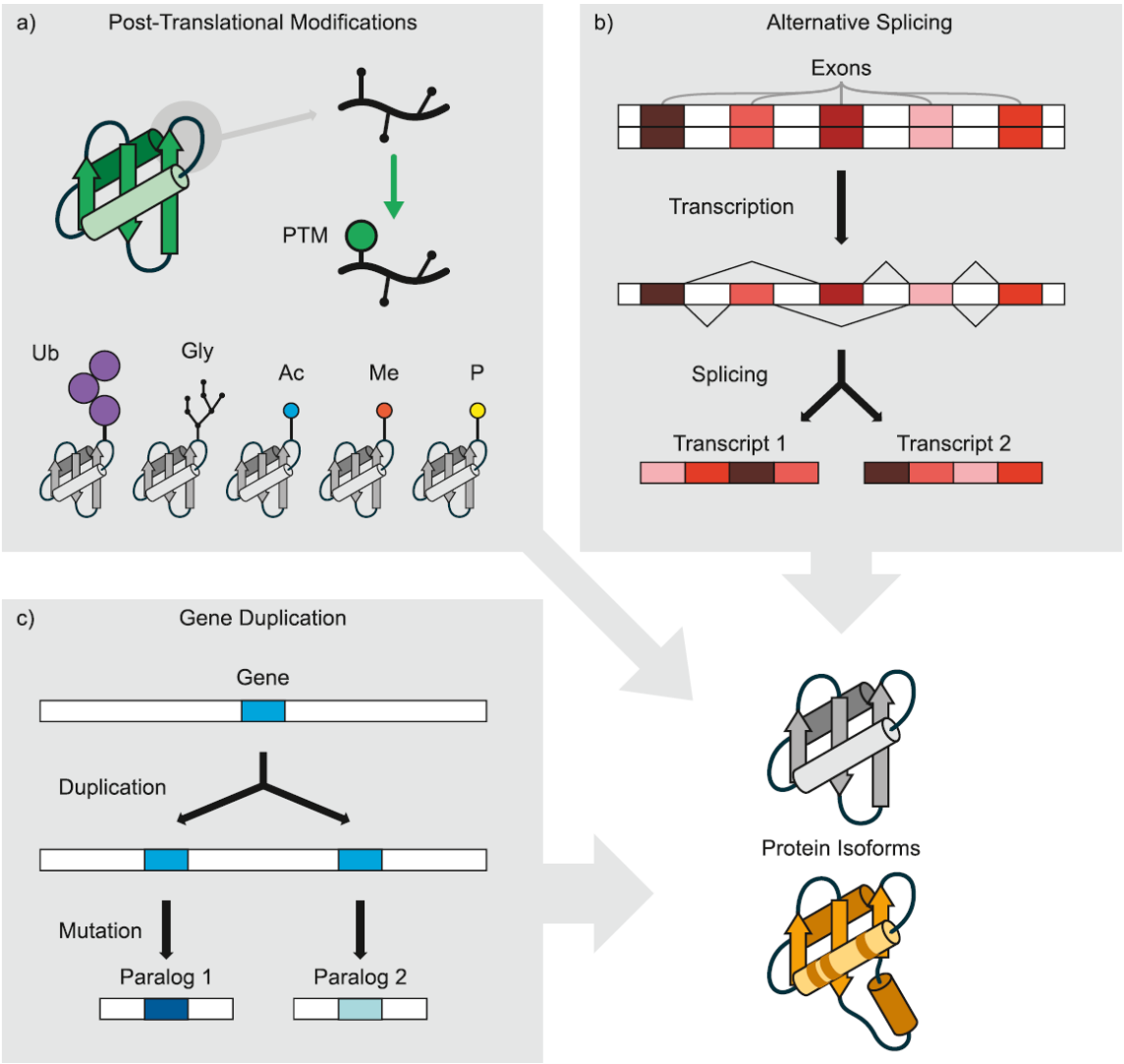

Figure 6: Mechanisms producing numerous versions of protein (Goldtzvik et al., 2023)

Post-translational modifications (PTMs) are chemical groups that bind one or more amino acid residues to the protein by covalence binding (a). Alternative Splicing (AS) generates different protein isoforms from the same gene through alternative combinations of its exons during the splicing process (b). Gene duplication events generate multiple copies of a single gene, named paralogs. The paralogs accumulate mutations through evolution, resulting in different versions of the same gene (c). Abbreviations: Ub: ubiquitination; Gly: glycosylation; Ac: acetylation; Me: methylation; P: phosphorylation.

Three main mechanisms are responsible for producing multiple versions of the same protein. The first is a post-translational modification, where chemical groups are added to or removed from amino acids after the protein is synthesised. The second is gene duplication, where an ancestral gene is copied and separated into two distinct genes within a lineage, resulting in paralogs. The third mechanism is AS, which rearranges and assembles distinct exons from a single gene, producing numerous variants named isoforms.

Furthermore, AS allows one gene to generate multiple functions or properties, contributing to the proteomic diversity of multicellular organisms. In addition to AS, post-translational modifications, such as phosphorylation, contribute to diverse protein-protein interactions that are essential for maintaining cellular homeostasis (Kim et al., 2022; Zhong et al., 2023) (Figure 6).

AS enables the production of multiple functionally distinct mRNAs in a tissue-, cell type-, and developmental stage-specific manner (Jobbins et al., 2023; Kim et al., 2018; Marasco & Kornblihtt, 2023; Marcheva et al., 2020; Tazi et al., 2009; Vuong et al., 2016). This tightly regulated process is essential in maintaining cellular and physiological functions, including those related to metabolism. In the context of glucose homeostasis, the circadian clock has been shown to control the rhythmic expression and AS of genes within pancreatic β-cells, which are crucial for insulin secretion.

Marcheva et al. demonstrate that disruptions in circadian clock components, such as BMLA1 and CLOCK, lead to significant changes in the splicing of critical genes involved in insulin secretion, including *Cask* and *Madd*. These disruptions impair glucose-stimulated insulin release and contribute to metabolic disorders like diabetes. These findings highlight the essential role of AS in the regulation of glucose metabolism and underscore its contribution to the development and progression of metabolic diseases such as diabetes. This raises important considerations regarding the implications of this research on AS and its potential impact on metabolic health.

1.6.1 Dynamics of alternative splicing events and RabGAP proteins

The spliceosome is a complex assembly of small nuclear RNAs (snRNAs) and numerous associated protein factors, which together form a complex named small nuclear ribonucleoproteins (snRNPs). Together, they ensure the expression of the mature form of the mRNA by precisely removing non-coding regions (introns) and retaining the coding regions (exons) of the gene. The mRNA's transcription is regulated by a promoter, a DNA sequence located upstream of the gene, that controls its transcription by serving as a binding site for the RNA polymerase, initiating the production of the mRNA. Once matured, the mRNA is translated into proteins (Belfiore et al., 2017; Black, 2003; Morais et al., 2021; Nagasawa & Garcia-Blanco, 2023)

AS events are classified into common and uncommon categories. Common categories of AS include exon skipping, mutually exclusive exons, retained intron, alternative acceptor, alternative acceptor 3´splice sites, alternative donor, and alternative 5´splice sites. The uncommon group comprises the alternative promoter, alternative terminator, new intron, and retained exon (Figure 7).

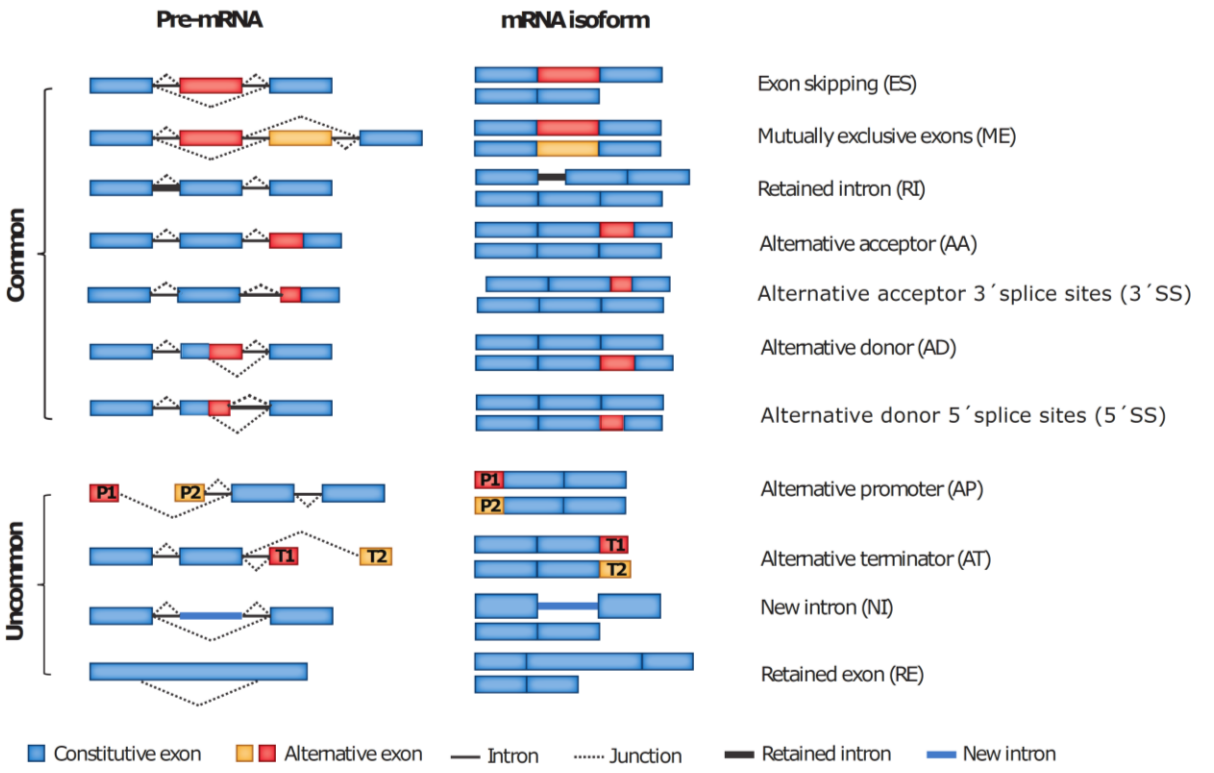

Adapted from Su,T., et al.(2023) Annual Review of Biomedical Data Science

Figure 7: Illustration of the nine types of alternative splicing events (Su et al., 2023)

AS is grouped into exon skipping (ES), mutually exclusive exons (ME), retained intron (RI), alternative acceptor (AA), alternative acceptor 3´splice sites (3´SS), alternative donor (AD), alternative donor 5´splice sites (5´SS), alternative promoter (AP), alternative terminator (AT), new intron (NI), retained exon (RE). P1 and P2 represent two possible promoters, and T1 and T2 represent two terminators. Abbreviations: mRNA, messenger RNA; pre-, precursor.

Through evolution, mammals, including humans and chimpanzees, have evolved to carry more than double the number of genes that can undergo AS compared to other metazoan species (Kim et al., 2018). This evolutionary advancement allows for greater diversity in gene expression and protein function, within these more complex organisms (Figure 8). The variability in AS patterns across species underscores how evolutionary adaptations have contributed to proteome complexity in more advanced organisms (Kim et

al., 2018; Su et al., 2023) (Figure 8a). In mammals and vertebrates, exon skipping is the predominant form of AS, whereas it is much less common in invertebrates (Figure 8b). Furthermore, in mammalian genomes, AS leads to the generation of new introns within existing exons and transforms previously annotated introns into exons, with alternative promoter and terminator events being less frequent. Transcripts generated through alternative promoter events contain multiple initiator exons.

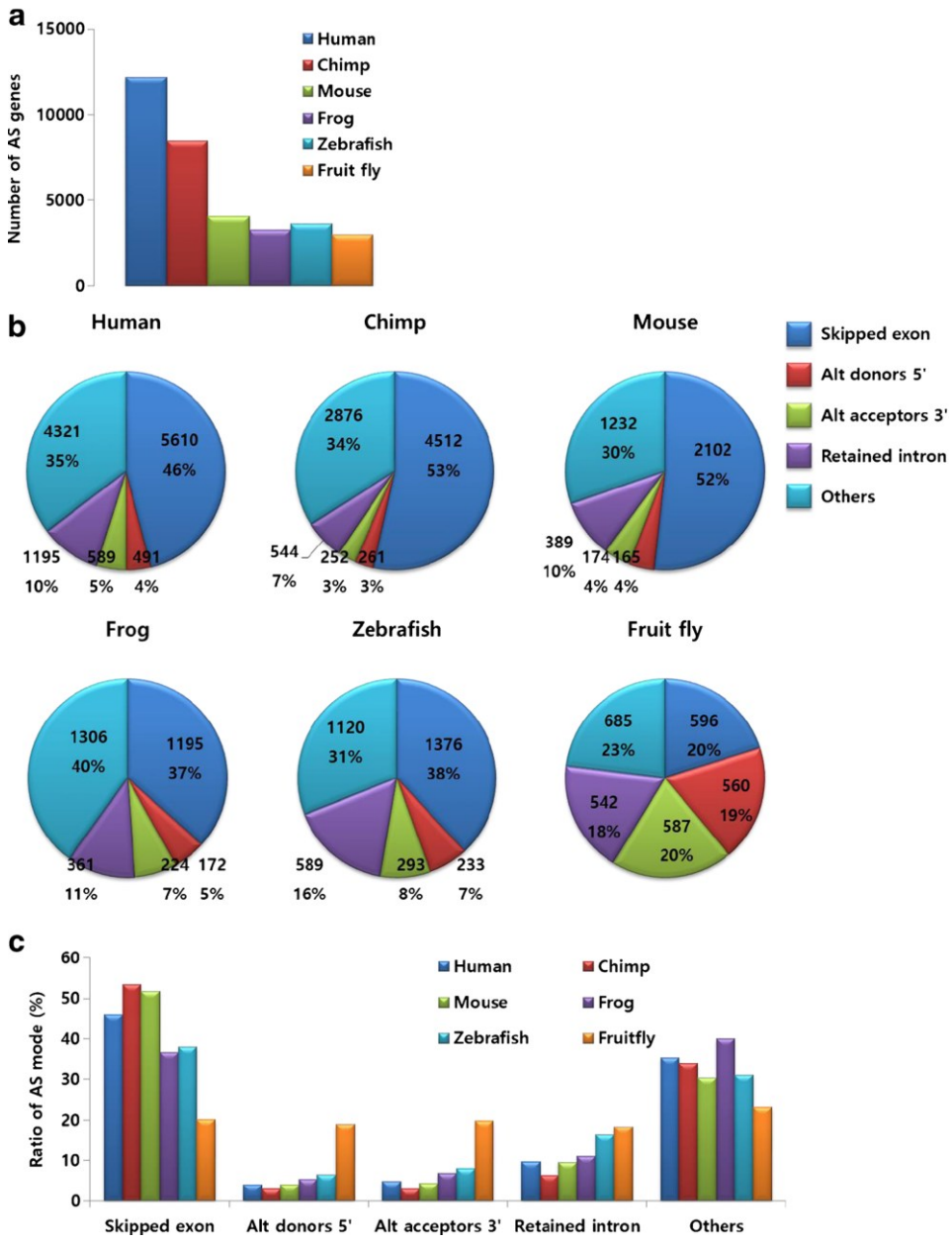

<u>Figure 8</u>: Prevalence of alternative splicing events (AS) and modes in six metazoans (Kim et al., 2018)

The total number of identified AS-modulated genes in the indicated species (a), the occurrence rate (% of all AS), and the number of genes for each AS mode (b), and a comparison of AS mode rates in six animals (c).

This distribution reflects the increased complexity and diversity of the human proteome despite the relatively limited genome size (Figure 8c). Studies report that AS regulates the activity and sensitivity of the transcripts related to pancreatic beta cell apoptosis, insulin synthesis or secretion, and insulin receptors in the context of glucose homeostasis. These findings highlight the significant role of AS in the development of insulin resistance and T2DM (Belfiore et al., 2017; Dlamini et al., 2017; Kim et al., 2018; Malakar et al., 2016).

1.6.2 Alternative splicing events in human and rodents

As presented in section 1.5.2, the two related RabGAP proteins, TBC1D1 and TBC1D4, are associated with obesity-related traits and T2DM in mice and humans (Mafakheri, Chadt, et al., 2018). Mutations in these RabGAPs can lead to substantial changes in the trafficking and subcellular distribution of the insulin-responsive GLUT4, disturbing energy substrate metabolism. A previous study of mouse 3T3L1 adipocytes identified alternatively spliced variants in genes associated with T2DM, which could alter the humoral autoreactivity or the expression of specific protein forms (Lui et al., 2021). For instance, the sortilin protein, which is involved in GLUT4 trafficking and glucose uptake in adipocytes, has an alternatively spliced variant that increases insulin resistance. This suggests that AS regulates gene expression related to T2DM and metabolic syndrome.

Further, a study in the Greenlandic population identified two splice variants of TBC1D4 protein, short and long, with the long isoform carrying a nonsense p.Arg684Ter variant. This variant, when present in homozygous carriers, affects TBC1D4 signaling in skeletal muscle but does not impact β-cells, liver, or adipose tissue (Moltke et al., 2014). Another study found a novel splice variant of TBC1D4 in rat muscle cells, which, compared to the full-length TBC1D4, lacks two specific segments (exons 11 and 12) and leads to new regulation of glucose transport, positively impacting glucose uptake in rates (Baus et al., 2008).

Unlike its related protein TBC1D4, TBC1D1 has not been extensively studied in the context of glucose homeostasis and T2DM. There is limited information about the mutations and AS of mRNA during the gene expression of *TBC1D1*. Cross-species genetic studies indicate that TBC1D1 is important for muscle and body mass development, highlighting its substantial function in muscle biology (Fontanesi et al., 2011; Fontanesi et al., 2012; Peng et al., 2015; Rubin et al., 2010; Wang et al., 2014). In humans, the R125W mutation in *TBC1D1* gene has been associated with obesity-related traits across various populations, as demonstrated by studies in different populations (Meyre et al., 2008; Stone et al., 2006; Volckmar et al., 2016).

Furthermore, a whole-exome sequencing study on male patients with congenital anomalies of the kidneys and the urinary tract has identified three heterozygous rare inherited missense variants in *TBC1D1*, predicted to be deleterious and potentially contributing to congenital anomalies of the kidneys and urinary tract (CAKUT) disease (Kosfeld et al., 2016). However, there is no evidence in the literature reporting AS events related to the TBC1D1 gene to date.

1.6.3 Investigating alternative splicing and its role in glucose homeostasis

Understanding the role of AS in diabetes raises many open questions, particularly regarding T1DM and T2DM (Chen & Manley, 2009; Dlamini et al., 2017; Pan et al., 2008; Wang et al., 2008). As described in section 1.6, AS significantly influences the regulation of genes involved in glucose metabolism and insulin signalling. Several studies have demonstrated a connection between diabetes and altered splicing patterns (Malakar et al., 2016; Norgren et al., 1994; Prokunina-Olsson et al., 2009; Savkur et al., 2004; Song & Richard, 2015). However, there is limited understanding of how specific splicing events contribute to the pathophysiology of diabetes.

In the context of β-cell function, splicing factors like *NOVA1* play a crucial role, yet the broader networks of splicing regulation and their impact on glucose homeostasis remain underexplored (Brahma et al., 2022; Wilhelmi et al., 2021). Moreover, AS affects glucose homeostasis by altering the expression of key insulin receptor isoforms, particularly IRA and IRB. The increased prevalence of IRA isoform in insulin-resistant tissues impairs glucose uptake and contributes to the development of insulin resistance. Furthermore, aberrant splicing of the GLUT4 gene (*SLC2A4*) exacerbates glucose metabolism issues, increasing the risk and severity of T2DM (Kim et al., 2018).

The discussion about using AS as a potential therapeutic target in diabetes is ongoing (Boucher et al., 2014; Qiao et al., 2021; Song & Richard, 2015). One promising feature will be using AS to modulate the expression of specific isoforms to enhance insulin sensitivity and glucose uptake, offering a novel approach to treat T2DM (Bennett et al., 2019; Bennett & Swayze, 2010; Roberts et al., 2020). Research is already oriented toward so-called antisense oligonucleotides (AONs) that correct for aberrant splicing events as promising strategies for restoring normal insulin signalling pathways in T2DM patients. However, further research is needed to effectively translate this new opportunity of using AS as a target for therapeutic interventions into clinical strategies (Baralle & Baralle, 2021; Kim et al., 2018).

1.7 Aim of the dissertation

Previous studies highlight the critical role of alternative splicing (AS) in various diseases, including cardiovascular, neurological, immunological, infectious diseases, and diabetes. They also mention the importance of AS in understanding the regulation of gene expression and its consequences in cellular trafficking processes for a wide range of health conditions (Belfiore et al., 2017; Dlamini et al., 2017; Kim et al., 2018; Makeyev et al., 2007; Malakar et al., 2016).

In the context of glucose homeostasis, skeletal muscle is a major site for both insulin- and exercise-induced glucose uptake. Rab GTPase proteins play a pivotal role in directing the subcellular localisation of GLUT4, the insulin-responsive glucose transporter in skeletal muscle. Key protein kinases, such as AKT2 and AMPK, along with their regulatory partners, such as the Rab substrates and the cytoplasmic tail of IRAP (cIRAP) associated with the cargo of GSVs, are involved in controlling these protein interactions and ensuring the correct glucose distribution within the cells.

In the development of T2DM, the Rab GTPase-activating protein (RabGAP) TBC1D1 has been associated with the regulation of metabolic flexibility within skeletal muscle tissue. Additionally, the dysfunction in TBC1D1's role is linked to insulin resistance and the progression of diabetes (Chadt et al., 2015; Corbeel & Freson, 2008; Hatakeyama & Kanzaki, 2013; Stockli et al., 2015). While the effects of genetic ablation or inhibition of TBC1D1 have been studied, the effects of AS events and the consequent impact on TBC1D1-mediated glucose homeostasis remain unexplored.

This dissertation is the first to investigate the RabGAP activity function of different *TBC1D1* splice variants detected in skeletal muscle and to elucidate how these splice variants of *TBC1D1* interact with their regulatory effectors, such as Rab substrates and cIRAP. Therefore, the dissertation aims to address the following research objectives:

I. Validate the presence of AS events of the *TBC1D1* gene in skeletal muscle

II. Investigate TBC1D1 isoforms' RabGAP activity and protein interactions with Rab substrates (Rab8A and Rab10) and cIRAP

III. Explore TBC1D1 isoforms' molecular function under phosphorylation events mediated by AKT2 and AMPK

This study focuses on understanding how the muscle-specific splice variants of *TBC1D1* RabGAP activity might influence the glucose uptake into cells, primarily facilitated by glucose transporter GLUT4 in muscle cells, thereby affecting glucose homeostasis.

This work investigates the functional outcomes of these splice variants and aims to uncover novel molecular mechanisms that regulate metabolic processes. This could lead to the development of targeted therapies tailored to address specific TBC1D1 splice profiles and their impact on cellular function.

A comprehensive approach was employed to achieve these objectives, combining comparative genomics, PCR-based strategies, and biochemical investigation using *ex vivo* models and cell-free systems. Furthermore, commercially available primary human skeletal muscle myoblast cells, as well as human muscle biopsies obtained from the *vastus lateralis* muscle, were selected for *in vitro* and *ex vivo* investigation of RabGAP function of TBC1D1 isoforms and the role of the isoforms dependent on AKT2 and AMPK stimulation. This approach ensures that the conclusions drawn from the datasets are based on accurate information, offering novel insights into the role of TBC1D1 splice variants in regulating glucose metabolism.

2. Material & Methods

2.1 Material

The kits, software, enzymes, instruments, chemicals, antibodies, buffers, solutions, *ex vivo* models and reagents listed in the following tables describe the material used in the context of the research conducted for this dissertation.

Table 2: Ex vivo models applied in this study

Denomination	Manufacturer
Escherichia coli (*E. coli*) strain DH5α	Thermo Fisher Scientific, Heiligen, Germany
Escherichia coli (*E. coli*) strain BL21	New England BioLabs, Frankfurt, Germany
Human Embryonic Kidney (HEK-293) cells	ATTC, Manassas, VA
Spodoptera frugiperda (SF9) cell (B82501)	Thermo Fisher Scientific, Heiligen, Germany
Human Skeletal Muscle Myoblast Cells (hMSCs)	Lonza, Basel, Switzerland
Muscle biopsies obtained from vastus lateralis muscle	Gift from Prof. Dr. med. Horst Harald Klein, Bochum University (Reference: Giebelstein J, Poschmann G, Højlund K, Schechinger W, Dietrich JW, Levin K, Beck-Nielsen H, Podwojski K, Stühler K, Meyer HE, Klein HH. The proteomic signature of insulin-resistant human skeletal muscle reveals increased glycolytic and decreased mitochondrial enzymes. Diabetologia. 2012 Apr;55(4):1114-27. doi: 10.1007/s00125-012-2456-x. Epub 2012 Jan 27.)
Muscle biopsies obtained from vastus lateralis muscle from the RNA Sequencing study	The biopsies were obtained after informed written consent and in accordance with the ethical standards of the Regional Committee for Medical and Health Research Ethics (REK) South East, Oslo, Norway (reference numbers: S-04133, S-09078d 2009/166, 2011/2207, and 2015/124) and REK North, Tromsø, Norway (reference number: 2011/882)

Table 3: Cell culture medium applied in this study

Compound	Manufacturer
Skeletal muscle cell basal medium 2 (SkBM-2)	© 2009 Lonza Rockland, Inc.
Sf9 Grace supplemented and serum-free (Sf-900TM II SFM) media	Life Technologies, Carlsbad, CA

Compound	Manufacturer
Advanced Dulbecco's Modified Eagle Medium (DMEM)/F12	Thermo Scientific, Waltham, MA, USA
Phosphate buffered saline (PBS) without Ca2+ Mg2+	Gibco, Carlsbad, California
Trypsin/Ethylenediaminetetraacetic acid (EDTA)	Thermo Scientific, Waltham, MA, USA
Fetal bovine serum (FBS)	Thermo Fisher, Waltham, MA, USA

Table 4: Software applied in this study

Software	Manufacturer
ImageLab Version 6.0.1	BioRad Laboratories, Hercules, USA
Nanodrop 2000/2000c software	Thermo Scientific, Peqlab, Wilmington, MA, USA
SnapGene Viewer 5.1.5	GSL Biotech LLC, San Diego, USA
GraphPad Prism 10	GraphPad Software, Inc, San Diego, CA, USA
Microplate Manager 6	BioRad Laboratories, Hercules; CA; USA
Thermo QuantStudio™ 7 Flex Real-Time PCR System	Applied Biosystems, Foster City, CA, USA

Table 5: Instruments applied in this study

Instrument	Manufacturer
ChemidocTM XRS+ System	BioRad Laboratories, Hercules, USA
Nanodrop2000	Thermo Scientific, Wilmington, USA
Centrifuge 5427 R	Eppendorf, Hamburg, Germany
Centrifuge 5810 R	Eppendorf, Hamburg, Germany
Centrifuge 5417 R	Eppendorf, Hamburg, Germany
Sorvall RC 5B Plus centrifuge	Thermo Scientific, Wilmington, USA
CH-4103 Incubator	INFORS AG, Bottmingen, Switzerland
Eporator	Eppendorf, Hamburg, Germany
BioPhotometer plus	Eppendorf, Hamburg, Germany
MagneSphere® Magnetic Separation Stands	Promega, Gutenbergring, Germany
Biometra Casting System Compact	Analytik Jena AG, Germany

Instrument	Manufacturer
Biometra Electrophoresis Power supply PS 304	Analytik Jena AG, Germany
Biometra Eco-Mini	Analytik Jena AG, Germany
iMark ™ Microplate Reader	Biorad laboratories, Munich, Germany
Thermomixer Compact	Eppendorf, Wesseling-Berzorf, Germany
TissueLyser II	Qiagen, Hilden Germany
Uniprep Gyrator	UniEquip, Munich, Germany

Table 6: Reaction kits applied in this study

Kits	Manufacturer
QIAprep Spin Miniprep Kit	Qiagen, Hilden, Germany
QIAGEN Plasmid Maxi Kit	Qiagen, Hilden, Germany
QIAGEN Plasmid *Plus* Maxi Kit	Qiagen, Hilden, Germany
QIAquick Gel Extraction Kit	Qiagen, Hilden, Germany
Pierce anti-DYKDDDDK Magnetic Agarose	Thermo Fisher Scientific, Wilmington, USA
Pierce Anti-HA Magnetic beads IP/Co-IP Kit	Thermo Fisher Scientific, Wilmington, USA
BCA Protein Assay Kit	Pierce, Rockford; IL, USA
GoTaq ®qPCR Master Mix	Promega, Madison WI, USA
RNeasy Mini Kit	Qiagen, Hilden, Germany
Western Lightning ECL Pro and Ultra	Perkin Elmer, Waltham, MA, USA

Table 7: Enzymes applied in this study

Enzyme	Manufacturer
S7 Fusion Polymerase	Mobidiag, Espoo, Finland
PstI	New England Biolabs, Ipswich, USA
BamHI-HF	New England Biolabs, Ipswich, USA
XhoI-HF	New England Biolabs, Ipswich, USA
SalI-HF	New England Biolabs, Ipswich, USA
NcoI-HF	New England Biolabs, Ipswich, USA

Table 8: Media used for E.coli cultivation

Medium	Ingredients
LB-Agar	10 g Peptone 5 g Yeast Extract 10 g NaCl 15 g Agar Ad 1000 ml H_2O
2xYT Medium, pH 7.4	16 g Tryptone 10 g Yeast Extract 5 g NaCl Ad 1000 ml H_20
SOC Medium	0.5 % Yeast extract 2 % tryptone 10 mM NaCl 2.5 mM KCl 10 mM $MgCl_2$ 10 mM $MgSO_4$ 20 mM Glucose

Table 9: Chemicals applied in this study

Chemical	Manufacturer
Acetic Acid	Carl Roth, Karlsruhe, Germany
Acrylamide (30%)	BioRad, Germany
Agar	Carl Roth, Karlsruhe, Germany
Agarose	AppliChem, Darmstadt, Germany
Ampicillin	Sigma-Aldrich, St. Louis, USA
Ammonium persulfate (APS)	MP Biomedicals, USA
Bromophenol blue	Marck, Darmstadt, Germany
BSA Fraction V	Sigma-Aldrich, St. Louis, USA
Chlorophorm	AppliChem, Darmstadt, Germany
Chloramphenicol	Carl Roth, Karlsruhe, Germany
Coomassie® Brillant Blue R-250	AppliChem, Darmstadt, Germany

Chemical	Manufacturer
Complete proteinase inhibitor	Roche Diagnostics, Mannheim, Germany
Desoxyribonucleotide triphosphate mix	Roche Diagnostics, Mannheim, Germany
Dithiothreitol (DTT)	Sigma Aldrich, Steinheim, Germany
Ethanol absolute	AppliChem, Darmstadt, Germany
Ethylene diamine tetraacetic acid (EDTA)	Serva, Heidelberg, Germany
Ethylene glycol tetraacetic acid (EGTA)	Serva, Heidelberg, Germany
Gamma-32P- triphosphate ([ɣ-^{32}P] GTP)	Hartmann Analytics, Braunschweig, Germany
Glutathione Sepharose™4 Fast Flow	GE Healthcare, USA
Glycerol	Aros Organics, USA
Hydrochloric acid (HCl)	Carl Roth, Karlsruhe, Germany
HDGreen Plus DNA Stain	INTAS Science Imaging Instruments, Göttingen, Germany
HEPES (H3375-500G)	Sigma-Aldrich, St. Louis, USA
Isopropanol	Carl Roth, Karlsruhe, Germany
Imidazole (56749-50G)	Sigma-Aldrich, St. Louis, USA
Liquid scintillation universal cocktail	Carl Roth, Karlsruhe, Germany
Lipofectamine2000	Thermo Scientific, Wilmington, USA
Mercaptoethanol	Merck, Germany
Methanol	Carl Roth, Karlsruhe, Germany
Ni-NTA Agarose	Qiagen, Germany
Peptone	Carl Roth, Karlsruhe, Germany
Phosphate Buffered Saline (PBS)	LifeTechnologies, USA
PhosSTOP Phosphatase inhibitor cocktail	Roche Diagnostics, Mannheim, Germany
Protease inhibitor cocktail tablets, EDTA-free	Roche Diagnostics, Germany
Saccharose (A2211)	PanReac Applichem, VWR, Germany
Sodium chloride (NaCl)	Carl Roth, Karlsruhe, Germany
Sodium dodecyl sulfate (SDS)	Applichem, Darmstadt, Germany
Skim milk powder	Carl Roth, Karlsruhe, Germany
Tryptone	Carl Roth, Karlsruhe, Germany
Yeast extract	Carl Roth, Karlsruhe, Germany
Tetramethylethylenediamine (TEMED)	Carl Roth, Karlsruhe, Germany
Tris-HCl	Applichem, Darmstadt, Germany

Chemical	Manufacturer
Triton X-100	MP Biomadicals, Solon, USA
Tween 20	MP Biomedicals, USA

Table 10: Plasmids applied in this study

Plasmid	Supplier	Application
pcDNA3.1-3xFLAG	Peiqing Liu /Genscript	Cloning vector
pcDNA3.1-HA	Peiqing Liu /Genscript	Cloning vector
pcDNA3.1-Myc	Peiqing Liu /Genscript	Cloning vector
pcDNA3.1-3xFLAG-TBC1D1-LONG	generated in this study	HA-TBC1D1-LONG protein
pcDNA3.1-HA-TBC1D1-LONG-GAPdel	generated in this study	HA-TBC1D1-LONG-GAPdel protein
pcDNA3.1-Myc-TBC1D1-SHORT	generated in this study	HA-TBC1D1-SHORT protein
pAcSG2—6xHis	Peiqing Liu /Genscript	Cloning vector
pAcSG2—6xHis – TBC1D1 – LONG	generated in this study	pAcSG2—6xHis – TBC1D1 – LONG protein
pAcSG2—6xHis – TBC1D1 – LONG-GAPdel	generated in this study	pAcSG2—6xHis – TBC1D1 – LONG-GAPdel protein
pAcSG2—6xHis – TBC1D1 – SHORT	generated in this study	pAcSG2—6xHis – TBC1D1 – SHORT protein
pEGFP-N1	Samaneh Eickelschulte	eGFP protein
pGEX-4T-1 plasmid parent	Peiqing Liu /Genscript	Cloning vector
pGEX-4T-1- mGST Rab10 & Rab8a	Samaneh Eickelschulte	GST- Rab10 & Rab8a fusion proteins
pGEX3x-GST-IRAP-cytosolic domain	Samaneh Eickelschulte	GST-cIRAP cytosolic domain protein
PGEX4T-1-hTBC1D1(GAP+C-214-K10)	generated in this study	GST-GAP domain truncated protein
PGEX4T-1-hTBC1D1(GAP+C-201-K2)	generated in this study	GST-GAP domain intact protein
pAcSG2—6xHis - hTBC1D1-X4-R947L (pACSG2-6xHis-hTBC1D1-RK)	generated in this study	6xHis-hTBC1D1-RK protein

Table 11: Primers applied in this study

Application/Primer		Sequence 5' - 3'
Cloning		
pcDNA3.1-3xFLAG-TBC1D1-LONG		
	Fwd	CAGGAACCTCCACAACCTG
	Fwd	CCTGCTACAAAGCTGAGACC
pcDNA3.1-HA-TBC1D1-GAP-VAR		
	Fwd	AGAGGCGTTTAAAATGCTCA
	Rev	ACCGCTCCAGTTCTAAGGT
pcDNA3.1-Myc-TBC1D1-Short		
	Fwd	CAGGAACCTCCACAACCTG
	Rev	TCTCCCAGCTCTGAATAATC
pcDNA3.1-hTBC1D1-GAP-214-K10-NcoI-SalI		
	Fwd 1	ATCCATGGTAGCCTCTGAAAATGATTTGCTG
	Fwd 2	ATCCATGGTAGCCTCTGAAAATGATTTGC
	Rev	AGCCCACGGGCGACTGAGTCGACAT
pcDNA3.1-hTBC1D1-GAP-201-K2-BamHI-SalI		
	Fwd	ATGGATCCATGCACTCGGCTGTTG
	Rev	GATTCTGCAGCATGAATGAGTCGACGT
pcDNA3.1		
	Fwd	TTCCAAGTCGTAACAAC
	Rev	ACAGTGGGAGTGGCACCTTC
pAcSG2		
	Fwd	GTTGCTGATATCATGGAG
	Rev	GGAAACTTCAAGGAGAATTTC
M13		
	Fwd	CAGGAAACAGCTATGAC
	Rev	GTAAAACGACGGCCAG

Application/Primer		Sequence 5' - 3'
Quantitative real-time PCR		
TBC1D1		
	Fwd	CTGTGAGAGGATAGAGGGAATGA
	Rev	TAGTCGCCTGCTCCTGATTG
TBC1D1-Short		
	Fwd	AGACGCCTCATGAACGAAAG
	Rev	CTCCCAGCTCTGAATAATCTTCA
TBC1D1-Long		
	Fwd	CCCAGGTCAGTCTTCAGCTC
	Rev	CGCAGGGCATTACGGTAGG
Desmin		
	Fwd	GAGAGGAGAGCCGGATCAATCT
	Rev	ACCTCAGAACCCCTTTGCTCAG
Myogenic factor 5(MYF5)		
	Fwd	CCACCTCCAACTGCTCTGAT
	Rev	GCAATCCAAGCTGGATAAGG
Myogenin factor (MYOG)		
	Fwd	ACCCTACAGATGCCCACAAC
	Rev	TGGTTTCATCTGGGAAGGCC
Myoblast determination protein 1 (MYOD)		
	Fwd	CGGCATGATGGACTACAGCG
	Rev	CAGGCAGTCTAGGCTCGAC
Myosin heavy chain 2 (MYH2)		
	Fwd	GAAAGTCTGAAAGGGAACGCA
	Rev	CGCCACAAAGACAGATGTTTTG
Beta-2-microglobulin (B2M)		
	Fwd	CTATCCAGCGTACTCCAAAG
	Rev	GAAAGACCAGTCCTTGCTGA

Application/Primer	Sequence 5' - 3'
Polymerase Chain Reaction (PCR)	
pcDNA3-3xFLAG-TBC1D1-LONG/ GAP-VAR / SHORT (exon 11 toward C-terminal domain)	
Fwd	AAACACCCTGAGTCACTTCC
Rev	CAAGGTTCTGTTTGCGTAAG
pcDNA3-3xFLAG-TBC1D1-LONG/ GAP-VAR / SHORT (full-length)	
Fwd	CTGTGAGAGGATAGAGGGAATGA
Rev	TAGTCGCCTGCTCCTGATTG
siRNA knockdowns of *TBC1D1*	
Custom TBC1D1 duplex 1 (CTM-523806)	GAACAGAGGUCAUAUUUAAUU
Custom TBC1D1 duplex 2 (CTM-523808)	GCUUUAAGUCUGUUGGGAAUU
Custom TBC1D1 duplex 3 (CTM-523809)	CGAGGUUGCUUCAUGAUUAUU
ON-TARGETplus non-targeting (D-001810-01-20)	
TaqMan probe of *TBC1D1-LONG-GAPdel*	
Accession no. NM_001253912.2 Padded context sequence from Thermo fisher amplicon size: ~ 78 pb	TGAGTGAGGAAGAGGCGTTTAAAATGCTCAAGTTTCTGATGTTTGACATG GGGCTGCGGAAACAGTATCGGCCAGACATGATTATTTTACAGATGGAAAA GACCATCAATCAGGTATTTGAAATGGACATCGCTAAACAGTTAC

<u>Table 12</u>: Reagents applied for PCR and qRT-PCR

PCR constituents	Amount
Template DNA / picked colony	100 ng / 20 ng
Forward Primer (100 nM)	25 pmol
Reverse Primer (100 nM)	25 pmol
DMSO (100%) *[1]	3 %
dNTP	200 µM
5x Fusion HF buffer	1x

PCR constituents	Amount
S7 Fusion DNA Polymerase	2 Units
Nuclease-free H_2O	Ad 50 µl

*[1] DMSO was only applied for colony PCR

Reaction mix for qRT-PCR

Constituents	Volume
2x GoTaq qPCR Master Mix	5 µl
Forward primer	0.5 µl
Reverse primer	0.5 µl
cDNA (1:40 dilution)	4 µl
Total	**10 µl**

Table 13: Buffers applied during this study

Buffer	Components
AMPK buffer	50 mM Tris, 10 mM $MgCl_2$, 0.5 mM DTT, 250 µM AMP (pH 7.4)
Wash buffer 1	150 mM NaCl, 1% IGEPAL CA-630, 0.5% sodium deoxycholate, 0.1% SDS, 50 mM Tris-HCl (pH 8.0)
Wash buffer 2	20 mM Tris HCl (pH 7.5)
Elution buffer	50 mM Tris HCl (pH 6.8), 50 mM DTT, 1 % SDS, 1mM EDTA, 0.005% bromophenol blue, 10% glycerol
Sf9 – wash buffer 1	50 mM HEPES, 50 mM Imidazole, 300 mM Na Cl, 1% (v/v) Triton X-100, pH 8
Sf9 – wash buffer 2	50 mM HEPES, 40 mM Imidazole, 300 mM Na Cl, 1% (v/v) Triton X-100, pH 8
Sf9 – lysis buffer	50 mM Hepes, pH8, 15 mM imidazole, o,25 M sucrose, 5 mM β-mercaptoethanol, EDTA-free protease inhibitor tablets, 0,5% (v/v) NP-40 or Triton-X100
Sf9 – elution buffer	80 mM imidazole,150 mMNaCl, EDTA-free protease inhibitor tablets, pH8
4x Laemmli sample buffer	20 % (w/v) Glycerol; 8 % (w/v) sodium dodecyl sulfate (SDS); 10 mM ethylenediaminetetraacetic acid (EDTA); 0.25 M Tris; 0,2 % (w/v) Bromophenol blue + 6% (w/v) DTT, pH 6.8

Buffer	Components
Protein lysis buffer	50 mM Tris-HCL, pH 8.0, 150 mM NaCl, 1 mM EDTA, 1 mM EGTA, 1 % Triton X-100, EDTA-free protease inhibitor tablets
Kinase buffer	2 mM adenosine 5´-triphosphate (ATP), 40 mMTris-HCl, pH7,4, 8 mM magnesium chloride (MgCl2), 200µM adenosine monophosphate (AMP) and 0.4 mM dithiothreitol (DTT)
RabGAP assay buffer	50 mM Tris-HCl, pH 8, 2.5 mM DTT and, 5 mM MgCl2
RabGAP assay elution	20 mM Tris-HCl, pH 7.5, 1 mM DTT, 10 mM reduced GSH, 2.5 mM MgCl2
GST lysis buffer	10 mM Tris, pH 8, 2.5 mM MgCl2, 5 mM beta-mercaptoethanol, 1 mM DTT and protease inhibitor mixture
GST wash buffer	500 µl of a buffer containing 50 mM Tris, pH 8, and 150 mM NaCl

Table 14: Chemicals applied for preparation of separation gels

Chemical	Separation gel (10%)	Separation gel (12%)
dH_2O	3.66 ml	3.06 ml
Separation buffer	2.34 ml	2.34 ml
Acrylamide	3 ml	3.6 ml
TEMED	18 µl	18 µl
APS	9 µl	9 µl

Table 15: Chemicals applied for preparation of stacking gels

Chemical	Stacking gel
dH_2O	1.83 ml
Stacking buffer	780 µl
Acrylamide	390 µl
Ammonium persulfate (APS)	6 µl
TEMED	3 µl

Table 16: Buffers applied for SDS-PAGE

Buffer	Components
10x Electrophoresis buffer	Tris 250 mM, Glycine 1.92 M, 1% SDS
1x Electrophoresis buffer	100 ml 10x Electrophoresis buffer, 900 ml dH_2O
Stacking buffer	1.5 M Tris, 0.4 % SDS, pH 8.8
Separation buffer	0.5 M Tris, 0.4 % SDS, pH 6.8

Table 17: Solutions applied for Coomassie staining

Solution	Components
Coomassie staining	0.25 g Coomassie® Brillant Blue R-250 in 100 ml Ethanol and 100 ml H_2O
Destaining solution 1	50 % ethanol, 10 % acetic acid
Destaining solution 2	10 % ethanol, 7% acetic acid

Table 18: Buffer applied for Western blotting

Buffer	Components
10x Transfer buffer	Tris 250 mM, 1.92 M
1x Transfer buffer	100 ml 10x Transfer buffer, 200 ml Methanol, 700 ml dH_2O
10x Washing buffer (TBS)	Tris 100 mM, NaCl 1.5 M
1x Washing buffer (TBS-T)	100 ml 10x Washing buffer, 900 ml dH_2O, 1 ml Tween 20
Blocking buffer	5 % (w/v) BSA in TBS-T

Table 19: List of primary antibodies applied in this study

Antibody	Species	Manufacturer
anti-DYKDDDDK (monoclonal)	Mouse	Sigma-Aldrich, St. Louis, USA
anti-GAPDH (monoclonal)	Rabbit	Cell Signaling Technology, Danvers, USA
anti-HA (monoclonal)	Rabbit	Cell Signaling Technology, Danvers, USA
anti-Myc (monoclonal)	Mouse	Sigma-Aldrich, St. Louis, USA
anti-Phospho-TBC1D1 (Ser237) (monoclonal)	Sheep	MRC-PPU, Dundee, UK
anti-Phospho-TBC1D1 (Ser507) (monoclonal)	Sheep	MRC-PPU, Dundee, UK
anti-Phospho-TBC1D1 (Ser667) (monoclonal)	Rabbit	Cell Signaling Technology, Danvers, USA
anti-Phospho-TBC1D1 (Ser700) (monoclonal)	Rabbit	Cell Signaling Technology, Danvers, USA
anti-Phospho-TBC1D1 (Thr596) (monoclonal)	Sheep	MRC-PPU, Dundee, UK
anti-TBC1D1 (monoclonal)	Rabbit	Bethyl Laboratories, Inc, Hamburg, Germany

Table 20: List of secondary antibodies applied in this study

Antibody	Manufacturer
Anti-Sheep IgG, HRP Conjugate	R&D Systems, Minneapolis, USA
Anti-Mouse IgG, HRP Conjugate	Promega, Madison, USA
Anti-Rabbit IgG, HRP Conjugate	Promega, Madison, USA

2.2 Methods

2.2.1 Microbiological methods

2.2.1.1 Cultivation of *Escherichia coli* (*E. coli*)

The *E. coli* strain DH5α as well as BL21 were cultured in a suspension culture using 2xYT (DYT) Medium containing 100 µg/ml Ampicillin (Roth) as selection marker and DYT medium containing 100 µg/ml Ampicillin and 50 µg/ml Chloramphenicol (Roth), respectively at 37°C and 180 rpm overnight (Table 8). Long-term storage of the transformed E. coli was created with 1 ml 80% glycerol mixed with 1 ml of the overnight bacterial culture using a 2 ml cryovial tube (Thermo Fisher Scientific, Heiligen, Germany) and was preserved at -80°C.

2.2.1.2 Transformation of competent *E. coli* cells

Electroporation was performed to transform the electrocompetent *E. coli* cells. The electroporation cuvette and desalted ligation product were pre-cooled on ice. The E. coli cells were thawed on ice and mixed with 7 µl desalted ligation product. The cells were transferred into the electroporation cuvette. The bacteria were electroporated by applying a voltage of 1700 V using the Eppendorf Eporator® (Eppendorf). The cells were immediately transferred into a 1 ml SOC medium, followed by 30 to 60 minutes of incubation at 37°C. Subsequently, the cells were plated on LB-Agar plates containing 100 µg/ml Ampicillin as a selection marker.

2.2.1.3 Cultivation of HEK293 cells

The Human Embryonic Kidney (HEK293) cells were cultivated in T75 flasks using Advanced Dulbecco's Modified Eagle Medium (DMEM)/F12 (Gibco) supplemented with 10% Fetal Bovine Serum (FBS), 1 % Penicillin/Streptomycin in the incubator at 37°C and 5% CO2. The cells were subcultured every 3-4 days to maintain the cell line. The cells were washed with phosphate-buffered saline (PBS) without Ca^{2+} and Mg^{2+}, then 0.05% Trypsin-EDTA was added, followed by 3 minutes of incubation at 37°C. A culture medium was added to stop the Trypsin action. The cells were diluted 1:5 with trypan blue and counted using an improved Neubauer chamber. The cells were centrifuged at 2000x g for 5 min. 0.5 – 1 $x10^6$ cells were seeded in a T75 cell culture flask for propagation.

2.2.1.4 Transfection of HEK293 cells

HEK293 cells at a density of 3x106 cells/ml in the T75 flask and $3.5x10^6$ cells/ml per well for 6-well plates were seeded for transfection and incubated overnight (O/N) at 37°C. The following day, the culture medium was replaced with serum-free Opti-MEM (Gibco). Then, 4 µg of DNA per well was used in 6-well plates, and 20 µg of DNA was used for T75 flasks for transfection. Then, 20 µg of each plasmid was used in the T75 flask for co-transfection. Lipofectamin 2000 transfection reagent (Invitrogen) was diluted in Opti-MEM medium and mixed with plasmid DNA at a rate of 1.3 µl Lipofectamin 2000 per µg plasmid DNA. The mixture was incubated for 20 minutes at room temperature to generate the DNA-Lipid complex required for transfection. Next, the DNA-Lipid mixture was added to the cells and incubated for 5 hours at 37°C. Next, the Opti-MEM medium was replaced by a culture medium. After two days of incubation at 37°C, cells were harvested by washing with ice-cold PBS and scraping with a cell scraper (Sarstedt), followed by centrifugation at 500x g for 5 minutes. The supernatant was discarded, and the cells were stored at -20°C for future use.

2.2.2 Molecular biology methods

2.2.2.1 Isolation of plasmid DNA from *E. coli*

The plasmid DNA had to be isolated from *E. coli* cells with high purity to verify the generated clones by sequencing. The QIAprep Spin Miniprep kit (Qiagen) was used following the manufacturer's protocol and using 4 ml of overnight *E. coli* culture.

To obtain a higher yield of plasmid DNA, a 150 ml overnight culture of the E. coli clone was used, and plasmid DNA was isolated using the QIAGEN Plasmid Maxi kit (Qiagen) or the QIAGEN Plasmid Plus Maxi kit (Qiagen) following the manufacturer's protocols.

2.2.2.2 Measurement of DNA concentration

The purity and the concentration of the plasmid DNA were assessed by Nanodrop200 (Thermo Fisher Scientific). The concentration was evaluated by measuring the optical density (OD) at a wavelength of 260 nm. The absorbance ratio at 260 nm/230 nm and 260 nm/280 nm were calculated to determine the sample purity.

2.2.2.3 Polymerase chain reaction (PCR)

PCR was applied to amplify any specific DNA fragment for cloning. Similarly, colony PCRs were used to screen several clones for the correct insert. The PCR was conducted using a T100 thermal cycler (Bio-Rad) following the conditions in Table 21.

Table 21: PCR for quantitative real-time PCR (qRT-PCR) conditions

Step	Temperature [°C]	Time
Initial denaturation	95	5 min
Denaturation	95	30 s
Annealing*[1]	55-65	30 s
Elongation*[2]	72	3 min
Final elongation	72	10 min

*[1] Annealing temperature was adjusted to the melting temperature of the respective primers

*[2] Elongation time was adjusted according to the fragment size of the PCR product

Program setup for qRT-PCR

Step	Temperature	Time	Cycles
Hot Start	95°C	2 min	1x
Denaturation	95°C	15 sec	40x
Primer annealing and extension	60°C	1 min	
Dissociation (Melting)	60-95°C	-	1x

2.2.2.4 Expansion & differentiation of human skeletal muscle myoblast cells

Human skeletal muscle myoblast cells (hMSCs) containing ≥ 750.000 cells/ml (Lonza Group Ltd, Basel, Switzerland) were cultivated at 37°C with 5% CO2 in Skeletal Muscle Cell Growth Medium (SKGM-2 – Lonza Group Ltd, Basel, Switzerland), supplemented with epidermal growth factor (EGF), corticosteroid as dexamethasone to support the mesenchymal stem cell (MSC) chondrogenesis, growth supplement as fetal bovine serum (FBS), amino acid supplement in L-glutamine, and antibacterial agent as gentamicin sulfate-amphotericin (GA). $2x10^5$ cells/well were seeded in 6-well plates, and at the confluence of 90-95%, differentiation was induced by switching to DMEM medium with 1 g/l glucose and 1% penicillin/streptomycin (Thermo Fisher Scientific), supplemented with 2% horse serum (HS). After six days, myotubes and myoblasts were harvested and lysed using RLT lysis buffer (QIAGEN, Hilden, Germany). Cell lysates were stored at -20°C until further use.

2.2.2.5 RNA extraction, cDNA synthesis & reverse transcription quantitative real-time PCR

Designing specific primers for reverse transcription quantitative real-time PCR (RT-qPCR) involves selecting sequences that anneal to our targets with high specificity, avoiding off-target amplification, and ensuring accurate quantification. Primer3 software with primer blast NCBI was used to design the primers. The total RNA extraction from hMSCs was converted into cDNA using reverse transcription, followed by the amplification of the target regions of the cDNA using real-time quantitative PCR to measure the amount of each splice variant.

Total RNA was extracted using the RNeasy Mini Kit (QIAGEN, Hilden, Germany). Per sample, according to the manufacturer's instructions, 1 µg of RNA was converted to cDNA using the GoScript™ Reverse Transcriptase system (Promega, Madison, WI, USA) and hexanucleotide primers (Roche). Primers were designed using the Primer3 software tool with the primer designing tool NCBI (Table 11).

Polymerase chain reaction (PCR) primers were used with the GoTaq® qPCR Master mix on a QuantStudio™ 7 Flex device (Applied Biosystems, Thermo Fisher Scientific, Waltham, Massachusetts) to measure mRNA expression. Gene expression analysis was performed using the $2^{-\Delta\Delta Ct}$ method and Beta-2-Microglobulin (*B2M)* as a reference gene (Livak & Schmittgen, 2001).

2.2.2.6 siRNA knockdown of *TBC1D1* splice variants in primary hMSCs

Four days differentiated hMSCs in 6 well plates were transfected with a smart pool of siRNA oligonucleotides using Dharmacon Custom duplex siRNA ON-TARGETplus (Horizon Inc. Canada) for TBC1D1 TOTAL (CTM-523806), TBC1D1 SHORT (CTM-523808), TBC1D1 LONG/GAP (CTM-523809) and randomised non-targeting siRNA control (D-001810-01-20). All siRNAs of 0.025 µM were re-suspended to a stock concentration of 100 µM in 1xsiRNA buffer. The stocks were diluted in serum-free and antibiotic-free DMEM to 50 nM. A 200 µl aliquot of Dharmafect transfection reagent was diluted in 200 µl of serum and antibiotic-free DMEM and incubated for 30 minutes at RT. The mixture was added to hMSCs with a final 25 nmol/ml concentration. The cells were differentiated for two more days in siRNA-containing media before being harvested and lysed using RLT lysis buffer (QIAGEN, Hilden, Germany).

2.2.2.7 Purification of DNA from agarose gels

After separating the DNA fragments by agarose gel electrophoresis, the specific PCR product or DNA fragment resulting from restriction digestion is extracted from the gel under UV light using a scalpel. The excised gene fragment is subsequently purified using the QIAquick gel extraction kit (QIAGEN, Hilden, Germany).

2.2.2.8 Restriction digestion

Restriction digestion was performed on adapted TBC1D1 fragment sequences from exon 18 to the C-terminal region by PCR to include the targeted restriction sites. The restriction enzymes used are listed in Table 6. The enzymatic reaction was performed at 37°C for 1 hour. Per µg of DNA, 20 to 40 units of each restriction enzyme were applied for double digestion. CutSmart® 10x buffer (New England Biolabs) was used according to the manufacturer's recommendations. The restriction enzymes were inactivated at 85°C for 20 minutes.

2.2.2.9 TaqMan assay & *TBC1D1-LONG-GAPdel* in primary human cells

The TaqMan assay is a real-time polymerase chain reaction (qPCR) subtype that uses a specific probe to quantify a target DNA sequence. The TaqMan probe is customised (Table 10 section 2.1) with dye FAM, a non-fluorescence quencher NFQ, and MGB moiety attached.

For quantitative PCR (qPCR) analyses, Thermo Fisher designs a double dye TaqMan probe to detect the target DNA LONG-GAPdel from the NCBI reference gene (NM_001253912.2) (see Table 11, section 2.1). The TaqMan probe spans the coding region of exon 18 toward the C-terminal area, framing the sequence from the nucleotide 3351 to 3494 nucleotide (Figure 9A). The expression vectors containing either TBC1D1-LONG or TBC1D1-LONG-GAPdel were used to generate a standard curve, assessing the accuracy of the LONG-GAPdel expression vector in expressing the target gene LONG-GAPdel with the designed TaqMan probe (Figure 9B). The TaqMan ™ Gene Expression Fusion Assays is designed to detect the fusion transcripts using real-time PCR. The reaction mix and the real-time PCR cycling conditions were prepared for a 10 µl reaction, as described in section 2.2.2.3. Serial dilutions of 30 times 1:2 were prepared and subjected to amplification by qPCR with the TaqMan probe (Table 11). The resulting cycle threshold (Ct) values were plotted against the log of the known quantities of the vector (copy numbers) to create a standard curve. The linear regression equation deriving from the standard curve equation helps determine the PCR efficiency of each expression vector and calculate the copy number of the LONG-GAPdel within the expression vector for the primary hMSCs and muscle biopsies.

2.2.2.10 Sequencing

DNA sequencing analysis was performed to confirm all the constructs using the Sanger sequencing approach outsourced to Eurofins Genomics (Eurofins Genomics, Ebersberg, Germany). For sequencing, 15 µl of plasmid DNA at a concentration of 50-100 ng/µl was mixed with 2 µl of sequencing primer (10 pmol/µl).

2.2.2.11 Generation of recombinant TBC1D1 isoforms from Sf9 cells

cDNA fragments of full-length of the three curated splice transcripts of *TBC1D1* (LONG 1262 amino acids, NP_001383888.1; GAP-VAR 1159 amino acids, NP_001240841.1; SHORT 1168 amino acids, NP_055988.2) were cloned into a His6-tagged pAcSG2 baculovirus expression vector (BD Bioscience, Heidelberg, Germany) to generate recombinant baculoviruses as previously described (Baer et al., 2005; Mafakheri, Florke, et al., 2018). For expression, Sf9 insect cells were grown to a density of $2x10^6$ cells/ml in 500 ml GRACEs Insect Medium (Life Technologies, Carlsbad, CA) in spinning flasks. Next, the cells were transfected with a multiplicity of infection (MOI) of 10 and were harvested 24 hours post-infection. Cells were lysed by mild sonication at 4 an °C in Sf9 lysis buffer and subsequently eluted using Sf9 elution buffer (Table 13). For the described procedure, only freshly prepared baculovirus vectors were used.

A

Homo sapiens TBC1 domain family member 1 (TBC1D1), transcript variant 2, mRNA

Query ID NM_001253912.2

Query Length 3480 nucleic acids

Subject Length 144 nucleic acids

Score	Expect	Identities	Gaps	Strand	Frame
267 bits(144)	2e-75	144/144(100%)	0/144(0%)	Plus/Plus	

```
Query  3351  TGAGTGAGGAAGAGGCGTTTAAAATGCTCAAGTTTCTGATGTTTGACATGGGGCTGCGGA  3410
             ||||||||||||||||||||||||||||||||||||||||||||||||||||||||||||
Sbjct  1     TGAGTGAGGAAGAGGCGTTTAAAATGCTCAAGTTTCTGATGTTTGACATGGGGCTGCGGA  60

Query  3411  AACAGTATCGGCCAGACATGATTATTTTACAGATGGAAAAGACCATCAATCAGGTATTTG  3470
              ||||||||||||||||||||||||||||||||||||||||||||||||||||||||||||
Sbjct  61    AACAGTATCGGCCAGACATGATTATTTTACAGATGGAAAAGACCATCAATCAGGTATTTG  120

Query  3471  AAATGGACATCGCTAAACAGTTAC  3494
              ||||||||||||||||||||||||
```

B

Expression vector	Plasmid size (bp)	Insert size (bp)	Starting amount (pg)[1]
pcDNA3.1-3xFLAG-TBC1D1-LONG	9311 bp	3788	6.114 x10^3
pcDNA3.1-HA-TBC1D1-LONG-GAPdel	8930 bp	3479	6.114 x10^3

[1]To ensure that the cycle threshold values (Ct) of the samples fall within the linear range of the standard curve for accurate quantification of the copy number of the LONG-GAPdel target sequence within the expression vector.

Figure 9: BLAST analysis of the padded sequence localization in LONG-GAPdel coding sequence (A) with the expression vectors of LONG and LONG-GAPdel (B)

2.2.3 Biochemical methods

2.2.3.1 SDS-PAGE & immunoblotting of the denatured protein

Proteins are separated by molecular weight using the Sodium dodecyl sulfate-polyacrylamide gel electrophoresis (SDS-PAGE) approach. The SDS detergent binds to the hydrophobic residues of the proteins and denatures them, leading to linearisation. The porous polyacrylamide matrix separates the proteins in proportion to their mass. N, N, N', N', N'-TEMED and APS are responsible for the cross-linking and polymerisation of the acrylamide and bis-acrylamide molecules forming the pores of the gel. The composition of the gels is listed in Tables 14-16.

Per sample, 20 µg proteins were separated by SDS-PAGE and subsequently transferred onto a polyvinylidene fluoride (PVDF) membrane. The membrane was incubated for 1 hour in blocking buffer at RT (Table 18) and then incubated with specific TBC1D1 and phospho-TBC1D1 antibodies (Table 19-20) overnight (O/N) at 4°C. Then, membranes were washed three times in 1x Tri-buffered saline with tween 20 (TBS-T), followed by incubation with secondary antibodies. The immunodetection was performed using the enhanced chemiluminescence (ECL) solution (Pro or Ultra; PerkinElmer, Hamburg, Germany). The signal detection was performed using the ChemiDoc XRS+ System (BioRad, Hercules, California).

2.2.3.2 Coomassie staining

This protein staining approach enables the visualisation of all proteins on a polyacrylamide gel after electrophoresis. This allows for the analysis of the quality and the quantity of the purified protein upon the intensity of the bands compared to a standard curve generated from proteins of known concentration to estimate the amount of protein in each lane (Table 17). After SDS-PAGE, the gel was transferred to Coomassie staining solution and incubated overnight with agitation. The next day, the Coomassie staining solution was replaced by destaining solution 1 for 1 hour under agitation, followed by 3 hours incubation in destaining solution 2. Finally, the gel was transferred to dH2O and incubated for 2 hours. Imaging was carried out using ChemiDoc XRS+ (BioRad).

2.2.3.3 Western blot analysis

Western blotting enables the transfer of proteins onto a membrane. Per sample, 20 µg of proteins were separated by SDS-PAGE, then transferred to a PVDF membrane by tank blot technology using horizontal electrophoresis. In detail, the gel and membrane are surrounded by Whatman paper and sponges, placed in a tank filled with cold transfer buffer (Table 18), and refrigerated using a water-cooling system. The blotting time was chosen according to the molecular weight of the protein of interest (from 2 hours to o/n blotting) at a constant current of 200 mA. After transfer, the membrane was incubated for 1 hour in blocking buffer at room temperature (Table 18), then incubated with the respective primary specific antibodies and phospho-antibodies (1:1000 diluted in blocking buffer) O/N at 4°C. The membranes were washed 3 times in 1xTBS-T followed by incubation with the respective secondary antibodies (1:5000 diluted in blocking buffer) for 30 minutes at RT. Then, the membrane was washed for 30 minutes with TBS-T. The immunodetection was performed using enhanced chemiluminescence solution (ECL) (Pro or Ultra; PerkinElmer, Hamburg, Germany). The signal detection was performed using the ChemiDoc XRS+ system (BioRad, Hercules, California).

2.2.3.4 Co/Immunoprecipitation & overexpression of TBC1D1 isoforms in HEK293 cells

Immunoprecipitation, as well as co-immunoprecipitation, were conducted to study the protein-protein interaction by using antibody-coated magnetic beads, which are incubated with the sample to be precipitated and then applied to a column placed in a magnetic field to precipitate one protein and, by association, pull-down other proteins bound to it. While non-bound proteins flow through the column, the magnetic beads with their bound proteins are held back inside the column and can be eluted afterwards. This leads to the purification of the specific protein and co-precipitation of the interaction partner of the protein.

LONG and GAP-VAR isoforms of TBC1D1, respectively, 1262 amino acids (NM_001396959.1) and 1159 amino acids (NM_001253912.2) were subcloned into mammalian expression vector pcDNA3.1 harbouring a 3xFLAG- and a HA-tag, respectively at the N-terminal region. The expression of the two protein isoforms was performed using HEK-293 cells. For the transfection, $3x10^6$ cells were seeded in T75 flasks overnight (Thermo Fischer Scientific, Heiligen, Germany). The next day, they were transfected either with 20 µg of pcDNA3.1-LONG-3xFLAG, 20 µg of pcDNA3.1-GAP-HA and, or co-transfected with 20 µg of both DNA constructs using Lipofectamine 2000 (Fischer Scientific, Heiligen, Germany).

The cells were harvested three days post-transfection and lysed in a protein lysis buffer (Table 13), followed by centrifugation of the clear lysate at 20,000 g for 10 min. The protein phosphorylation was carried out in kinase buffer containing 2 mM ATP, 40 mM Tris-HCl, pH 7.4, 8 mM MgCl2, 200 µM AMP, and 5 microunits purified AKT2/AMPK for 20 minutes at room temperature (RT). Magnetic beads pre-conjugated with anti-HA monoclonal antibodies (MACS HA-beads, Miltenyi Biotec GmbH, Bergisch Gladbach, Germany), as well as anti-DYKDDDDK monoclonal antibodies (Fischer Scientific, Heiligen, Germany) were used according to the manufacturer's instructions.

Antibody-coupled beads were mixed with protein lysate and incubated for 30 minutes at RT. Subsequently, the beads were washed (50 mM Tris, pH 8, and 150 mM NaCl). The protein complexes formed were eluted using 4xLaemmli sample buffer, then denatured at 95°C for 5 min, and analysed by SDS-PAGE, followed by immunoblotting using antibodies that bind specifically to the protein isoforms (Table 19-20).

2.2.3.5 Protein purification from *E. coli* BL21 cells

Bacterial cells lysis

The bacterial pellet was resuspended in cooled lysis buffer (PBS, 1 M DTT, 200 mM MgCl2, EDTA-free protease inhibitor, pH 7.5). The cells were sonicated three times for 10 seconds using the HD2070 ultrasound. The bacterial lysate was centrifuged for 30 minutes at 3200 x g and 4°C. The supernatant was collected and frozen at -20°C until further use.

Purification of the GST-tagged proteins using Glutathione Sepharose beads

Glutathione Sepharose beads were used to purify GST-tagged proteins. The lysate was centrifuged 20000xg for 10 minutes at 4°C. The glutathione Sepharose 4 Fast Flow beads were transferred to a filtration column (MoBiTec) and rinsed with a column volume of dH2O. The cleared supernatant was mixed with the Glutathione Sepharose beads and moved to a 15 ml falcon tube. The mixture was incubated for 2 hours at 4°C with gentle agitation, allowing the beads to bind to the GST-tagged protein. Then, the mixture was transferred to a column, and the flow was collected for analysis. The column was washed 3x times with Wash Buffer 1 (50 mM Tris-HCl, 2.5 mM DTT, 2.5 mM EDTA (pH 7.5)) and 1 time with Wash Buffer 2 (50 mM Tris-HCl, 2.5 mM DTT, 5 mM MgCl2 (pH 7.5)), the wash flow was collected as well for analysis. The GST-tagged protein was eluted in 500 µl elution buffer (containing 10 mM reduced glutathione, Tris-HCl pH 8.0). SDS-PAGE was performed to determine the purified protein's concentration, followed by Coomassie staining.

Purification of the His-tagged proteins using Ni-NTA agarose beads

The cleared lysate was mixed with 1000 µl of Ni-NTA agarose beads and incubated for 1 hour with gentle rocking at 4°C. After that, the suspension was loaded to the gravity column and subsequently washed 4x times with wash buffer (50 mM HEPES, 30 mM imidazole, 300 mM NaCl) and eluted with 3x250 µl of elution buffer (50 mM HEPES, 150 mM imidazole, EDTA free protease inhibitor). To determine the protein concentration of the purified His-Tagged protein, SDS-PAGE was performed, followed by Coomassie staining.

2.2.3.6 SF9 cells expansion & protein expression

In a shaker incubator, SF9 cells were maintained in Sf-900TM II SFM medium supplemented with 50 ml of FBS at 27°C in a spinner flask. To keep the cells in an exponential growth phase, they were propagated every 2-3 days at a cell density between $1x10^6$ and $2x10^6$ cells/ml.

To increase the virus stock (P0) provided by Dr Adam Chambers (Oxford Expression Technologies, Ltd, Oxford, United Kingdom), 25 ml of SF9 cells were infected, and the virus was harvested seven days post-infection. The supernatant containing the virus was clarified by centrifugation 1000xg 3 minutes and stored at 4°C protected from light.

For the protein expression, SF9 cells at a density of $2.5x10^6$ cells/ml were seeded in fresh culture medium at the MOI of 10 at 27°C. 24 hours post-infection, the cells were harvested by centrifugation at 1000xg for 5 minutes, the supernatant was discarded, and the pellet was stored at -80°C for further use. Subsequently, the pellet was resuspended in lysis buffer (Table 13) for a sonication three times for 10 seconds, and the protein was purified as described above.

2.2.3.7 Kinase-dependent phosphorylation kinetics

To induce phosphorylation, the Sf9 cell-derived recombinant human constitutively active AKT2 protein (Baer et al., 2005) and commercially available recombinant human trimeric AMPK ("α1/β1/γ1" from Thermo Fischer Scientific, Carlsbad, CA, USA) protein were separately mixed with different concentrations of recombinant full-length TBC1D1 LONG, and TBC1D1 GAP-VAR protein (range 0.25 µg to 4 µg), and kinase buffer (4 pmol AKT2 or AMPK, 2 mM adenosine 5´-triphosphate (ATP) solution, 40 mM Tris-HCl, pH7.4, 8 mM magnesium chloride ($MgCl_2$), 200 µM AMP and, 0.4 mM dithiothreitol (DTT)) in a total volume of 300 µl, and incubated for 5 minutes. Subsequently, the phosphorylation reaction was quenched by adding 4xLaemmli buffer (Table 13). The magnitude of variant-specific AKT2 and AMPK phosphorylation was confirmed by immunoblotting using phosphosite-specific antibodies in combination with ECL (PerkinElmer, Hamburg, Germany). The raw phosphosite-specific kinase activity of AKT2 and AMPK was fitted with a nonlinear Michaelis-Menten kinetics model using GraphPad Prism Software.

2.2.3.8 *In vitro* RabGAP activity assay

RabGAPs function is catalysing the GTP hydrolysis. LONG and GAP-VAR isoform GTP hydrolysis functions were explored. GST-Rab10 and GST-Rab8a fusion proteins were prepared as previously described (Mafakheri, Florke, et al., 2018; Zhou et al., 2017). Briefly, GST-Rab8a were expressed in *E. coli* BL21-CodonPlus (DE3)-RIL, and GST-Rab10 was expressed using the baculovirus system and purified as described (Mafakheri, Florke, et al., 2018; Zhou et al., 2017). Both substrates were lysed using ultrasound, and fusion proteins were bound to GSH-Sepharose columns and loaded with [ɣ-^{32}P] GTP (Hartmann Analytics, Braunschweig, Germany) in RabGAP assay buffer (Table 13).

The matrix was rinsed with the RabGAP assay buffer to remove unbound GTP, and [ɣ-^{32}P] GTP-bound substrates were eluted in the RabGAP assay elution buffer (Table 13). Then, GST-bound Rab GTPases were incubated at room temperature for 30 minutes with either isolated full-length TBC1D1 splice protein, the inactive TBC1D1-R854K mutant or the cloned GAP domain fraction located at the N-terminal region, respectively. The reaction was stopped by adding 0.2 M EDTA and activated charcoal suspension to separate [^{32}P] phosphate through filtration. Finally, we measured the GTP hydrolysis activity by scintillation counting (Zhou et al., 2017). The amount of [^{32}P] phosphate produced was normalised to the amount of radioactivity of [ɣ-^{32}P] GTP-bound Rab proteins.

2.2.3.9 Interaction of TBC1D1 with cytosolic domain of IRAP

The 110 amino acids-long cytosolic C-terminal tail of IRAP was fused to GST to yield a GST-cIRAP fusion protein (PMID: 30275018). Next, GST-cIRAP was expressed in *E.coli* BL21-CodonPlus (DE3)-RIL and lysed in GST pulldown lysis buffer (Table 13) using sonication. The isolated GST-cIRAP fusion protein was centrifuged at 20000 x g for 20 minutes at 4°C. At gentle rotary agitation, 2 ml of GST-cIRAP lysate was incubated with 250 µl of GSH Sepharose beads (Amersham, GE Healthcare, Sweden) for 2 hours at 4°C. As a negative control, the same amount of the beads were incubated with GST alone. Following incubation, GST-cIRAP-bound beads were washed 3x times with 500 µl GST pulldown wash buffer (Table 13). The GST-cIRAP-bound beads were incubated with 1 pmol of non-phosphorylated or previously phosphorylated (AKT2 or AMPK) TBC1D1 LONG or TBC1D1 GAP-VAR proteins for 30 minutes at RT. The GST-cIRAP-TBC1D1-bound beads were washed two times with the wash buffer, and then the GST-cIRAP-TBC1D1-bound complex was eluted with 4xLaemmeli sample buffer (Table 13). The eluted fractions were analysed using the SDS-PAGE approach and immunoblotting with TBC1D1 and phospho-TBC1D1 antibodies (Table 19-20).

2.2.3.10 Bioinformatic tools & statistical analysis

Coomassie-stained polyacrylamide gels, agarose gels and Western blotting imaging were performed using ImageLab Version 6.0.1 software (BioRad).

Sequencing results were analysed using SnapGene Viewer Version 5.1.5 (GSL Biotech LLC) and the Clustal Omega alignment tool (EMBL-EBI).

The results of this study are presented with three biological replicates and are provided as mean ± Standard Error of the Mean (SEM) unless indicated in the figures otherwise. Statistical differences between experimental groups were calculated with GraphPad Prism software 10 (GraphPad Software, Inc., La Jolla, CA). A p-value < 0.05 was considered statistically significant. Individually applied statistics are depicted in the figure description.

3. Results

3.1 RNA-Seq enables identification of transcript splice variants of *TBC1D1*

Unpublished data from the Pathobiochemistry Group, led by Prof. Hadi Al-Hasani at the Deutsche Diabetes Zentrum (DDZ) in Düsseldorf, in collaboration with Prof. Hege Thoresen at the University of Oslo, have confirmed the expression of the LONG-GAPdel variant in healthy human skeletal muscle (Figure 10). This study collected RNA samples from cells isolated from the vastus lateralis muscle of three healthy young male donors. The RNA was then subjected to Illumina RNA sequencing for a comprehensive gene expression profile. This sequencing approach consists of converting RNA into complementary DNA (cDNA), followed by sequencing to analyse the complete set of transcripts of each donor. This RNA-Seq analysis enabled the detection and quantification of the expression levels of various genes and their isoforms, encompassing the *TBC1D1* gene. Notably, the sequencing identified three distinct transcript splice variants of the gene, which exhibited moderate expression levels ranging from 1 to 5 Transcripts per Million (TPM), suggesting differential regulation of TBC1D1 isoforms in human skeletal muscle. These findings are significant as they provide insights into the potential functional diversity of TBC1D1, which may have implications for understanding its role in muscle function and metabolic processes.

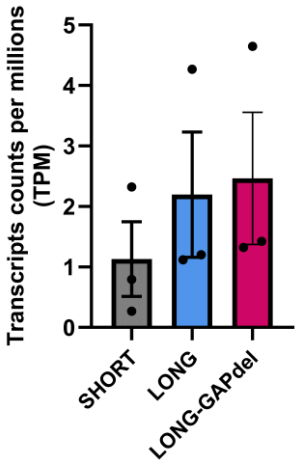

Figure 10: RNA-Seq Analysis reveals transcript counts of the three splice variants of *TBC1D1* in muscle biopsies

RNAs were collected from cells isolated from the vastus lateralis of three healthy young male donors under basal conditions for RNA sequencing using Illumina RNA sequencing. Kallisto is used to rationalise the analysis and visualise the RNA-Seq outcome. *TBC1D1* splice transcripts showed expression values within 1 to 5 TPM. ENST00000261439.9, ENST00000698857.1, and ENST00000508802.5 are referred to as SHORT, LONG, and LONG-GAPdel, respectively.

The consistent presence of these three specific *TBC1D1* transcripts, ENST00000261439.9, ENST00000698857.1, and ENST00000508802.5, which this study referrs to as, respectively, *TBC1D1-SHORT*, *TBC1D1-LONG*, and *TBC1D1-LONG-GAPdel* (Table 22), suggests their potential involvement in TBC1D1-associated biological processes such as the intracellular GLUT4 retention and GLUT4 traffic within skeletal muscle cells. These transcripts interact by regulating the activation state of the downstream Rab GTPases.

Among the three transcript variants, *TBC1D1-SHORT* and *TBC1D1-LONG* have been previously characterised, with analyses of their structural domains confirming their specific expression profiles across tissue types. *TBC1D1-SHORT* is predominantly expressed in non-muscular tissues, while *TBC1D1-LONG* shows a preference for expression in muscular tissues, as validated in murine *Tbc1d1* gene studies (Chadt et al., 2008).

The third variant, ENST00000508802.5, also named in this study *TBC1D1-LONG-GAPdel,* exhibits a close structural similarity to *TBC1D1-LONG* but reveals missing amino acids in the catalytic RabGAP domain. While the functional significance of this deletion is not fully understood, its expression in human skeletal muscle and its resemblance to TBC1D1-LONG open new avenues for investigating its role in RabGAP activity and, by extension, its regulatory role in energy metabolism in muscle tissue.

Table 22: Reference identifier of *TBC1D1* compiled and catalogued splice variants

Ensembl	NCBI	This study
ENST00000261439.9	NM_015173.4	*SHORT*
ENST00000698857.1	NM_001396959.1	*LONG*
ENST00000508802.5	NM_001253912.2	*LONG-GAPdel*

3.1.1 AS-driven nucleic acid structures in *TBC1D1* transcript variants

TBC1D1 splice variants were examined using amino acid alignments to address the conservation of the different domain structures (Figure 11). All three splice variants, SHORT, LONG, and LONG-GAPdel, depicted the two amino-terminal PTB domains. The first PTB domain is between amino acids 16 to 164, while the second PTB extends from 168 to 384. Across all three splice variants, the two PTB domains are conserved. The catalytic RabGAP domain structure is conserved between SHORT and LONG splice variants, spanning the amino acids 809 to 1247.

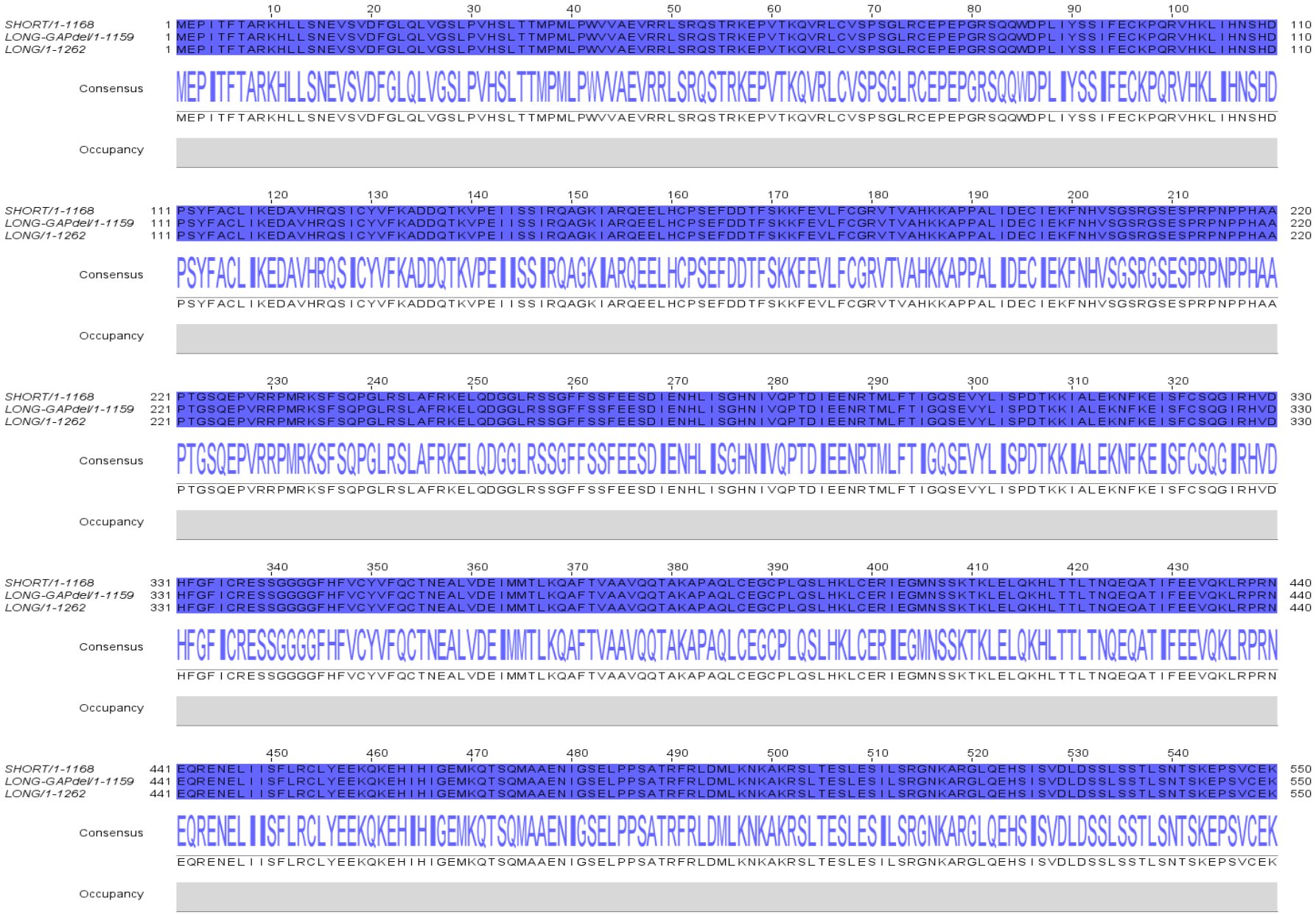
10 20 30 40 50 60 70 80 90 100
SHORT/1-1168 1 MEPITFTARKHLLSNEVSVDFGLQLVGSLPVHSLTTMPMLPWVVAEVRRLSRQSTRKEPVTKQVRLCVSPSGLRCEPEPGRSQQWDPLIYSSIFECKPQRVHKLIHNSHD 110
LONG-GAPdel/1-1159 1 MEPITFTARKHLLSNEVSVDFGLQLVGSLPVHSLTTMPMLPWVVAEVRRLSRQSTRKEPVTKQVRLCVSPSGLRCEPEPGRSQQWDPLIYSSIFECKPQRVHKLIHNSHD 110
LONG/1-1262 1 MEPITFTARKHLLSNEVSVDFGLQLVGSLPVHSLTTMPMLPWVVAEVRRLSRQSTRKEPVTKQVRLCVSPSGLRCEPEPGRSQQWDPLIYSSIFECKPQRVHKLIHNSHD 110
Consensus
Occupancy
120 130 140 150 160 170 180 190 200 210
SHORT/1-1168 111 PSYFACLIKEDAVHRQSICYVFKADDQTKVPEIISSIRQAGKIARQEELHCPSEFDDTFSKKFEVLFCGRVTVAHKKAPPALIDECIEKFNHVSGSRGSESPRPNPPHAA 220
LONG-GAPdel/1-1159 111 PSYFACLIKEDAVHRQSICYVFKADDQTKVPEIISSIRQAGKIARQEELHCPSEFDDTFSKKFEVLFCGRVTVAHKKAPPALIDECIEKFNHVSGSRGSESPRPNPPHAA 220
LONG/1-1262 111 PSYFACLIKEDAVHRQSICYVFKADDQTKVPEIISSIRQAGKIARQEELHCPSEFDDTFSKKFEVLFCGRVTVAHKKAPPALIDECIEKFNHVSGSRGSESPRPNPPHAA 220
Consensus
Occupancy
230 240 250 260 270 280 290 300 310 320
SHORT/1-1168 221 PTGSQEPVRRPMRKSFSQPGLRSLAFRKELQDGGLRSSGFFSSFEESDIENHLISGHNIVQPTDIEENRTMLFTIGQSEVYLISPDTKKIALEKNFKEISFCSQGIRHVD 330
LONG-GAPdel/1-1159 221 PTGSQEPVRRPMRKSFSQPGLRSLAFRKELQDGGLRSSGFFSSFEESDIENHLISGHNIVQPTDIEENRTMLFTIGQSEVYLISPDTKKIALEKNFKEISFCSQGIRHVD 330
LONG/1-1262 221 PTGSQEPVRRPMRKSFSQPGLRSLAFRKELQDGGLRSSGFFSSFEESDIENHLISGHNIVQPTDIEENRTMLFTIGQSEVYLISPDTKKIALEKNFKEISFCSQGIRHVD 330
Consensus
Occupancy
340 350 360 370 380 390 400 410 420 430
SHORT/1-1168 331 HFGFICRESSGGGGFHFVCYVFQCTNEALVDEIMMTLKQAFTVAAVQQTAKAPAQLCEGCPLQSLHKLCERIEGMNSSKTKLELQKHLTTLTNQEQATIFEEVQKLRPRN 440
LONG-GAPdel/1-1159 331 HFGFICRESSGGGGFHFVCYVFQCTNEALVDEIMMTLKQAFTVAAVQQTAKAPAQLCEGCPLQSLHKLCERIEGMNSSKTKLELQKHLTTLTNQEQATIFEEVQKLRPRN 440
LONG/1-1262 331 HFGFICRESSGGGGFHFVCYVFQCTNEALVDEIMMTLKQAFTVAAVQQTAKAPAQLCEGCPLQSLHKLCERIEGMNSSKTKLELQKHLTTLTNQEQATIFEEVQKLRPRN 440
Consensus
Occupancy
450 460 470 480 490 500 510 520 530 540
SHORT/1-1168 441 EQRENELIISFLRCLYEEKQKEHIHIGEMKQTSQMAAENIGSELPPSATRFRLDMLKNKAKRSLTESLESILSRGNKARGLQEHSISVDLDSSLSSTLSNTSKEPSVCEK 550
LONG-GAPdel/1-1159 441 EQRENELIISFLRCLYEEKQKEHIHIGEMKQTSQMAAENIGSELPPSATRFRLDMLKNKAKRSLTESLESILSRGNKARGLQEHSISVDLDSSLSSTLSNTSKEPSVCEK 550
LONG/1-1262 441 EQRENELIISFLRCLYEEKQKEHIHIGEMKQTSQMAAENIGSELPPSATRFRLDMLKNKAKRSLTESLESILSRGNKARGLQEHSISVDLDSSLSSTLSNTSKEPSVCEK 550
Consensus
Occupancy

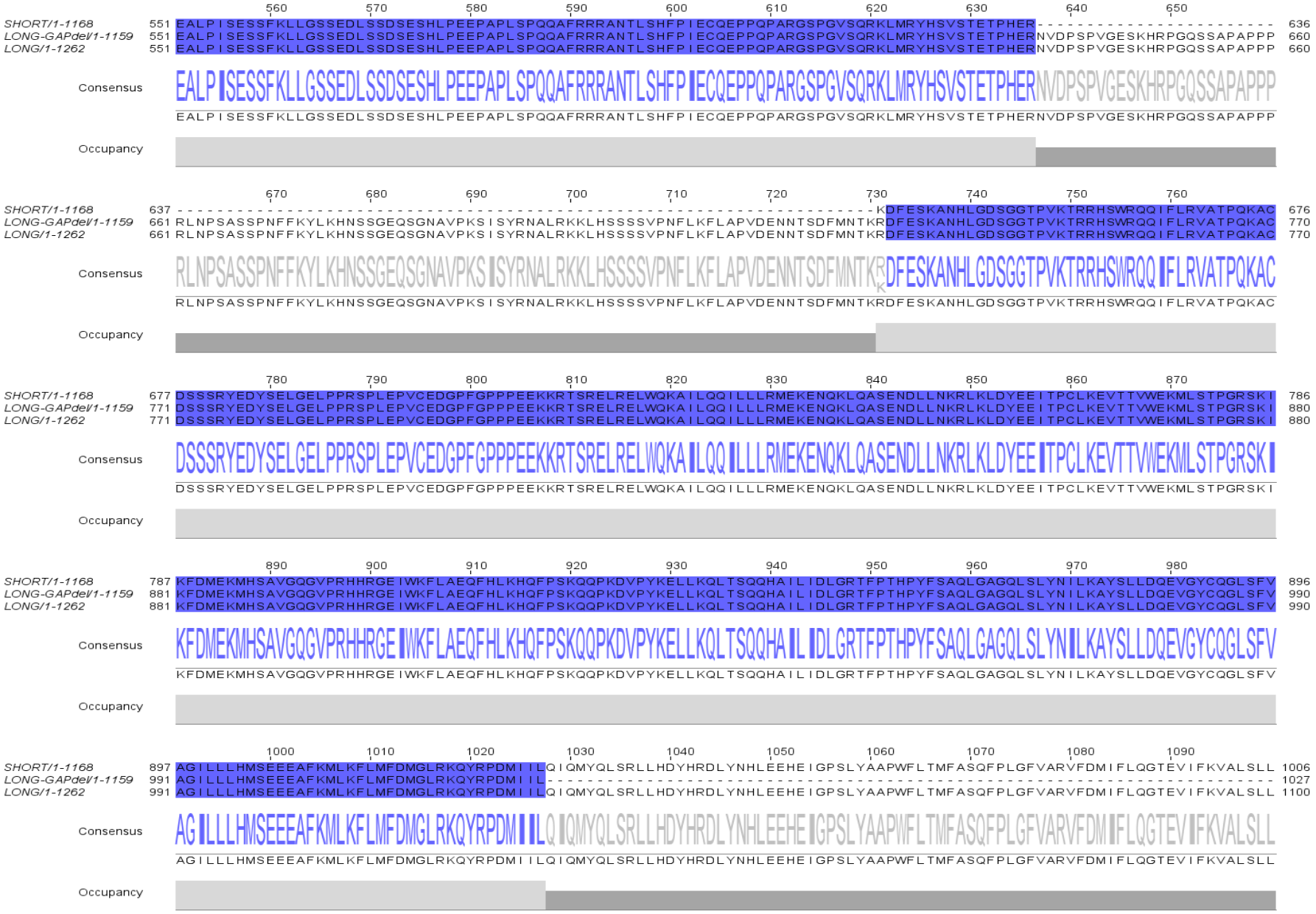
560 570 580 590 600 610 620 630 640 650
SHORT/1-1168 551 EALPISESSFKLLGSSEDLSSDSESHLPEEPAPLSPQQAFRRRANTLSHFPIECQEPPQPARGSPGVSQRKLMRYHSVSTETPHER 636
LONG-GAPdel/1-1159 551 EALPISESSFKLLGSSEDLSSDSESHLPEEPAPLSPQQAFRRRANTLSHFPIECQEPPQPARGSPGVSQRKLMRYHSVSTETPHERNVDPSPVGESKHRPGQSSAPAPPP 660
LONG/1-1262 551 EALPISESSFKLLGSSEDLSSDSESHLPEEPAPLSPQQAFRRRANTLSHFPIECQEPPQPARGSPGVSQRKLMRYHSVSTETPHERNVDPSPVGESKHRPGQSSAPAPPP 660
Consensus
Occupancy
670 680 690 700 710 720 730 740 750 760
SHORT/1-1168 637 KDFESKANHLGDSGGTPVKTRRHSWRQQIFLRVATPQKAC 676
LONG-GAPdel/1-1159 661 RLNPSASSPNFFKYLKHNSSGEQSGNAVPKSISYRNALRKKLHSSSSVPNFLKFLAPVDENNTSDFMNTKRDFESKANHLGDSGGTPVKTRRHSWRQQIFLRVATPQKAC 770
LONG/1-1262 661 RLNPSASSPNFFKYLKHNSSGEQSGNAVPKSISYRNALRKKLHSSSSVPNFLKFLAPVDENNTSDFMNTKRDFESKANHLGDSGGTPVKTRRHSWRQQIFLRVATPQKAC 770
Consensus
Occupancy
780 790 800 810 820 830 840 850 860 870
SHORT/1-1168 677 DSSSRYEDYSELGELPPRSPLEPVCEDGPFGPPPEEKKRTSRELRELWQKAILQQILLLRMEKENQKLQASENDLLNKRLKLDYEEITPCLKEVTTVWEKMLSTPGRSKI 786
LONG-GAPdel/1-1159 771 DSSSRYEDYSELGELPPRSPLEPVCEDGPFGPPPEEKKRTSRELRELWQKAILQQILLLRMEKENQKLQASENDLLNKRLKLDYEEITPCLKEVTTVWEKMLSTPGRSKI 880
LONG/1-1262 771 DSSSRYEDYSELGELPPRSPLEPVCEDGPFGPPPEEKKRTSRELRELWQKAILQQILLLRMEKENQKLQASENDLLNKRLKLDYEEITPCLKEVTTVWEKMLSTPGRSKI 880
Consensus
Occupancy
890 900 910 920 930 940 950 960 970 980
SHORT/1-1168 787 KFDMEKMHSAVGQGVPRHHRGEIWKFLAEQFHLKHQFPSKQQPKDVPYKELLKQLTSQQHAILIDLGRTFPTHPYFSAQLGAGQLSLYNILKAYSLLDQEVGYCQGLSFV 896
LONG-GAPdel/1-1159 881 KFDMEKMHSAVGQGVPRHHRGEIWKFLAEQFHLKHQFPSKQQPKDVPYKELLKQLTSQQHAILIDLGRTFPTHPYFSAQLGAGQLSLYNILKAYSLLDQEVGYCQGLSFV 990
LONG/1-1262 881 KFDMEKMHSAVGQGVPRHHRGEIWKFLAEQFHLKHQFPSKQQPKDVPYKELLKQLTSQQHAILIDLGRTFPTHPYFSAQLGAGQLSLYNILKAYSLLDQEVGYCQGLSFV 990
Consensus
Occupancy
1000 1010 1020 1030 1040 1050 1060 1070 1080 1090
SHORT/1-1168 897 AGILLLHMSEEEAFKMLKFLMFDMGLRKQYRPDMIILQIQMYQLSRLLHDYHRDLYNHLEEHEIGPSLYAAPWFLTMFASQFPLGFVARVFDMIFLQGTEVIFKVALSLL 1006
LONG-GAPdel/1-1159 991 AGILLLHMSEEEAFKMLKFLMFDMGLRKQYRPDMIIL 1027
LONG/1-1262 991 AGILLLHMSEEEAFKMLKFLMFDMGLRKQYRPDMIILQIQMYQLSRLLHDYHRDLYNHLEEHEIGPSLYAAPWFLTMFASQFPLGFVARVFDMIFLQGTEVIFKVALSLL 1100
Consensus
Occupancy

Figure 11: TBC1D1 splice variants conserved motifs and variability

Multiple sequence alignment of the full-length splice variants of TBC1D1 using the T-Coffee web server (Di Tommaso et al., 2011) and Jalview version 2.11.3.3 (Waterhouse et al., 2009). The splice variants are sorted by pairwise identity. The percentage identity is coloured with a threshold of ≥ 99% across all three splice variants. TBC1D1 regions corresponding to the structural domain of phosphotyrosine-binding domain 1 and 2 (PTB1: 16-164 aa; PTB2: 168 – 384 aa) are conserved across all three transcript variants. The catalytic RabGAP domain structure from 809 – 1247 aa is conserved in the SHORT and LONG with a consensus occupancy of 100%. The LONG-GAPdel depicted a gap of 103 aa in grey with a consensus occupancy of 67% (1027 – 1130 aa). Additionally, a gap of 94 aa motif in grey, with a consensus occupancy of 67% (637 – 731 aa), is depicted between the SHORT and LONG splice variants and does not occur within a domain structure region. Abbreviations: aa: amino acids.

However, a gap occurs between LONG and LONG-GAPdel, ranging from the amino acids 1027 to 1130, indicating a deletion of 103 amino acids. Additionally, a second gap of 94 amino acids occurs between the SHORT and LONG splice variants, extending from the amino acids 637 to 731. Unlike the first deletion, this gap is not within a functional domain structure region.

The three *TBC1D1* mRNA transcript variants, derived from the AS events, exhibit distinct nucleic acid arrangements. To identify canonical and AS sites within the gene's structure, the Splice Detector software was employed (Figure 12). This analysis revealed unique splicing patterns for each variant. *SHORT* depicts an exon skipping (ES) at exons 12 and 13, while *LONG* does not undergo any AS events.

LONG-GAPdel displays an ES at exon 19 and an alternative acceptor 3´splice sites (A3´SS) at exon 20. Of note, beyond the three transcript variants described, additional TBC1D1 variants are present, exhibiting further splicing variations. While these additional isoforms were not the focus of this dissertation, their presence indicates a greater diversity in TBC1D1 regulation than previously understood. For an overview of these additional variants, see supplementary Figure 2.

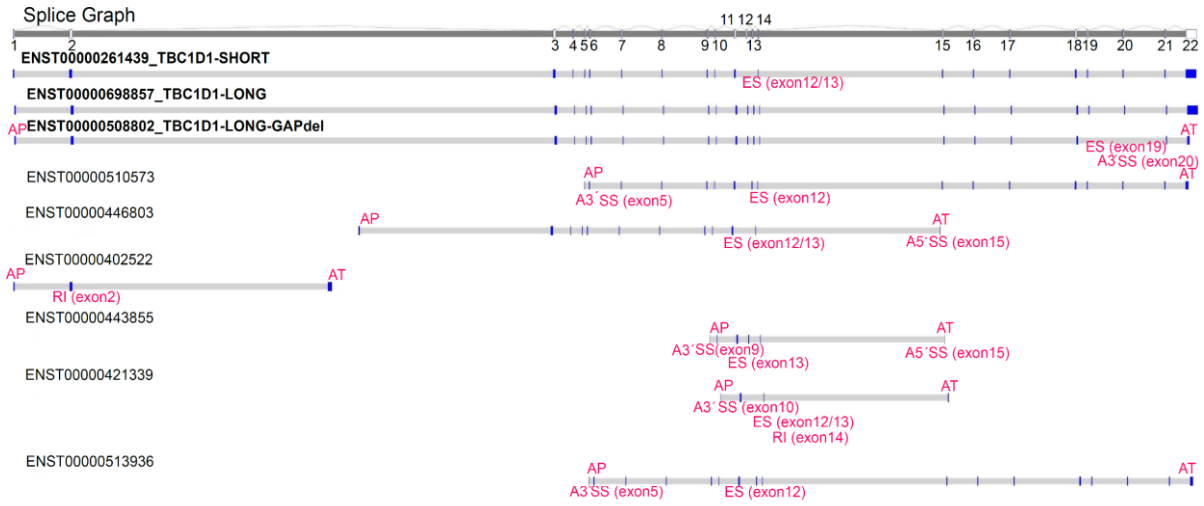

<u>Figure 12</u>: Illustration of the different types of alternative splicing and their distribution across *TBC1D1* transcript variants

Diagram of the AS events identified in *TBC1D1* transcripts using Splice Detector software (Baharlou Houreh et al., 2018). Abbreviations: AP: Alternative promoter; AT: Alternative Terminator; ES: Exon skipping; RI: Retained Intron; A3´SS: Alternative acceptor 3´splice sites; A5´SS: Alternative donor 5´splice sites.

The diagram in Figure 13 illustrates the three distinct spliced transcript variants of *TBC1D1*, each defined by unique nucleic arrangements and alternative splicing patterns. *SHORT* contains 20 exons, including alternatively spliced exons 12 and 13. *LONG* has 22 exons, while *LONG-GAPdel* exhibits 21 exons, with a deletion of about 309 nucleotides within the RabGAP domain structure resulting from the AS event ES at exon 19 and A3´SS at exon 20.

The conservation of the RabGAP catalytic domain structure across these isoforms indicates its preservation throughout evolution and highlights its essential role in biological processes. However, the structural deletion observed in *LONG-GAPdel* raises questions about how this alteration might affect the gene's function. Further comparative studies across species are needed to determine the evolutionary conservation of this modified RabGAP domain.

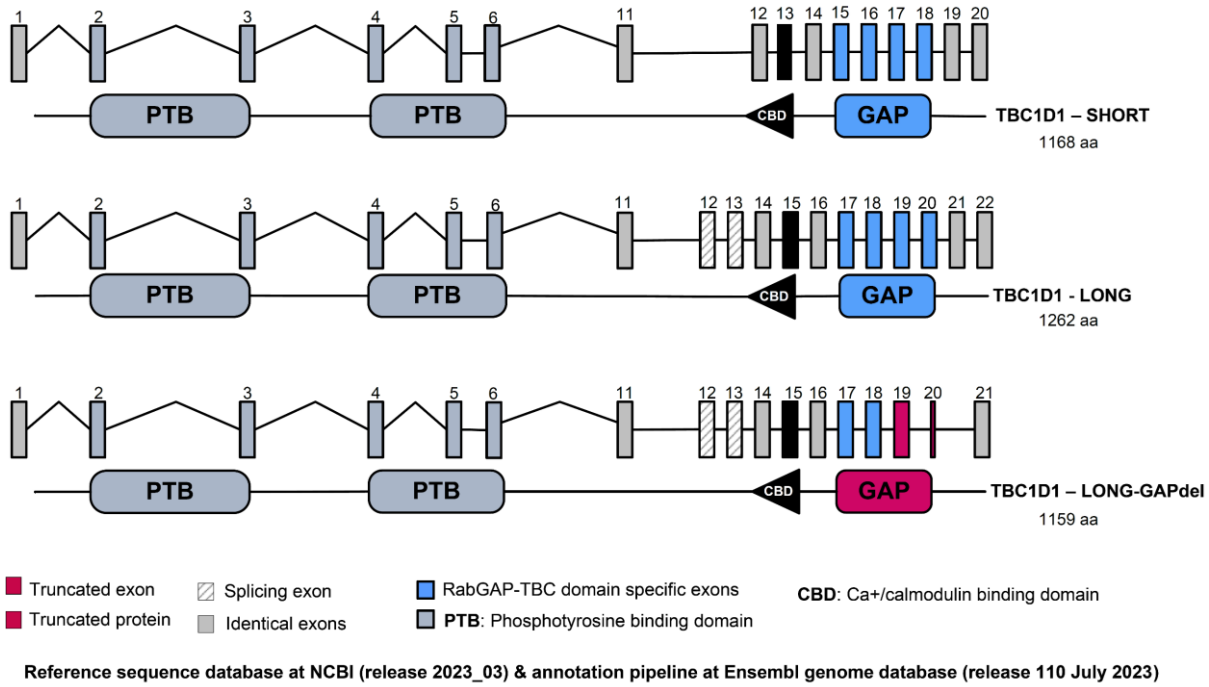

Figure 13: Diagram of the SHORT, LONG, and LONG-GAPdel transcript assembly catalogued and validated full-length transcript variants of *TBC1D1*

The gene structure of *TBC1D1* transcript variants is based on the NCBI RefSeq database, the annotation pipeline at the Ensembl genome database, and the proteins' proposed domain architecture.

3.1.2 Catalytic Rab-GAP TBC domain preserves across vertebrate lineages

A large-scale comparative genomics analysis was conducted to assess the conservation of the Rab-GAP TBC structural domain across species, aiming to investigate of the functional relevance of the truncated isoform identified as curated in the *in silico* analysis. An alignment of the genomic position of the Rab-GAP TBC domain region (chr4: 38,115,862 – 38,124,981) with 100 vertebrates across species (Figure 14) revealed that the catalytic Rab-GAP TBC domain is conserved among primates and canidae. However, some variation was observed in rodentia, where the domain showed minor discrepancies, and the catalytic Rab-GAP TBC domain is even less conserved further down the mammalian lineage.

A local hit alignment of the Rab-GAP TBC GAPdel domain, spanning amino acids 891 to 1130 (as shown in Figure 11) was performed to study gene conservation across a range of species. This analysis was executed on approximately 122 aa long, the amino acids 976 to 1097, containing the gap motif using local alignment to distinguish homologous sequences (Figure 15). The region containing the gap motif, the amino acids 976 to 1097, approximately 122 aa long, was selected for BLAST analysis across primates, rodents, domesticated cattle (Bos taurus), and birds to study gene conservation (Cheng et al., 2022; Miklos & Rubin, 1996).

Subsequently, a Multiple Sequence Comparison by Log-Expectation (MUSCLE) for sequence alignment in Jalview was performed to analyse the conservation of the 122 aa motifs across species. The motifs PDMIIL and QMEK were used to direct the insertion and deletion sequences. The Rab-GAP TBC domain depicted sturdy homologous relationships among the species with the motif PDMIIL. However, domesticated Cattle displayed moderate homology, with discrepancies in residues as the Threonine residue is less prevalent. In contrast, the QMEK motif is absent across the examined species. The small size of the residues making up the QMEK motif may contribute to their lower prevalence.

The structure of the Rab-GAP TBC domain appears well-conserved across specific vertebrate lineages such as primates, rodents, domesticated Cattle, and Birds. It is absent in the invertebrates, such as plants and fungi. The available data suggest that the domain may have evolved primarily in vertebrates. However, further research is needed to confirm its presence across other vertebrate groups and to explore whether it is consistently absent in non-vertebrate lineages.

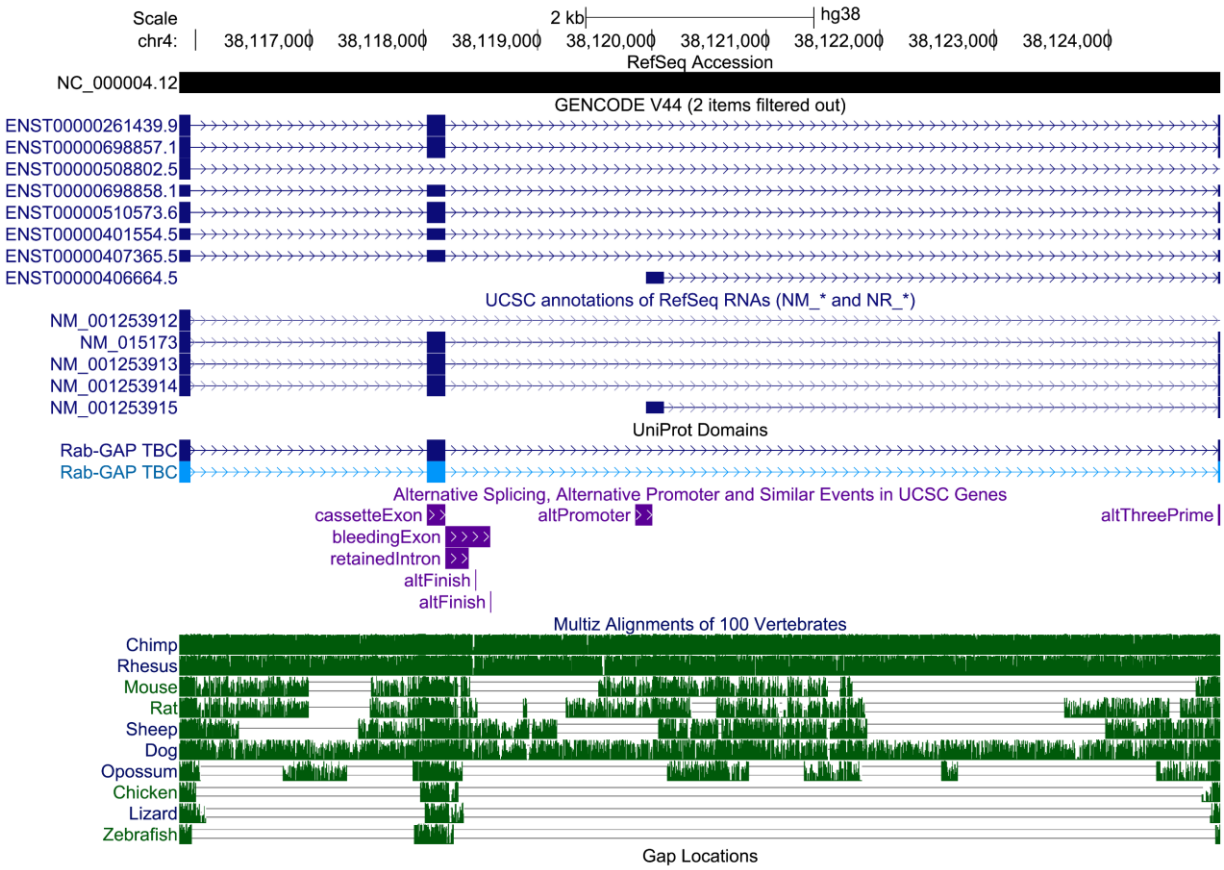

Figure 14: Graphical visualisation of Rab-GAP TBC domain of TBC1D1 on human assembly (GRCh38/hg38) using UCSC Genome Browser version Dec.2013 initial release; June 2022 patch release 14

The Rab-GAP TBC domain genomic coordinates (38,115,862 – 38,124,981) are displayed in the graph. Four different tracks are represented: the GENCODE V44, showing the genomic codons of the splice variants and their Ensembl ID; the UniProt Domains, followed by the AS track, indicating all various types of AS events at that location and the conservation of genomic elements of the Rab-GAP TBC domain elements across the vertebrate species.

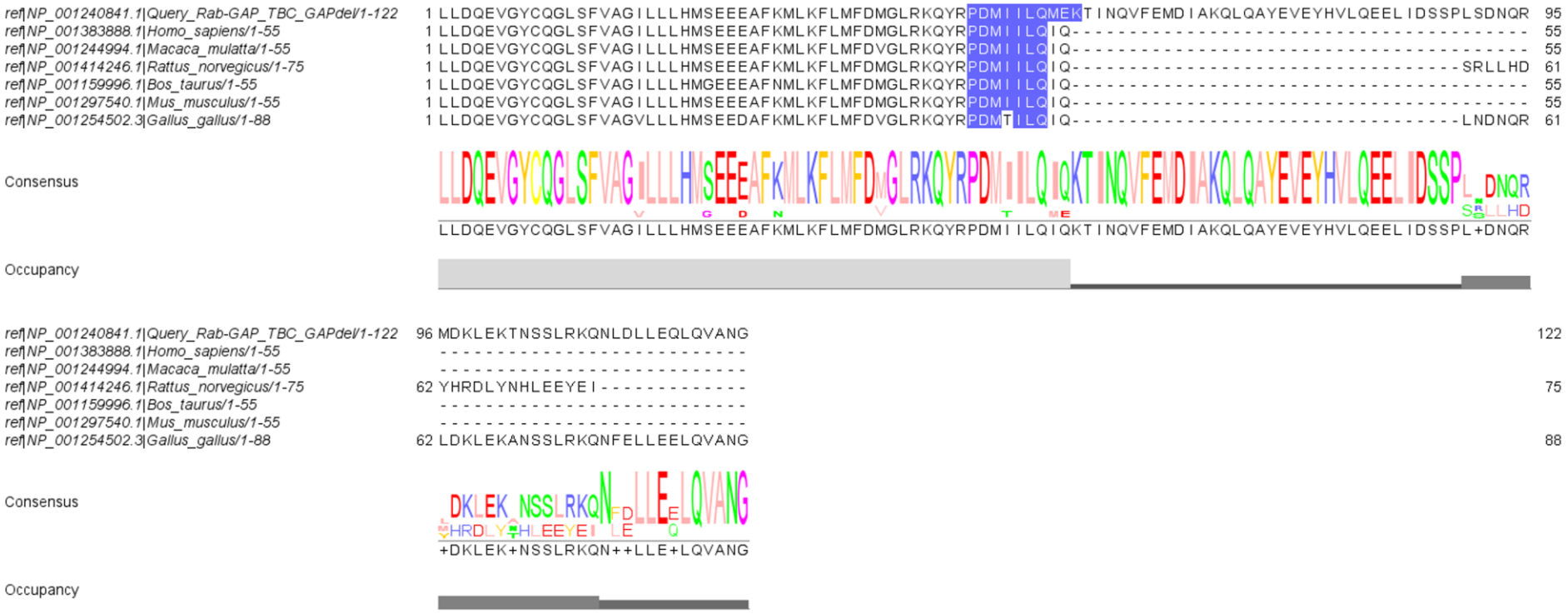

<u>Figure 15</u>: MUSCLE Alignment of Rab-GAP TBC domain fragment (amino acids 976-1097) across species visualized with Jalview version 2.11.3.3

Alignment of the query motif of the Rab-GAP TBC domain fragment amino acids coordinate (976 – 1097) spanning the gap region is displayed in the graph against the canonical set of protein sequences (NPs) from different species. The motifs PDMIIL and QMEK fragments indicate the extent of insertions and deletions. This consensus occupancy remains constant for the motif PDMIIL across the species. A discrepancy appears among the species with the motif QMEK.

3.2 *In vitro* validation of *TBC1D1* splice variants in primary cell cultures

3.2.1 Primary human mesenchymal stem cells differentiation into myotubes

Commercially available primary hMSCs were cultivated and differentiated in myoblast and subsequently into myotubes (Figure 16 and section 2.2.2.4) to study the expression of the *TBC1D1* variants *SHORT, LONG,* and *LONG-GAPdel*.

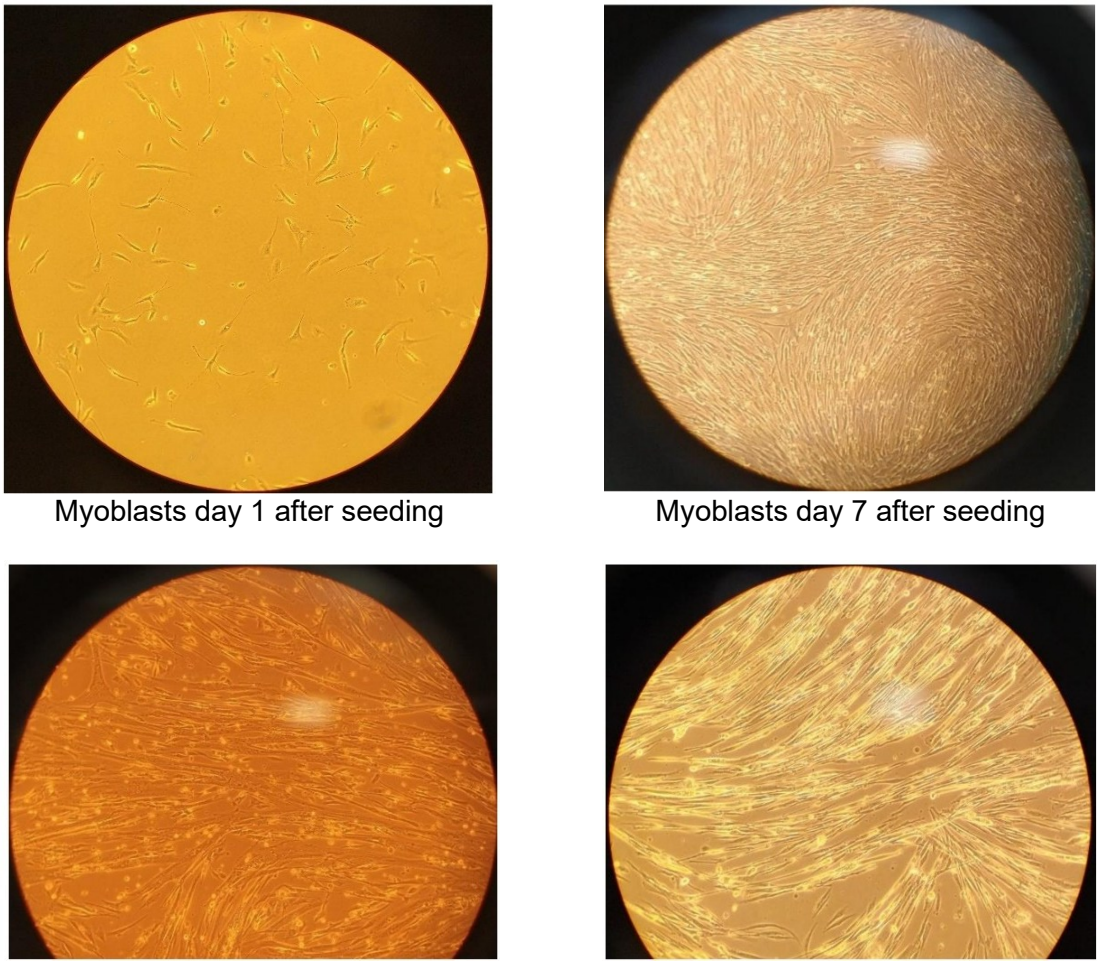

Figure 16: Primary hMSCs under a light microscope

Myoblasts, mononucleated cells at 90% confluence (top), fuse on a large, centrally located multinucleated myotube (bottom).

To further ensure the adequate differentiation of the satellite cells into myoblasts and myotubes, we assessed the expression levels of myogenic regulatory factors (MRFs) such as *MYF5*, *DESMIN*, and *MYH2* using RT-qPCR (see section 2.2.2.5). Differentiation of the cells from myoblasts to myotubes *in vitro* was confirmed (Figure 17). Thus, the mRNA expression level of the myoblast-specific factor *MYF5* was significantly decreased in the myotubes compared to the myoblasts (Figure 17A). In contrast, the expression level of the myotube-specific factor *MYH2* was significantly increased in the myotubes compared to the myoblasts (Figure 17C). Additionally, the expression level of *DESMIN*, a marker of muscle cells' structural integrity, was significantly elevated in myotubes relative to myoblasts (Figure 17B).

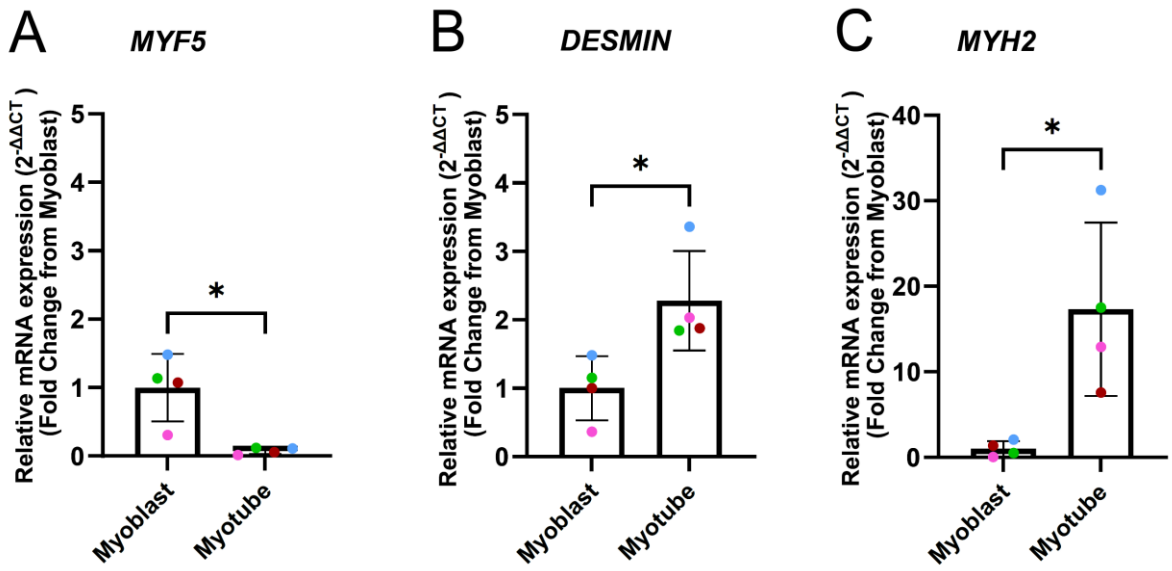

Figure 17: Relative mRNA expression of myogenic regulatory factors of differentiated myoblasts and myotubes

(A) myoblast-specific factor *MYF5*, (B) marker of the integrity of the muscle cells *DESMIN* and (C) myotube-specific factor *MYH2*. Data is represented as mean ± SEM and was analysed by paired t-test, two-tailed, from 4 biological donors. P-values are indicated, and *, p-value <0.05 was considered statistically significant (paired t-test and Dunnett's multiple comparisons test).

3.2.2 MRFs & MSPs validation in primary human cells

Quantitative analyses of myogenic regulatory factors (MRFs) such as Myf5, MyoD, and MyoG and muscle structural proteins (MSPs), specifically Desmin and Myh2 expression, were conducted to confirm the myogenicity of the primary cell, evaluate the cell line's differentiation state, and establish a consistent baseline for inter-experimental comparisons (Figure 17 and supplementary Figure 2).

To facilitate accurate quantification of differential expression, beta-2-microglobulin (B2M) was selected as a reference gene (RG) due to its stable expression as part of the MHC class I molecules, which is present on the surface of all nucleated cells (see supplementary Figure 2 for details).

The expression profiles of MRFs represented the myogenic characteristics and differentiation state of the cells. The expression of *MyoD*, an indicator of stem cell activity and cell cycle engagement, is comparable in both primary hMSCs and muscle biopsies (Figure 18A). In contrast, the *MyoG* factor, an indicator of terminal differentiation and fusion of the myocytes into myofibers, showed significant expression in the myotubes compared to myoblasts (Figure 18B). Conversely, *DESMIN* and *Myh2*, indicators of mature muscle cells and myotubes displayed elevated expression levels in the muscle biopsies compared to the myoblasts (Figure 18C-D).

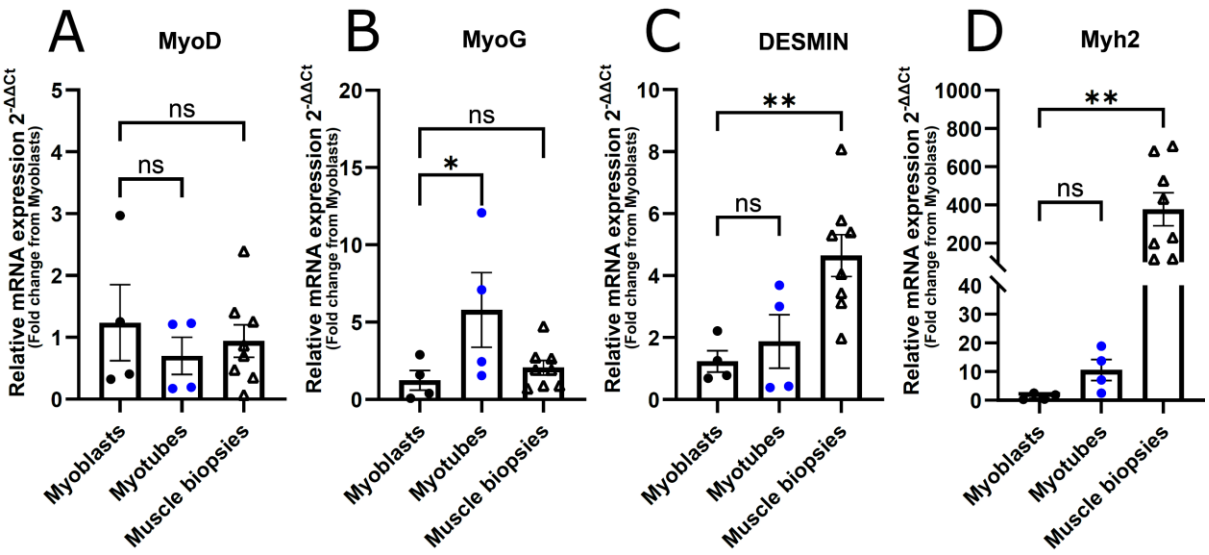

<u>Figure 18</u>: Relative mRNA expression of the Myogenic Regulatory Factors (MRFs) and the Muscle Structural Proteins (MSPs) genes

Relative mRNA expression fold change from myoblasts of the MRFs (A-B) and MSPs (C-D) genes in primary hMSCs (n=4) and muscle biopsies (n=8). Triangles indicate muscle biopsies, dark circles indicate myoblasts, and blue circles indicate myotubes. Data is presented as mean ± SEM. For statistical analysis, one-way ANOVA was computed using myoblasts versus myotubes and muscle biopsies. *, $p<0.05$; **, $p<0.01$ (Dunnett's multiple comparisons test).

3.2.3 Abundance of *TBC1D1* splice variants in primary human cells

3.2.3.1 Optimised primers design for RT-qPCR detection of the splice variants

Specific primers were successfully validated via gel electrophoresis for the detection of *TBC1D1* splice variants in primary hMSCs and muscle biopsy samples (Figure 19). Three sets of primers, each targeting distinct regions of the *TBC1D1* gene, were designed to assess the expression of *TBC1D1* in these samples.

The first set of primers spans exon 6 and exon 7, a region conserved across all *TBC1D1* variants and is referred to as *TBC1D1 TOTAL*. These primers consistently produced a DNA fragment of ~ 92 bp across the myoblasts, myotubes, and muscle biopsies (Figure 19A), confirming the presence of *TBC1D1* mRNA in each cell type. The relative mRNA expression of all 3 variants remains consistent across myoblasts, myotubes, and muscle biopsies.

A second set of primers, specific to the *TBC1D1 SHORT* variant, produced a DNA fragment at the expected size of ~ 177 bp (Figure 19B). The relative mRNA expression in this set is significantly lower in myotubes and muscle biopsy samples compared to myoblasts.

The last set of primers, specific to the *LONG* and *LONG-GAPdel* variants, produced a DNA fragment at the expected size of ~ 150 bp (Figure 19C). The relative mRNA expression of *TBC1D1 LONG* and *LONG-GAPdel* is significantly higher in both myotubes and muscle biopsies compared to myoblasts. This result provides essential evidence enlightening the *LONG* and *LONG-GAPdel* as the muscle-specific splicing variants.

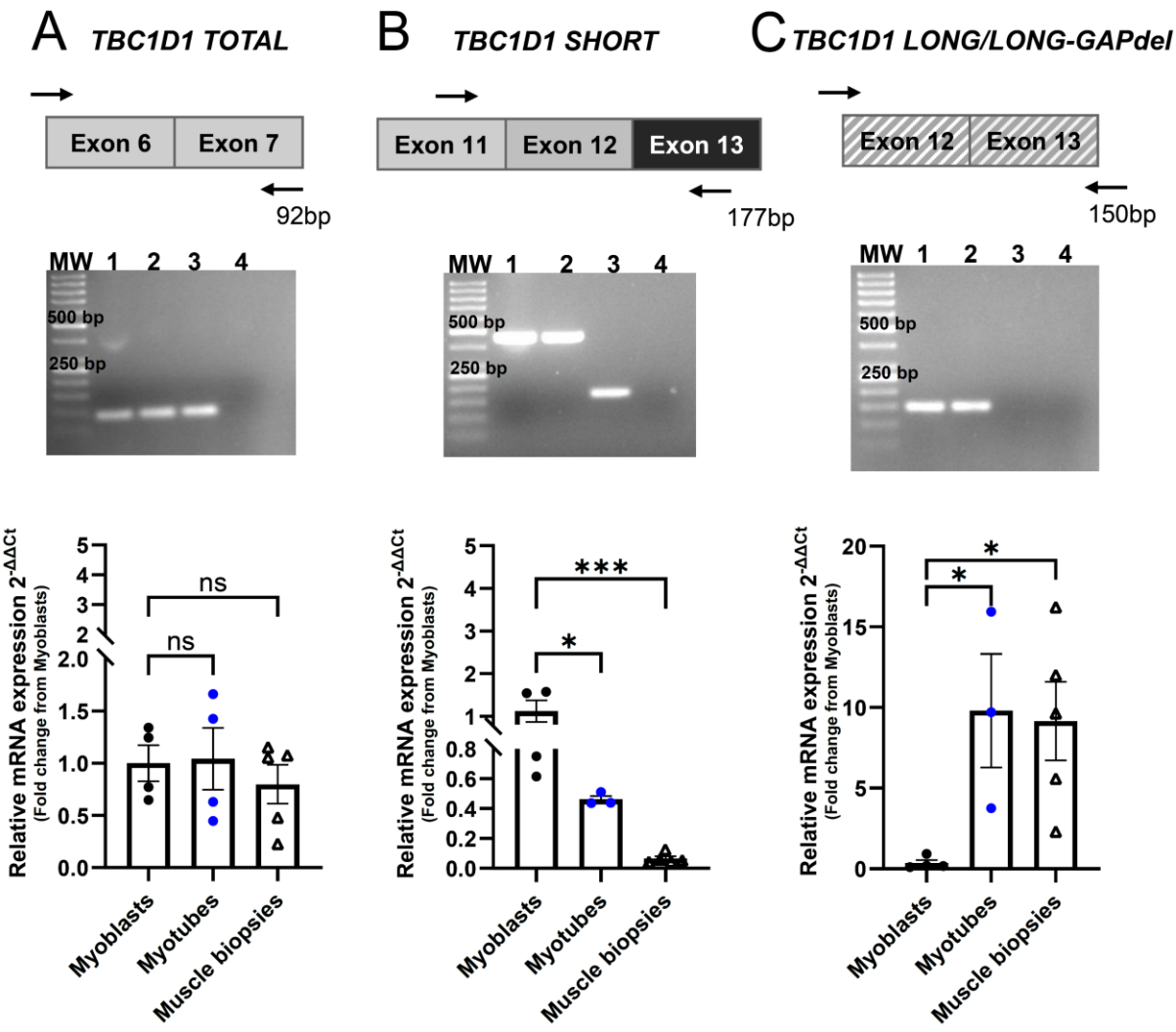

<u>Figure 19</u>: Schematic diagrams depicting the primer location for detecting *TBC1D1* splicing isoforms and their distribution in primary hMSCs (n=3-4) and muscle biopsies (n=5)

The boxes represent the exons, and the arrows indicate the primers' locations. The expected fragment sizes are indicated. MW: molecular weight used 50bp DNA ladder. Lines 1, 2, 3, and 4 on the gel electrophoresis indicate the plasmid reference for LONG, LONG-GAP, and SHORT, respectively, and the negative control. The triangle indicates the biopsies; dark circles indicate the myoblasts; blue circles indicate the myotubes. (A) Relative mRNA expression fold change from myoblasts of all three splicing isoforms in primary hMSCs and muscle biopsies. (B) Relative mRNA expression fold change from myoblasts of SHORT in primary hMSCs and muscle biopsies. (C) Relative mRNA expression fold change from myoblasts of LONG and LONG-GAP in primary hMSCs and muscle biopsies. Data is presented as mean ± SEM. For statistical analysis, one-way ANOVA was computed using myoblasts versus myotubes and muscle biopsies. *, $p<0.05$; **, $p<0.01$; ***, $p<0.001$ (Dunnett's multiple comparisons test).

3.2.3.2 *TBC1D1 LONG-GAPdel* expression in primary hMSCs & muscle biopsies

The validation of the *LONG-GAPdel* splicing variant through RT-qPCR using the standard SYBR Green method could not be achieved. This limitation likely arises from SYBR Green's lower specificity. SYBR Green binds to double-stranded DNA, including non-specific PCR products or primer dimers, which can lead to inaccurate detection. To achieve precise detection of *LONG-GAPdel*, a TaqMan probe-based approach was adopted, which offers higher specificity by targeting unique sequences within the variant (Figure 20).

To accurately quantify the cellular expression levels of the *LONG-GAPdel* splicing variant, a specific TaqMan probe was developed, designed to span the region from exon 18 toward the c-terminal region of the gene. This target area includes the deletion of amino acids characteristic of the *LONG-GAPdel* variant compared to the *LONG* variant (see section 2.2.2.9; Figure 20A). The efficiency of the qPCR assay depends on the sequence specificity of the probe, the complexity of the template and the experimental cycling conditions (Cao & Shockey, 2012).

Therefore, both expression vectors (pcDNA3.1-3xFLAG-TBC1D1-LONG and pcDNA3.1-HA-TBC1D1-LONG-GAPdel) were used to construct standard curves through a series of serial 1:2-fold dilutions to compare their efficiency in expressing the target gene *LONG-GAPdel* (Figure 20B). Results indicated that the TaqMan probe is bound to both vectors of expression. However, analysis of the linear regression equation revealed that the LONG-GAPdel vector exhibited an expression efficiency of approximately 99.79%, a value within the ideal standard slope range of -3.3 to -3.6, which correlates with efficiencies between 90% and 110% (Ruijter et al., 2021). This confirms that the TaqMan probe was accurately designed and specifically detects the LONG-GAPdel expression in samples.

Following the validation of the TaqMan probe, the expression levels of LONG-GAPdel were quantified in primary hMSCs and muscle biopsies cDNA samples, equivalent to 1 µg of RNA (Figure 20C). Copy numbers were determined for each sample type using the linear relationship between the Ct (cycle threshold) values and the logarithmic concentration of the LONG-GAPdel expression vector. The myoblasts and the myotubes depicted average C_T values of 32.697 and 32.092, respectively, while the muscle biopsies depicted an average C_T value of 35.70 (Supplementary Figure 3). *LONG-GAPdel* expression was not significantly different in the myoblasts or the myotubes, with an average copy number of approx. 0.027 in myoblasts, while myotubes showed a slightly higher expression at 0.045 copies on average. In the muscle biopsies, the *LONG-GAPdel* demonstrated the lowest expression with an average copy number of approximately 0.004, significantly less than in the cultured myotubes. Overall, all cell line samples expressed a very low abundance of *LONG-GAPdel*.

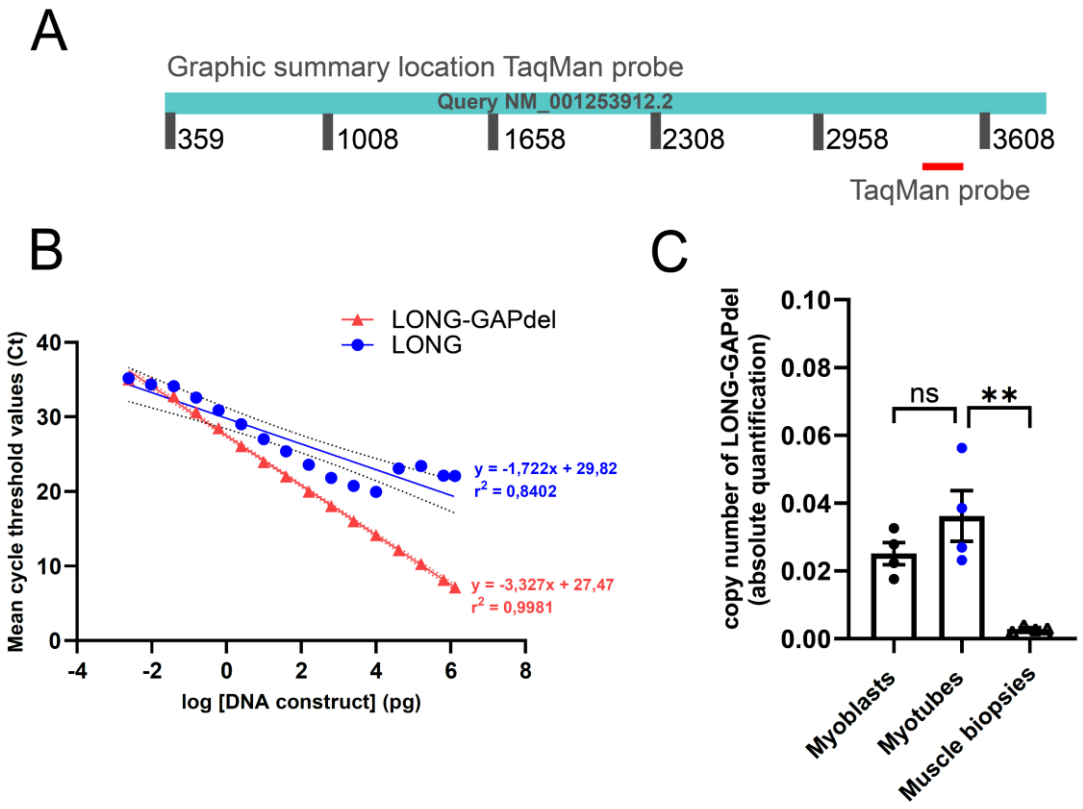

<u>Figure 20</u>: Quantifying the log amount of TBC1D1-LONG-GAPdel in primary hMSCs and muscle biopsies

(A) Graphical illustration of the TaqMan probe location. (B) The linear relationship between Ct values and log quantities (copy number) of the LONG and LONG-GAPdel expression vectors. The qPCR standard curve linear relationship equation **y=mx+n** with **y** standing for the C_T value, **x** denoting the log of the starting quantity of the DNA copy number, **m** is the slope of the line, and n represents the y-intercept. (C) The comparison of detection and quantification of LONG-GAPdel among the myoblasts, the myotubes, and the muscle biopsies. Data are mean values ± SEM (n=4), and one-way ANOVA was computed using myotubes versus all conditions. ns: non-significant, **, p<0.01 (Dunnett's multiple comparisons test).

3.3 TBC1D1-LONG & TBC1D1-LONG-GAPdel molecular functions

A series of biochemical assays were conducted to investigate the muscle-specific expressed isoforms' upstream and downstream regulatory pathways. Previous studies have highlighted a wide range of upstream and downstream regulators of TBC1D1 and its involvement in GLUT4 translocation (Cheng et al., 2014; Hatakeyama & Kanzaki, 2013; Ishikura & Klip, 2008; Jordens et al., 2010; Keller et al., 1995; Mafakheri, Florke, et al., 2018; Miinea et al., 2005; Pehmoller et al., 2009; Roach et al., 2007; Sakamoto & Holman, 2008; Sun et al., 2010; Sun et al., 2014; Zhou et al., 2017).

The upcoming sections of this dissertation aim to provide insight into the functional mechanisms of the two muscle-specific isoforms, providing a detailed analysis of their regulatory networks. By exploring how these isoforms are modulated, the study seeks to uncover their roles in metabolic processes and their potential impact on cellular glucose management and insulin signaling in muscle.

3.3.1 LONG & LONG-GAPdel GTP hydrolysis activity with small GTPase substrates

To unveil the GTP hydrolysis activity of the muscle-specific TBC1D1 isoforms LONG and LONG-GAPdel, Rab8a and Rab10 were used as substrates (Figure 21). The difference between the two isoforms is that the LONG-GAPdel isoform lacks about 103 amino acids in the catalytic site compared to the LONG isoform. The catalytic site is located at the GAP domain structure. Therefore, purified cloned of the GAP domain structure, as well as the purified full-length of both splice protein, LONG and LONG-GAPdel, were expressed as recombinant GST fusion protein in *E. coli* BL21-CodonPlus (DE3)-RIL, and the baculovirus system, respectively (see sections 2.2.3.5 and 2.2.3.6). The GTPase assays were performed with the TBC1D1-specific small GTPases Rab8a and Rab10 (Roach et al., 2007; Zhou et al., 2017). Additionally, the GAP domain of the mutant form of the TBC1D1, in which the critical arginine "finger" residue was substituted with lysine (R854K), served as a positive control for the inactivity of the GAP domain function (Pan et al., 2006; Roach et al., 2007; Will & Gallwitz, 2001) (Figure 21A).

An enhanced GTP hydrolysis activity of Rab8a and Rab10 was observed when incubated with the purified recombinant cloned GAP domain of TBC1D1-LONG compared to TBC1D1-LONG-GAPdel (Figure 21B). In contrast, there is no GTP hydrolysis activity of Rab8a and Rab10 after incubation with the purified recombinant cloned TBC1D1 GAPdel domain structure (Figure 21C).

In line with these findings, the GTP hydrolysis activity of both Rab8a and Rab10 was substantially increased when subjected to the recombinant TBC1D1 LONG full-length protein. However, incubation of the small Rab GTPases with the full-length TBC1D1 GAPdel splice protein did not lead to an increase of intrinsic GTP hydrolysis. Similarly, no increase in GTP hydrolysis was observed when the small Rab GTPases were exposed to the GAP-inactive TBC1D1-R854K mutant (Figure 21 D-E).

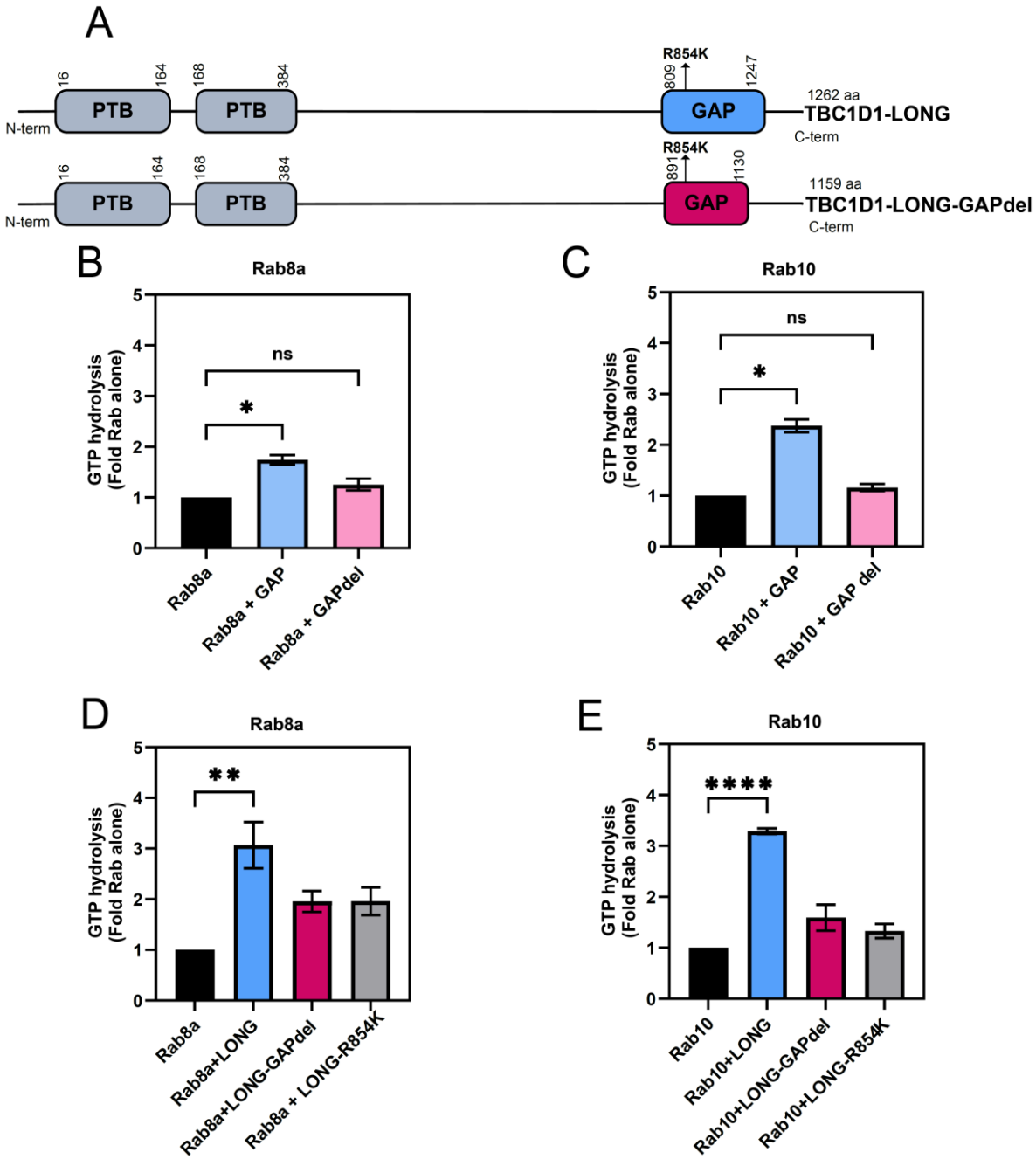

Figure 21: GTP hydrolysis activity of purified RabGAP domain structure and full-length protein isoforms of TBC1D1 and TBC1D1-R854K mutant *in vitro*

(A) Domain structure of TBC1D1 LONG, LONG-GAP-VAR, and the position of the mutated residue R854K. (B-C) RabGAP assays were performed with Rab8a and Rab10 in the presence of 2 pmol purified RabGAP domain structure and (D-E) in the presence of 2 pmol of purified full-length protein of TBC1D1 -LONG, TBC1D1 -LONG-GAPdel, and TBC1D1-R854K mutant (RK). The reaction was stopped after 30 minutes, and the mixture of aliquots was filtrated and quantified as described in the methods section 2.2.3.8. Phosphate production from the endogenous GTP hydrolysis activity of Rab8a and Rab10 was subtracted. Data is represented as mean ± S.E.M from three independent experiments. One-way ANOVA with Dunnett's multiple comparisons tests. *, $p<0.05$; **, $p<0.01$; ****, $p<0.0001$.

3.3.2 LONG & LONG-GAPdel apparent affinity for upstream kinases AKT2 & AMPK

TBC1D1 has been reported to be regulated by various kinases such as AKT2 and AMPK (Chen et al., 2008; Eickelschulte et al., 2021; Jessen et al., 2011; Rutti et al., 2014; Taylor et al., 2008; Treebak et al., 2014; Vichaiwong et al., 2010). This study explored the interaction between these two kinases and the muscle-specific TBC1D1 isoforms, LONG and LONG-GAPdel, to determine kinase-substrate affinity and specificity differences. The phosphorylation events on these substrates trigger the insulin signaling in the cells, activate the translocation of the GLUT4 storage vesicles to the plasma membrane, and mediate glucose uptake. As depicted in Figure 22A, both muscle-specific isoforms, LONG and LONG-GAPdel, showed identical phosphosites compared to the SHORT isoform missing the Ser^{707} site.

At the phosphosites, Ser^{237}, Ser^{507}, and Thr^{596}, both kinases, AKT2 and AMPK, promote the phosphorylation of the LONG and LONG-GAPdel substrates in the same manner (Figure 22B-D), as indicated by the identical apparent affinity (K_m) values. Moreover, at the phosphosite Ser^{507}, the K_m is at its highest, about 73 µM, for the LONG isoform substrate under AMPK stimulation (Figure 22C). However, AMPK displayed a significantly lower K_m value for the LONG isoform substrate at the phosphosites Ser^{707} and Ser^{667}, with K_m values around 3 µM and 4 µM, respectively (Figure 22 E-F).

The kinase AKT2 showed similar apparent affinities for both LONG and LONG-GAPdel substrates across phosphosites, indicating a uniform interaction between these isoforms and AKT2. AMPK, on the other hand, exhibits a higher apparent affinity for the LONG isoform substrate than the LONG-GAPdel isoform substrate. Furthermore, AMPK kinase promotes phosphorylation of the LONG isoform substrate at lower concentrations than the GAPdel isoform substrate, as indicated by the phosphorylation signals observed at both latter phosphosites on the blots.

AKT2 and AMPK kinases are upstream regulators of TBC1D1 involved in this cascade signaling, but their interactions with its isoforms differ significantly. AMPK shows a clear preference for the LONG isoform substrate compared to the LONG-GAPdel isoform, effectively promoting phosphorylation even at low substrate concentrations. Conversely, AKT2 displays a comparable affinity for both LONG and LONG-GAPdel, indicating a relatively weak interaction between the isoforms' substrates and AKT2 kinase. This lower affinity suggests that higher concentrations of both isoforms are necessary for AKT2 to promote phosphorylation effectively.

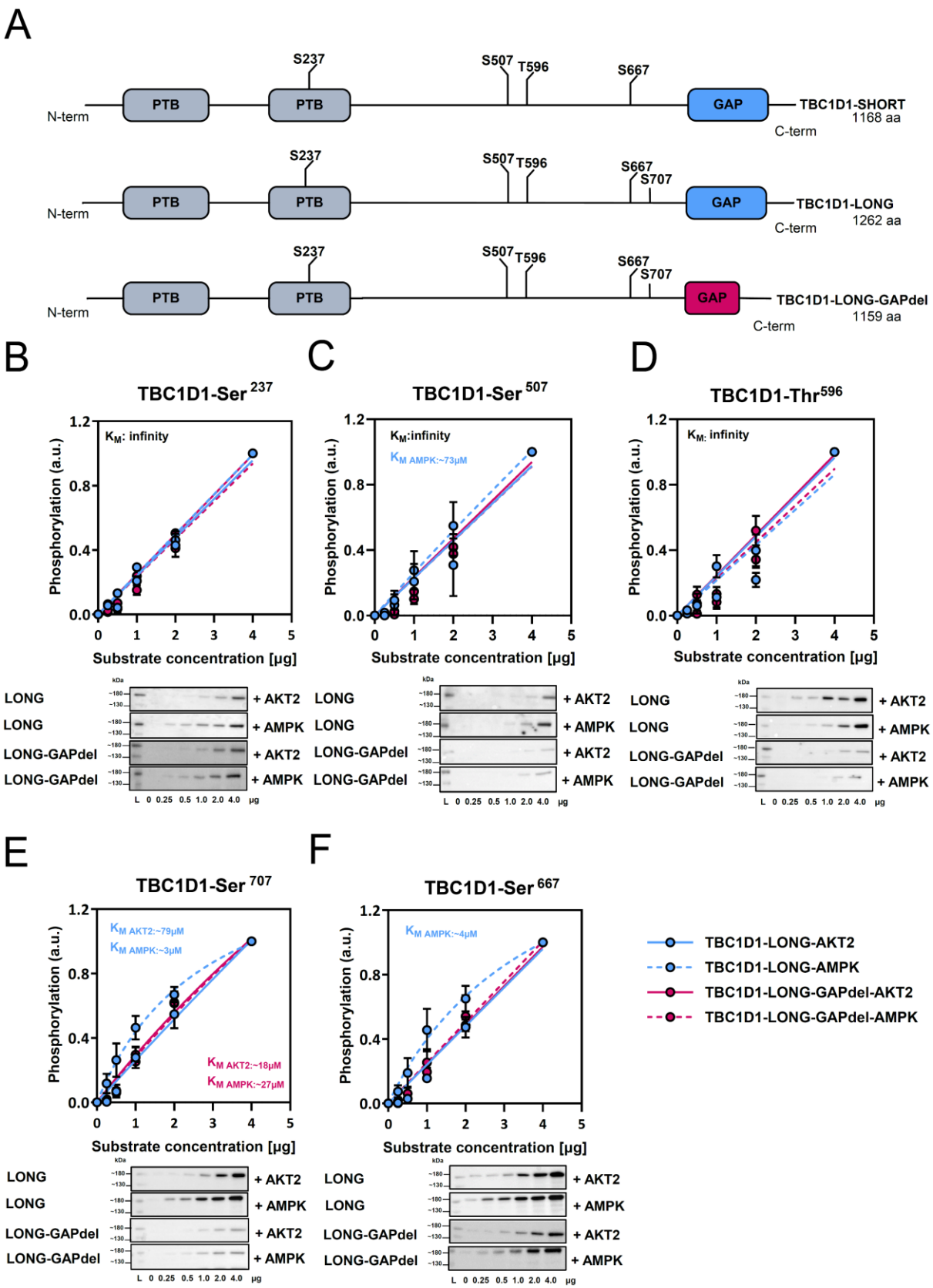

Figure 22: Profiling human substrates TBC1D1-LONG and TBC1D1 GAP-VAR specificities for the kinases AKT and AMPK *in vitro*

(A) The domain structure of TBC1D1-LONG, TBC1D1-LONG-GAPdel, and the position of crucial phosphorylation sites (Chen et al., 2008; Taylor et al., 2008; Treebak et al., 2014). Purified AKT2 and AMPK kinases were used to phosphorylate purified full-length TBC1D1-LONG protein as well as LONG-GAPdel protein (from a range of 0.25 µg to 4 µg) for 5 minutes at the specific phosphosite regulated by the kinases was confirmed by Western blots using phospho-TBC1D1 antibodies against Ser^{237} (B), Ser^{507} (C), Thr^{596} (D) and the two phosphosites located at the splice variant site, Ser^{667} (E) and, Ser^{707} (F). The data were subjected to a nonlinear curve fitting to Michaelis-Menten kinetics using GraphPad Prism Software. Data represent mean values ± SEM from three independent experiments.

3.3.3 LONG & LONG-GAPdel interaction with the cytoplasmic tail of IRAP

Earlier studies have described the insulin-regulated aminopeptidase IRAP as a resident protein of the GLUT4 storage vesicles (Bogan & Kandror, 2010; Jordens et al., 2010). We have previously shown that murine *Tbc1d1* interact with IRAP in a phosphorylation-dependent manner. Non-phosphorylated TBC1D1 demonstrates a specific binding to the cytoplasmic domain of IRAP (cIRAP), but this interaction is abolished after phosphorylation of TBC1D1 by AKT2 or AMPK kinases (Mafakheri, Florke, et al., 2018). To characterise the binding interaction of the cytoplasmic domain of IRAP with the two muscle-specific isoforms, the respective proteins were expressed as GST fusion proteins in *E. coli* Bl21 cells, then purified, and utilised to perform a GST-pulldown assay and co-immunoprecipitation *in vitro* after pre-incubation of the two isoforms with either AKT2 or AMPK (see sections 2.2.3.4, 2.2.3.5, 2.2.3.9 and Figure 23).

The pre-incubation of TBC1D1-LONG isoform with AKT2 or AMPK led to its phosphorylation at two key sites, Thr^{596} and Ser^{667}. The Ser^{667} site demonstrates an enhanced phosphorylation response when stimulated by AMPK (Figure 23A).

Likewise, pre-incubation of TBC1D1-LONG-GAPdel isoform with AKT2 and AMPK also led to the phosphorylation of both sites under AMPK compared to the LONG. However, the Thr^{596} phosphorylation site was exclusively activated after the incubation with AKT2 (Figure 23B). The pulldown of GST-cIRAP confirmed that both non-phosphorylated TBC1D1-LONG (Figure 23C) and TBC1D1-LONG-GAPdel (Figure 23D) co-precipitate. Moreover, the specific binding of both TBC1D1 isoforms to GST-cIRAP was significantly decreased in the presence of AKT2 and AMPK.

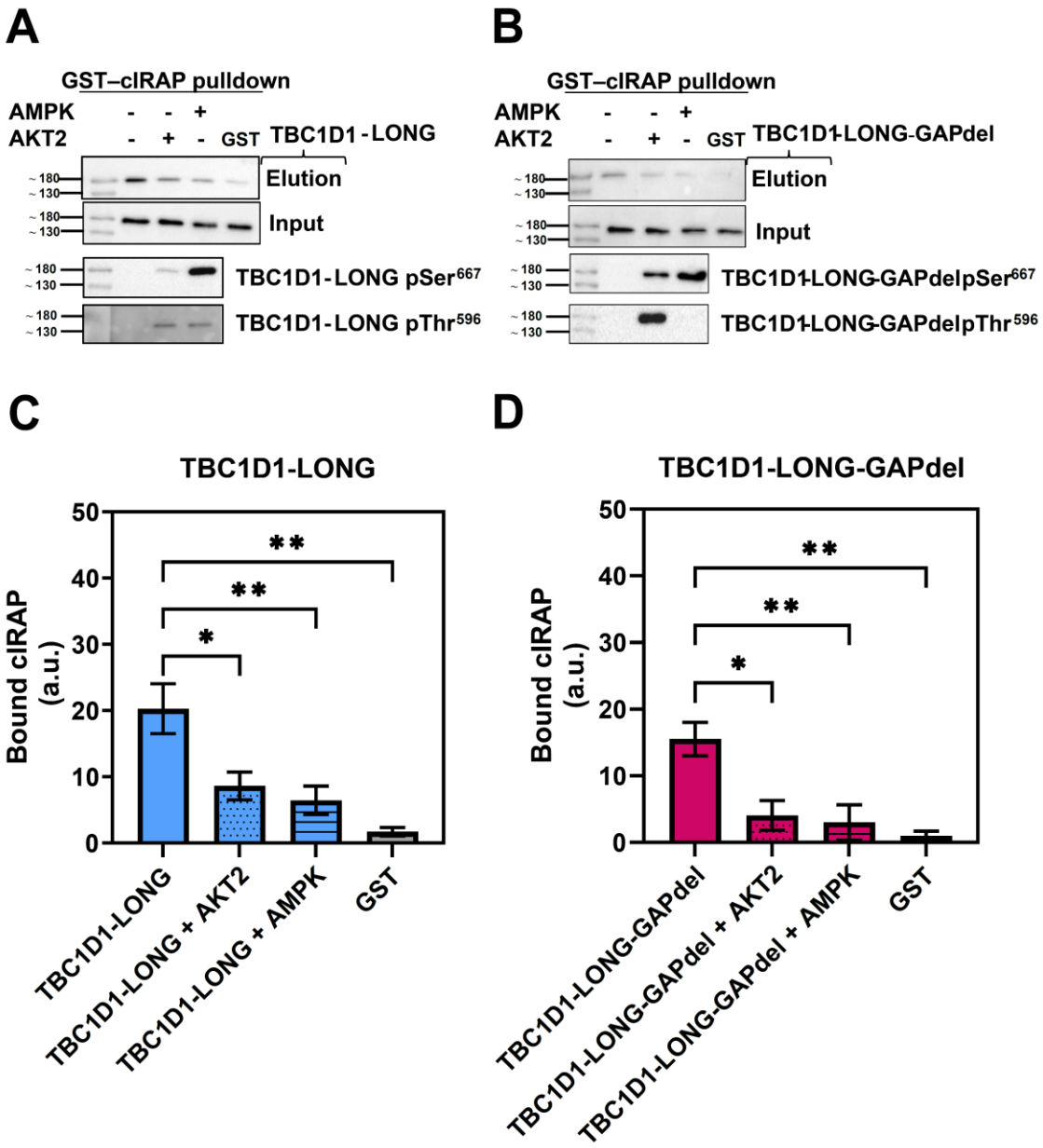

Figure 23: Interaction of TBC1D1-LONG and TBC1D1-LONG-GAPdel with the cytoplasmic tail of insulin-regulated aminopeptidase (cIRAP) *in vitro*. The carboxy-terminal region secondary structure of TBC1D1-LONG and LONG-GAPdel and their binding interactions

(A-B) Blots of GST pulldown assay and co-immunoprecipitation *in vitro* after pre-incubation of each isoform of TBC1D1 with either AKT2 or AMPK. (B) full-length TBC1D1-LONG-GAPdel protein. Bar plots indicate the ratio of GST-cIRAP input bound to TBC1D1-LONG and TBC1D1-LONG-GAPdel across the different phosphorylation conditions (non-phosphorylated, AKT2 and AMPK phosphorylated). Data is represented as mean ± SEM from three independent experiments. For statistical analysis, one-way ANOVA was computed to the respective non-phosphorylated TBC1D1 isoform as control, *p<0.05, **p<0.01.

Both isoforms (TBC1D1-LONG and TBC1D1-LONG-GAPdel) interact with the cytoplasmic tail of IRAP. This interaction is significantly reduced in the presence of the kinases, AKT2 and AMPK. A detailed analysis was conducted using Jalview software to gain a more comprehensive understanding of the protein structure of TBC1D1-LONG compared to TBC1D1-LONG-GAP. Both isoforms depicted a large amount of α-helices complex compared to β-strands in all domain structures (Figure 24). Notably, the C-terminal region of TBC1D1 shows a particularly dense arrangement of α-helices, which, as reported in prior studies, is advantageous for RabGAP dimerization (Woo et al., 2017). Therefore, full-length recombinant 3xFLAG-tagged TBC1D1-LONG and HA-tagged TBC1D1-LONG-GAPdel were expressed in HEK293 cells.

The lysates expressing the full-length 3xFLAG-tagged TBC1D1-LONG, HA-tagged TBC1D1-LONG-GAPdel, or both tagged proteins were used in a co-immunoprecipitation approach. The immune complex formed is eluted using magnetic beads pre-conjugated with anti-3xFLAG and HA-monoclonal antibodies and analysed by SDS-PAGE, followed by immunoblotting using TBC1D1 antibody and phospho-specific antibody TBC1D1-Thr^{596}. Homo- and heterodimerisation of TBC1D1-LONG and TBC1D1-LONG-GAPdel were explored before and after pre-incubation with either AKT2 or AMPK (see section 2.2.3.4 and Figure 25).

The full-length 3xFLAG-tagged TBC1D1-LONG homodimer complex is a distinct band on the TBC1D1 immunoblot, whereas homodimerization is not affected by phosphorylation of TBC1D1-Thr^{596} by AKT2 compared to AMPK kinase (Figure 25A). The TBC1D1-LONG-GAPdel variant also forms homodimers, as shown by immunoprecipitation of the HA-labelled isoform from the mammalian cell system. Consistent with the TBC1D1-LONG isoform, TBC1D1-LONG-GAPdel homodimerization is unchanged in the presence of AKT2 and associated TBC1D1-Thr^{596} phosphorylation blot (Figure 25B). Yet, in the presence of AMPK stimulation, the homodimerization is affected as the protein on the immunoblot is faintly represented. The effect of AKT2 stimulation was maintained in the heterodimerisation complex of 3xFLAG-tagged TBC1D1-LONG co-precipitated with the HA-TBC1D1-LONG-GAPdel isoform (Figure 25C). The physical interaction between the two isoforms, TBC1D1-LONG and TBC1D1-LONG-GAPdel, has been experimentally confirmed by this study, and the kinase AKT2 catalyses this interaction compared to AMPK.

Importantly, this technique validated the previous work of our group on murine TBC1D1 and demonstrated as tetramer upon the apparent molecular mass of about 600 kDa from the size exclusion chromatography (Mafakheri, Florke, et al., 2018). Aligned with the aforementioned study, the current dissertation confirms that both human TBC1D1 isoforms are also available as monomers (~ 150 kDa) and can initiate homo-heterodimers complexes.

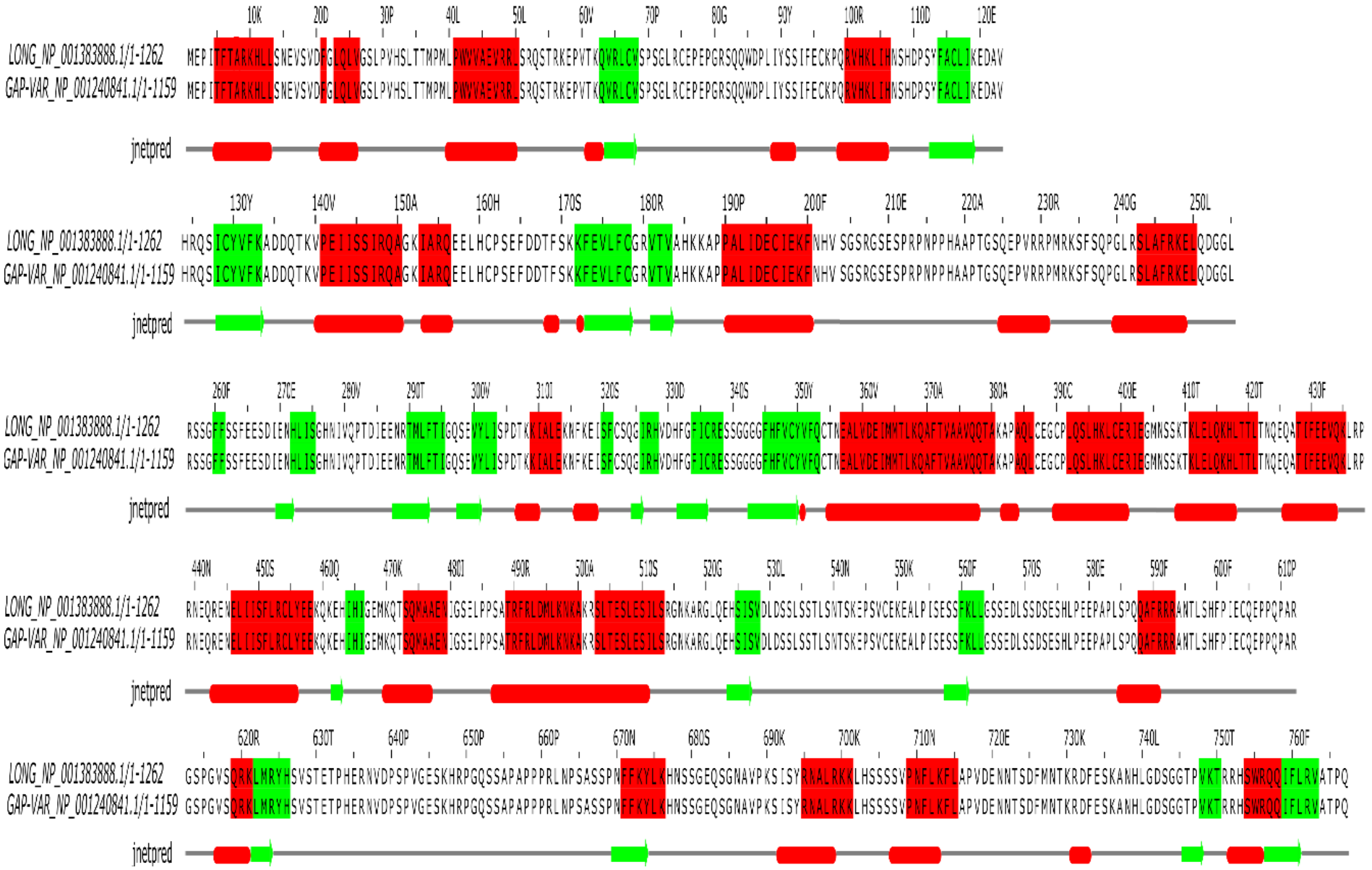
LONG_NP_001383888.1/1-1262
GAP-VAR_NP_001240841.1/1-1159
jnetpred

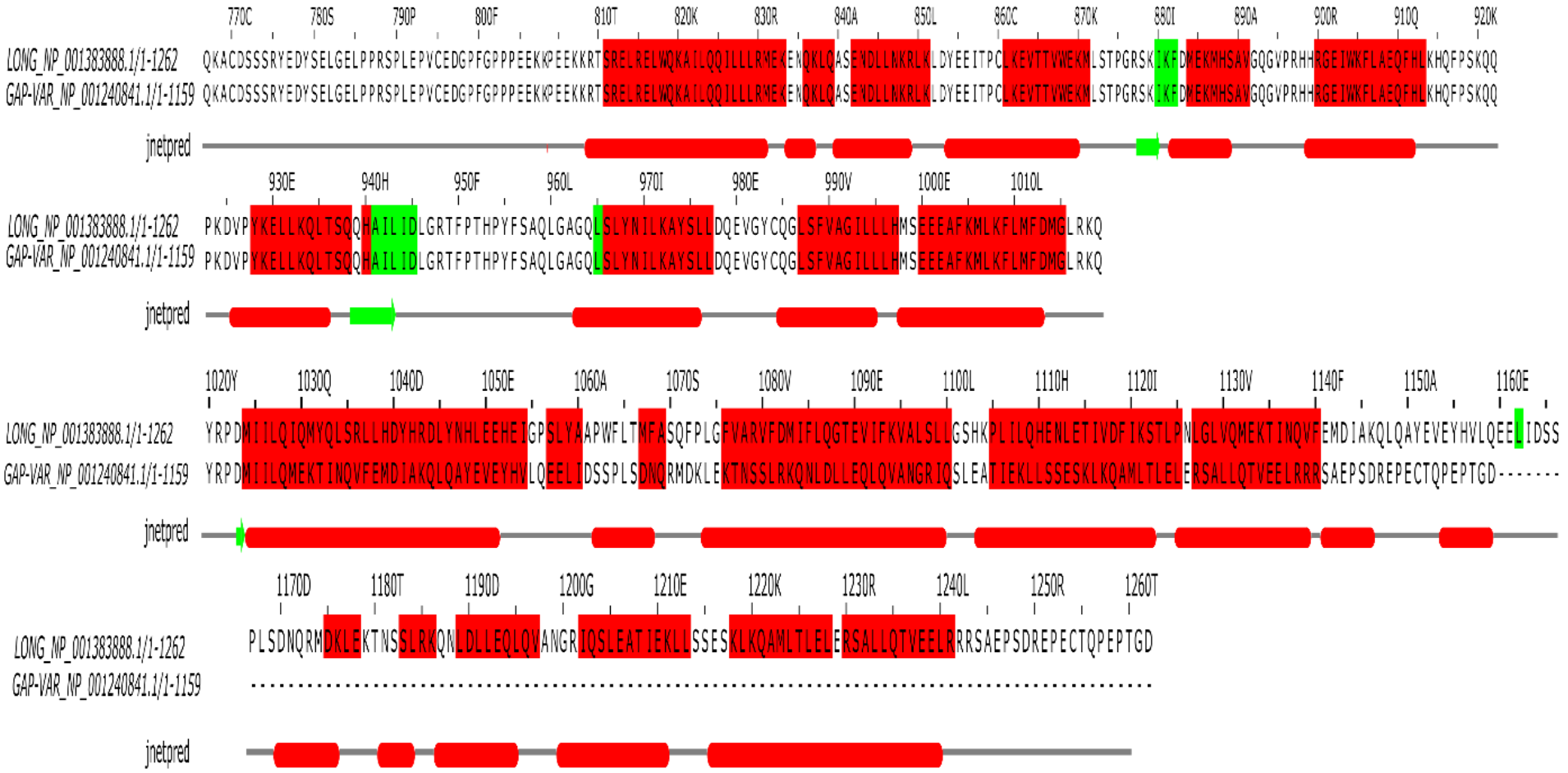

Figure 24: Structure-based multiple sequence alignment of TBC1D1-LONG and TBC1D1 LONG-GAPdel domains structure

Jalview version 2.11.2.7 – A multiple sequence alignment editor and JPred secondary structure prediction. Consensus JPred prediction for selected protein sequence is displayed in row "jnetpred". The helices are represented as red, and the beta-strands as green.

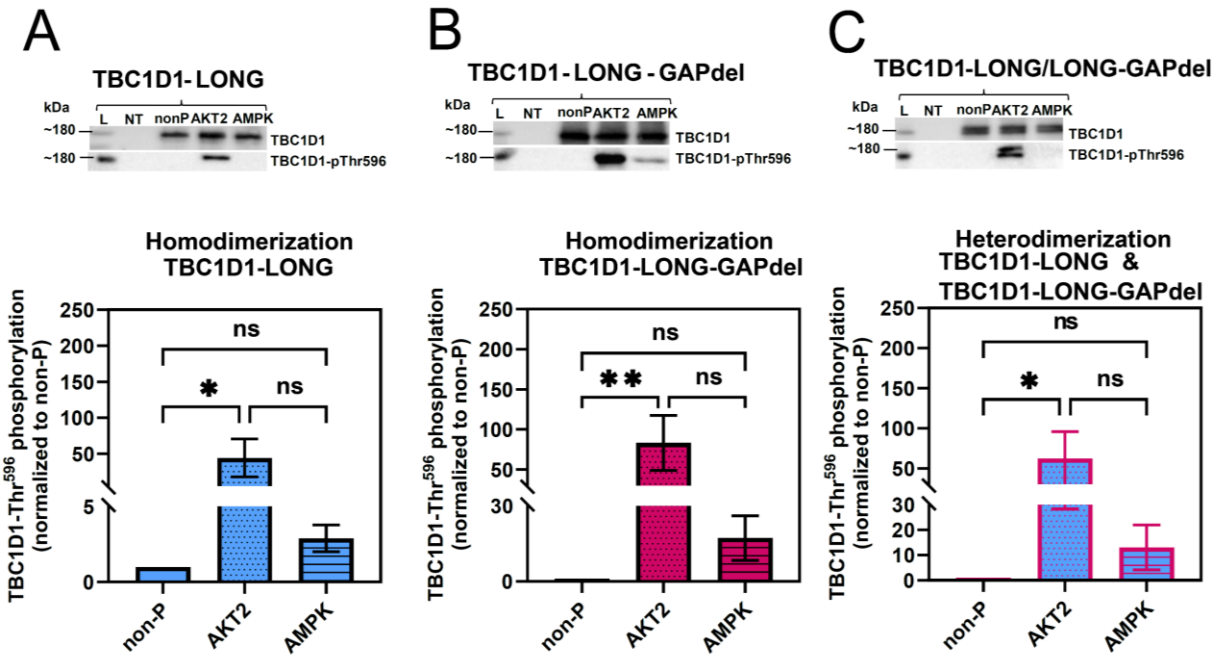

<u>Figure 25</u>: TBC1D1-LONG and TBC1D1-GAPLONG-VAR GAP full-length protein homo- and heterodimer complex in dependence of phosphorylation by AKT2 or AMPK in-vitro

Immunoprecipitation of (A) 3xFLAG-TBC1D1-LONG as well as (B) HA-TBC1D1-GAP-VARLONG-GAP and co-immunoprecipitation of (C) 3xFLAG-TBC1D1-LONG and HA-TBC1D1-GAP-VARLONG-GAP. Data is represented as mean ± SEM from four independent experiments. A one-way ANOVA with Dunnett's multiple comparisons test was computed for statistical analysis using the respective non-phosphorylated (nonP) TBC1D1 isoform as a control. *p<0.05, **p<0.01. L: Ladder, NT: non-transfected.

Further, due to the pivotal role of the substantially identical number of α-helix complexes in all their domain structures, for both isoforms, the heterodimerization is not affected by the lack of about 103 amino acids in the TBC1D1-LONG-GAPdel isoform, nor is its homodimerization.

The *in vitro* investigation of the two muscle-specific isoforms, LONG and LONG-GAPdel, revealed some critical molecular interactions and regulatory mechanisms both upstream and downstream of these isoforms. These are essential to unravelling the complex biological processes involved in the molecular pathway behind regulating muscle glucose transport in the context of insulin and physical exercise.

4. Discussion

Previous studies have consistently demonstrated the distinct and cooperative roles of the paralogous Rab-GTPase-activating proteins (RabGAPs), TBC1D4 and TBC1D1, in regulating muscle glucose transport, particularly in response to insulin and physical exercise (An et al., 2010; Binsch et al., 2023; Chadt et al., 2015; Fontanesi & Bertolini, 2013; Hatakeyama & Kanzaki, 2013; Hatakeyama et al., 2019; Larsen et al., 2022; Springer et al., 2024). Both proteins contribute to regulating GLUT4 vesicle translocation to the plasma membrane, a fundamental process for insulin-stimulated glucose uptake in muscle tissue. Understanding how TBC1D4 and TBC1D1 interact with other regulatory molecular effectors along the signaling pathways has thus allowed for a better comprehension of the mechanisms that support skeletal muscle metabolism and glucose homeostasis.

This dissertation addresses three primary research objectives. The first is the investigation of alternative splicing (AS) events present in TBC1D1 and characterising the expression levels of its distinct transcript variants in skeletal muscle. Various AS events were identified through a combined *in silico* and *in vitro* approach, revealing a transcriptional regulation for TBC1D1. By characterising these AS events in TBC1D1, the thesis highlights how AS expands the functional potential of TBC1D1.

The second objective is to investigate the functional properties of the muscle-specific LONG and LONG-GAPdel isoforms of TBC1D1. The findings revealed that these isoforms exhibit distinct GTP hydrolysis activity with small GTPase substrates, such as Rab8a and Rab10.

The third objective is dedicated to exploring the molecular functions of the specific TBC1D1 isoforms, particularly their roles in insulin- and exercise-stimulated glucose uptake in skeletal muscle. This analysis focused on phosphorylation events mediated by key kinases such as AKT2 and AMPK, both central regulators of glucose metabolism.

Collectively, the results revealed that these isoforms display distinct functional roles in glucose uptake. Their unique responses within the regulatory network suggest a functional specialisation supporting the precise and dynamic regulation of glucose transport in skeletal muscle cells.

4.1 *TBC1D1*: An integrative model for AS and evolutionary dynamics in muscle metabolic regulation

Recent advances in genomic sequencing and analysis make bioinformatics invaluable for studying AS (Modrek & Lee, 2003; Sorek & Ast, 2003; Sugnet et al., 2004). Bioinformatics includes computational methods for analysing vast genomic datasets, enabling researchers to identify AS events with greater precision (Figures 12 and 14).

High-throughput technologies and computational tools for predicting regulatory control mechanisms in biological systems and mapping specific splicing factors continue to advance (Cartegni et al., 2002; Shepard & Hertel, 2008; Song et al., 2024). Yet, despite considerable technological progress—consider e.g. comparative genomic methods for analysing conservation across species and enabling the identification of alternative exons and regulatory elements—tools and technologies available for analysing AS have their limitations (Beye et al., 2003; Hasselmann et al., 2008). At the same time, technological advances help to explore and analyse the evolutionary flexibility of AS and its function in different species (Calarco et al., 2007; Clamp et al., 2007; Graveley, 2008; Zhang & Chasin, 2006).

4.1.1 Alternative splicing in TBC1D1 regulation

Previously, the pathobiochemistry group led by Prof. Hadi Al-Hasani at the Deutsche Diabetes Zentrum in Düsseldorf identified a variant of the murine *Tbc1d1* gene, resulting from a post-transcriptional regulatory mechanism affecting the gene expression (Chadt et al., 2008). This discovery, alongside other studies, underscores the role of AS in a range of diseases such as neurodegenerative disorders, cancer, cardiovascular diseases, and metabolic conditions and provides the foundation for this dissertation's investigation into AS in the context of post-transcriptional regulatory mechanisms of the human *TBC1D1* gene (Alvelos et al., 2018; Lipscombe et al., 2013; Paronetto et al., 2016; Rajan et al., 2010).

In this study, AS events were identified within *TBC1D1,* including exon skipping (ES) and alternative 3′ splice sites (A3´SS) in the *TBC1D1-SHORT* and *TBC1D1-LONG-GAPdel* isoforms, which are common events in mammalians (Figure 12). Analysis of the RabGAP domain gene sequences confirmed the presence of an A3´SS splice event, which introduces a gap of approximately 103 aa in the catalytic RabGAP domain of TBC1D1-LONG-GAPdel (Figure 13). Comparative genomic analysis revealed that this domain structure is conserved among primates and canidae (Figure 14). The conservation pattern of this domain structure suggests that the RabGAP domain has been preserved across different animal species

throughout evolution due to its essential biological role, likely related to glucose metabolism and cellular signaling, whereas discrepancies between species exist (Calixto et al., 2020; Park et al., 2011; Wilmes & Kummel, 2023).

Further, local alignment identified two motifs, PDMIIL and QMEK, indicating structural stability by accommodating insertions and deletions within the RabGAP domain (Figure 15). These motifs are highly conserved in primates, with slight modifications in Mus musculus, and absent in non-mammalian species such as Drosophila melanogaster, Arabidopsis thaliana, and Saccharomyces cerevisiae.

This study provides evidence on the TBC1D1 splice transcript variants diagram using a collection of AS tools, techniques and relevant genomic databases (Figures 11, 12 and 13). Analysis of the *TBC1D1* gene sequence revealed the conservation of two key motifs, PDMIIL and QMEK, in Homo sapiens and other primates. In Mus musculus, only the PDMIIL motif showed partial conservation, indicating the relevance of the RabGAP domain structure in cellular communication, development, physiology, and regulatory networks that are specific to animals (Thompson et al., 2015). The conservation of the two motifs indicates that the RabGAP domain function can exist in multiple forms, leading to proteins with varied functions. The divergence observed in the Mus musculus points to potential evolutionary adaptations, with sequence divergence potentially arising from gene duplication, functional redundancy, or other species-specific modifications (Sahm et al., 2018; Tigano et al., 2020).

The retention of these motifs across species suggests that evolutionary pressures conserved these sequences for their functional importance in primates, while organisms like plants and fungi either lack these processes or have evolved alternative mechanisms to fulfil similar cellular roles (Romero et al., 2012). The conservation in primates reflects the varying selective pressures that shaped *TBC1D1's* evolution. Accordingly, these motifs may have provided evolutionary advantages depending on environmental and genetic contexts. This hypothesis is supported by findings of *in vitro* investigations in this dissertation that reveal two muscle-specific variants of *TBC1D1, LONG* and *LONG-GAPdel*, along with the *SHORT* variant, whose expression is restricted to myoblasts. These findings are in accordance with previous research in the lean SJL mice strain, which identified two splice variants of *Tbc1d1*: a *Short* variant predominantly expressed in white adipose tissue and a *Long* variant identified in mouse skeletal muscle (Chadt et al., 2008).

Early research on closely related RabGAP protein TBC1D4 (also known as AS160) identified variant 2 (AS160_v2), which lacks exons 11 and 12. This deletion enhances insulin- and IGF-1-stimulated glucose uptake in skeletal muscle without affecting glucose uptake when stimulated by AICAR or metformin (Baus et al., 2008). Moreover, research has shown that the

long isoform of Tbc1d4 is particularly abundant in the mouse heart. Thus, RabGAP mRNA splicing and expression may be similarly regulated in cardiac muscle and the oxidative fibers of skeletal muscle (Binsch et al., 2023). This expression pattern underscores the tissue-specific demands for RabGAP activity, which could support the regulation of glucose transport and metabolic flexibility in high-energy tissues like the heart and skeletal muscle.

Consistent with the abovementioned findings, this dissertation demonstrates that the human *TBC1D1* gene exhibits both muscle-specific and non-muscular tissue variants. In addition, this work introduces a novel muscle-specific variant, LONG-GAPdel, which, unlike the full-length LONG isoform, undergoes AS events in the RabGAP domain gene sequence, resulting in a truncated RabGAP domain region with a completely unknown function. AS is a post-translational mechanism responsible for a single gene to produce different mRNA and protein isoforms, thereby contributing to the expansion of the transcriptome complexity and enhancing protein diversity. Its importance has attracted interest in various research areas, including metabolic disease since AS can impact the regulation of genes involved in metabolism and glucose uptake (Alvelos et al., 2018; Paronetto et al., 2016).

4.1.2 AS role in the genetic diversity and functional complexity of TBC1D1

A recent study, e.g. highlighted the influence of AS on the beta-cell response to inflammatory signals in type 1 diabetes mellitus (T1DM) progression, whereas the role of AS in type 2 diabetes mellitus (T2DM) remains an unexplored knowledge gap (Wu et al., 2021). This thesis investigates this knowledge gap by exploring how TBC1D1 AS contributes to glucose uptake in muscle under various physiological cues in the context of cellular energy processes. The findings herein broaden our understanding of the regulatory impact of AS on glucose metabolism and may open new avenues for therapeutic exploration in metabolic disorders. The dissertation contributes to understanding the genetic diversity and regulatory complexity of the human *TBC1D1* gene by having discovered a new splice variant of *TBC1D1*. The findings of this study enhance our understanding of the genetic diversity and regulatory intricacies of the human *TBC1D1* gene, marking the first characterisation and report of a novel splice variant that lacks amino acids within the RabGAP domain, resulting in the loss of RabGAP function in TBC1D1. Accordingly, this newly identified variant, TBC1D1-LONG GAPdel, is an indicator of regulatory complexity associated with AS and offers novel insight into the evolutionary development of the RabGAP domain function in humans compared to other species. The observations underscore how the RabGAP domain has adapted to specific metabolic cues, reflecting broader evolutionary flexibility.

The above aligns with recent findings in NAR Genomics and Bioinformatics that discuss the existence of multiple distinct evolutions of protein domain functions, called “domain isotypes” in humans. The literature traditionally has viewed protein domains as static, highly conserved structures. This view is being challenged by an emerging isoform-centric approach that emphasises functional diversity within a single gene (Juan-Mateu et al., 2016; Vitting-Seerup, 2023). By demonstrating the tissue-specific expression of alternative isoforms and the distinct RabGAP structure in LONG-GAPdel, this dissertation contributes to this emerging approach, showing that TBC1D1 exemplifies domain diversity at the protein level. The AS events observed in the data collected for this dissertation support the notion that isoform-centric research is essential to fully understand the functional variability introduced by AS in the regulation of critical metabolic pathways.

4.2 *TBC1D1* transcript variant expression and their RabGAP domain

4.2.1 *TBC1D1-LONG* and *TBC1D1-LONG-GAPdel* expressed in muscle

This dissertation validated the presence of *TBC1D1* splice variants in primary hMSCs and muscle biopsy samples, demonstrating distinct expression patterns. *TBC1D1-SHORT* variant is predominantly expressed in myoblasts, whereas the *LONG* and *LONG-GAPdel* splice variants are more prevalent in differentiated muscle cells (Figure 19). These findings highlight the role of AS in regulating TBC1D1 expression in muscle cell differentiation.

This thesis used two ex vivo cell models: primary hMSCs and muscle biopsies. Both models showed comparable expression patterns for the analysed MRFs and MSPs (Figure 18 and Supplementary Figure 2). *MyoD* plays a crucial role in driving myoblast differentiation into myotubes, so elevated expression of *MyoD* was expected in myotubes. However, *MyoD* expression was relatively low in both myotubes and muscle biopsy samples compared to myoblasts. This observation indicates a state of dormant differentiation, potentially reflective of the shift toward terminal differentiation. *MyoG*, an indicator of late-stage differentiation, showed significant expression in myotubes but was minimally expressed in mature muscle biopsy samples (Asfour et al., 2018; Engquist & Zammit, 2021). These observations support the tissue-specific expression patterns of the *SHORT*, *LONG*, and *LONG-GAPdel* splice variants in primary hMSCs and underscore the transition from early to late differentiation states in muscle cells. The minimal expression of *MyoD* in mature muscle tissue, despite its critical role in promoting myoblast differentiation, suggests a shift toward terminal differentiation. This is further supported by elevated *MyoG* expression in myotubes, notably absent in mature

muscle biopsies. The findings demonstrate that *TBC1D1* splice variants, particularly *LONG-GAPdel*, are intricately linked to differentiation states and muscle-specific functionality. The identification of *LONG-GAPdel* as a muscle-specific isoform with unique structural features provides new insights into the regulation of RabGAP domain activity and its potential role in muscle physiology.

4.2.2 Muscle-specific *LONG-GAPdel* splice variant characterisation

This thesis identifies the LONG-GAPdel isoform as a muscle-specific isoform with no known functional homolog in TBC1D4. This isoform possesses two distinct AS events within its RabGAP domain structure: an exon skipping (ES) combined with an alternative 3´splice site (A3´SS), resulting in a truncated protein structure that lacks RabGAP activity (Figures 12, 13, and 21). The *LONG-GAPdel* isoform was detected in three healthy male donors using RNA sequencing, a technique that enabled broader and more sensitive detection of low-abundance transcripts across the genome (Figure 10).

The PCR-based methods employed in this study, particularly when studying TBC1D1-*LONG-GAPdel* expression dynamics, generated only output focused on pre-selected regions of interest. Therefore, this approach was limited in exploring low-abundant transcripts or detecting minor and yet significant gene expression changes. The primers designed for this study faced challenges due to the high sequence homology between *LONG-GAPdel* and *LONG,* reducing amplification efficiency for the *LONG-GAPdel* isoform (Figure 20). These limitations underscore the need for advanced sequencing technologies to achieve comprehensive isoform detection and characterisation.

4.2.3 Challenges in muscle-specific splice variant characterisation

The RabGAP TBC domain region in the LONG and LONG-GAPdel variants is rich in purines (adenine and guanine) and pyrimidines (cytosine and thymine), making their discrimination more complex when analysed with the methods used in this dissertation (Supplementary Figure 5). To overcome the target region’s rich content in purines and pyrimidines, multiple strategies were implemented, including primer design optimisation for GC content, touchdown PCR, Nested PCR, and a Polymerase Chain Reaction-Restriction Fragment Length Polymorphism (PCR-RFLP) analysis, followed by sequencing of the PCR product (data not shown). Despite these measurements, the distinction between *LONG* and

LONG-GAPdel remained challenging, likely due to extreme sequence homogeneity exceeding the discriminatory power of traditional PCR-based methods. Moreover, the binding kinetics in this purine/pyrimidine-rich region may not be sufficiently favourable for differential amplification.

Detecting *LONG-GAPdel* expression may be influenced by different genetic variations within the primary hMSCs and mature muscle biopsy samples. This dissertation establishes that the *LONG-GAPdel* transcript variant may arise from genetic alterations caused by DNA sequences, resulting in gene expression and protein function changes. This finding aligns with the concept of mosaicism, a condition in which an individual has genetically distinct cell populations across different tissues. Mosaicism has been reported in various genetic alterations, including trisomy, monosomy, deletions, duplications, and other rare alterations (Campbell et al., 2015; Freed et al., 2014; Kerwin et al., 2023; Spinner & Conlin, 2014).

The clinical manifestation of mosaicism depends on the mutation type, the proportion of cells affected by that mutation, and the tissue distribution of the genetic change, making the identification of low-level mosaic pathogenic variants particularly challenging. Given the low abundance of the *LONG-GAPdel* transcript variant observed in this dissertation (Figure 20), it is plausible that this variant represents a somatic mutation, which may occur later in the cell lifespan, generally affecting fewer cells (Supplementary Figure 4).

In cellular signaling, cells communicate with each other and respond to various internal and external stimuli. Each cell type, including myoblasts and myotubes, responds uniquely to molecular interactions, meaning that a mosaic mutation could alter signaling responses differently across cell types. The presence of a loss-of-function mutation as a mosaic in a subset of myotubes would create a heterogeneous cell population, with both standard and mutated myotubes. This mosaic mutation, *LONG-GAPdel*, appears to disrupt GTP hydrolysis function by causing substantial dysfunction in the regulation of GLUT4 transportation.

In short, this dissertation points out the complexity of cellular responses to mutations, highlighting how the same mutation can have different impacts across cell types. This understanding is crucial for studying diseases driven by mosaic mutations, as it explains why specific cells within tissues may be severely affected while others are exempt (Supplementary Figure 4).

The broader concept of different splice variants influencing various diseases is well-documented (Kim et al., 2018). For example, a recognised loss-of-function mutation in TBC1D4 has been associated with postprandial hyperglycemia and an increased risk of type 2 diabetes (T2D), explicitly affecting the LONG muscle isoform of the protein (Moltke et al., 2014). Similarly, earlier research has investigated the role of AS in osteoclasts related to

Paget's disease of bone (PDB). Their analysis identified six AS events significantly associated with PDB, implicating genes like TBC1D25 and underscoring the role of AS in osteoclast biology (Klinck et al., 2014).

In conclusion, the findings presented in this section contribute to a deeper understanding of how splicing variations, especially when coupled with mosaicism, influence disease mechanisms. Mosaic mutations and splice variants such as *LONG-GAPdel* illustrate how genetic diversity within cells can lead to distinct physiological effects, particularly in complex diseases. The findings here emphasise the importance of exploring genetic heterogeneity and splicing variations to unravel the nuanced mechanisms underlying metabolic disorders and other diseases that AS influences.

4.3 TBC1D1-LONG and LONG-GAPdel functions characterisation

To explore the molecular functions of muscle-specific *TBC1D1* variants, this dissertation focused on the *LONG-GAPdel* variant compared to the wild-type *LONG* isoform, applying *in vitro* approaches. Studying these specific isoforms, resulting from AS of *TBC1D1*, provides insights into the complex regulatory mechanisms underlying the transport of glucose from the bloodstream into the cells, facilitated by GLUT4 translocation to the plasma membrane of the cells (Belfiore et al., 2017).

4.3.1 RabGAP activity of TBC1D1 LONG and TBC1D1 LONG-GAPdel

This dissertation provides evidence of the molecular function of the two muscle-specific TBC1D1 variants, specifically that LONG-GAPdel is enabled to hydrolyse GTP compared to LONG (Figure 21), although both isoforms exhibit essential structural elements of GTP hydrolysis, including the "arginine finger" and "glutamine finger," which are essential to the RabGAP catalytic activity (Majumdar et al., 2017; Pan et al., 2006; Park et al., 2011).

As illustrated by Figure 21B-D, neither the recombinant RabGAP domain assays nor the full-length LONG-GAPdel proteins exhibit significant catalysis of GTP hydrolysis activity toward Rab8a and Rab10, two key downstream targets of TBC1D1 (Benninghoff et al., 2020; Ishikura & Klip, 2008; Jaldin-Fincati et al., 2017; Roach et al., 2007). The observed GTP hydrolysis of the downstream Rab GTPases upon interaction with the GAPdel variant is comparable to that of a TBC1D1 protein with a disruption of the GAP domain function induced

by replacing the “arginine finger” with a lysine (R/K mutant) (Mafakheri, Florke, et al., 2018; Park et al., 2011; Zhou et al., 2017).

This observation suggests a more complex regulatory function of the TBC1D1 RabGAP domain structure beyond the conventional finger-like interaction structures, possibly involving additional regulatory roles influenced by AS events. Figure 12 highlights the presence of ES and an A3´SS event, both AS events are commonly associated with tissue-specific expression patterns (Lee et al., 2023; Wang et al., 2008). These splicing events contribute to the misregulation of the conserved TBC-GAP protein domain by missing amino acids carrying the catalytic function of the LONG-GAPdel isoform (Fukuda, 2011; Gavriljuk et al., 2012; Park et al., 2011; Sano et al., 2003).

4.3.2 Phosphorylation dynamics on TBC1D1 isoforms

In addition to structural analysis, kinase assays were applied to explore further how phosphorylation impacts the function of TBC1D1 isoforms. Previous studies, including work from Prof. Hadi Al-Hasani’s pathobiochemistry group at the Deutsche Diabetes Zentrum in Düsseldorf, have shown that the kinases AKT2 and AMPK play key roles in insulin-stimulated and contraction-induced GLUT4 translocation in skeletal muscle by distinct phosphorylation patterns of TBC1D1 (Chen et al., 2008; Fritzen et al., 2016; Kjobsted et al., 2019; Mafakheri, Florke, et al., 2018; Taylor et al., 2008; Treebak et al., 2014).

In this dissertation, kinase assays with recombinant full-length TBC1D1-LONG and TBC1D1-LONG-GAPdel proteins, pre-incubated with either AKT2 or AMPK, revealed comparable phosphorylation patterns for both isoforms at the primary AMPK target site, Ser^{237}, and the predominant AKT2 site, Thr^{596}. Incubation with AKT2 did not result in differences in the phosphorylation state of Ser^{667} or Ser^{707}, whereas AMPK effectively phosphorylated the LONG isoform at these sites (Figure 22).

These observations suggest that under AMPK stimulation, the LONG isoform undergoes enhanced phosphorylation, which likely inhibits its RabGAP function. Consequently, its inhibitory role on the Rab GTPases, which coordinate the translocation of GLUT4 to the plasma membrane, is removed.

4.3.3 TBC1D1 isoforms interaction with cIRAP and GSVs translocation

Previous studies have described the insulin-regulated aminopeptidase (IRAP) as a resident protein in the GSVs (Bogan & Kandror, 2010; Jordens et al., 2010). Our research group has previously shown that in murine models, the interaction between Tbc1d1 and cIRAP is phosphorylation-dependent, as the binding of non-phosphorylated Tbc1d1 to cIRAP is abolished upon phosphorylation by AKT2 or AMPK (Mafakheri, Florke, et al., 2018). However, this dissertation observed no significant difference in cIRAP binding between TBC1D1 isoforms LONG and LONG-GAPdel (Figure 23).

Upon phosphorylation, and regardless of the occurring phosphosites, Thr^{596} or Ser^{667}, both isoforms' interaction with cIRAP is significantly compromised and almost disrupted. This suggests that the localisation of both isoforms is adjacent to the GLUT4 vesicle-recruiting protein IRAP and is regulated through phosphorylation. Furthermore, the data indicate that AKT2 preferentially enhances the activity of LONG-GAPdel over LONG. This suggests that under AKT2 stimulation, LONG-GAPdel might become more abundant and potentially assume the functional role of LONG.

Without its GTP hydrolysis capability, LONG-GAPdel could lead to a shift in the signaling pathway of TBC1D1, resulting in a constitutively active state. This might cause Rabs to be loaded with GDP and effectively prevent GLUT4 translocation to the plasma membrane. This hypothesis aligns with the phosphorylation and binding patterns observed in Figure 22. In addition, the literature demonstrates the significance of the functional GAP and N-terminal PTB domains in TBC1D1 and TBC1D4, emphasising their role in regulating skeletal muscle energy metabolism. For example, heterodimers formed between the PTB domains of wild-type TBC1D4 and a loss-of-function mutation have been shown to cause acanthosis nigricans and postprandial hyperinsulinemia in humans, where the mutant form of TBC1D4 affect the RabGAP function in a dominant-negative manner (Dash et al., 2010; Dash et al., 2009). Additionally, TBC1D4 dimerization is facilitated by a largely α-helical region C-terminal to the RabGAP domain, including a coiled-coil motif (Woo et al., 2017).

Structural analysis in the present study revealed that both the TBC1D1 LONG and LONG-GAP isoforms primarily possess α-helical structures throughout their domain architectures, including the location of the RabGAP domain region (amino acids 875-1125), as shown in Figure 24. Both isoforms display no significant structural differences. Moreover, both isoforms can undergo dimerization, and the LONG-GAPdel isoform appears to affect the heterodimerisation complex in a dominant-negative manner, as depicted in Figure 25.

The results indicate that TBC1D1-LONG and TBC1D1-LONG-GAPdel are muscle-specific variants capable of dimerization, a process that has been previously linked to GLUT4 vesicle fusion with the plasma membrane (Koumanov et al., 2011; Park et al., 2011).

In summary, these results highlight the complex regulatory role of *TBC1D1* variants in glucose transport into muscle cells facilitated by GLUT4 transporters and underscore the potential for tissue-specific adaptations in muscle cells. The ability of the LONG-GAPdel isoform to affect TBC1D1 signaling through non-catalytic, structural interactions emphasises the broader importance of protein architecture and dimerization in metabolic regulation.

5. Conclusion & Outlook

This dissertation completes its research goals by providing evidence of the presence of AS in *TBC1D1* and the differential expression of the transcript variants in muscle cells. We demonstrate that the main difference between the two muscle-specific splice isoforms, TBC1D1-LONG and TBC1D1-LONG-GAPdel, is the absence of the RabGAP activity, notably the disturbed GTP hydrolysis function of the TBC1D1-LONG-GAPdel isoform. In addition, this thesis concludes that the dimerization of TBC1D1-LONG-GAPdel with TBC1D1-LONG appears unaffected by the truncated GAP domain. Therefore, we postulate that LONG-GAPdel outperforms LONG, altering the protein's original function. This misregulation likely affects Rab substrates and interactions with protein partners, such as cIRAP, potentially impairing the distribution of GSVs containing GLUT4 at the plasma membrane, thus altering glucose and fatty acid utilisation within cells. In conclusion, this research uncovered how the interactions between AKT2, AMPK, and TBC1D1 isoforms induce glucose uptake in muscle cells, elucidating the complexity of RabGAP function under insulin-contraction-mediated glucose uptake.

This dissertation provides new evidence on the intricate relationship between AS and the regulatory molecular mechanisms that govern RabGAP function in glucose uptake primarily facilitated by GLUT4 in skeletal muscle cells, a finding supported by *in vitro* analysis (Figure 26). The collective findings presented offer novel insights into the dynamics of glucose uptake regulation in response to AKT2 and AMPK, along with the TBC1D1 isoforms. These insights deepen the understanding of cellular adaptations to energy demands, exercise, and insulin signaling, illuminating the mechanisms by which cells adjust their metabolic pathways (de Wendt et al., 2021; Holman, 2020).

Moreover, the low affinity of AMPK for the LONG-GAPdel isoform, observed in this dissertation, suggests that the LONG-GAPdel isoform might act as a secondary regulatory checkpoint, maintaining Rab GTPases in an inactive state and promoting the retention of the GSVs under basal cellular conditions. By preventing excessive GLUT4 translocation to the plasma membrane, the LONG-GAPdel isoform can modulate cellular responses to metabolic cues, acting as a regulatory brake (Figure 26C). Accordingly, this dissertation contributes to a deeper understanding of the mechanisms involved in glucose uptake, which in turn may provide the scientific foundations for developing new antidiabetic therapies and treatments against insulin resistance. Further, this dissertation contributes to a broader understanding of the mechanisms involved in glucose uptake because RabGAP function has previously not been studied in the context of AS.

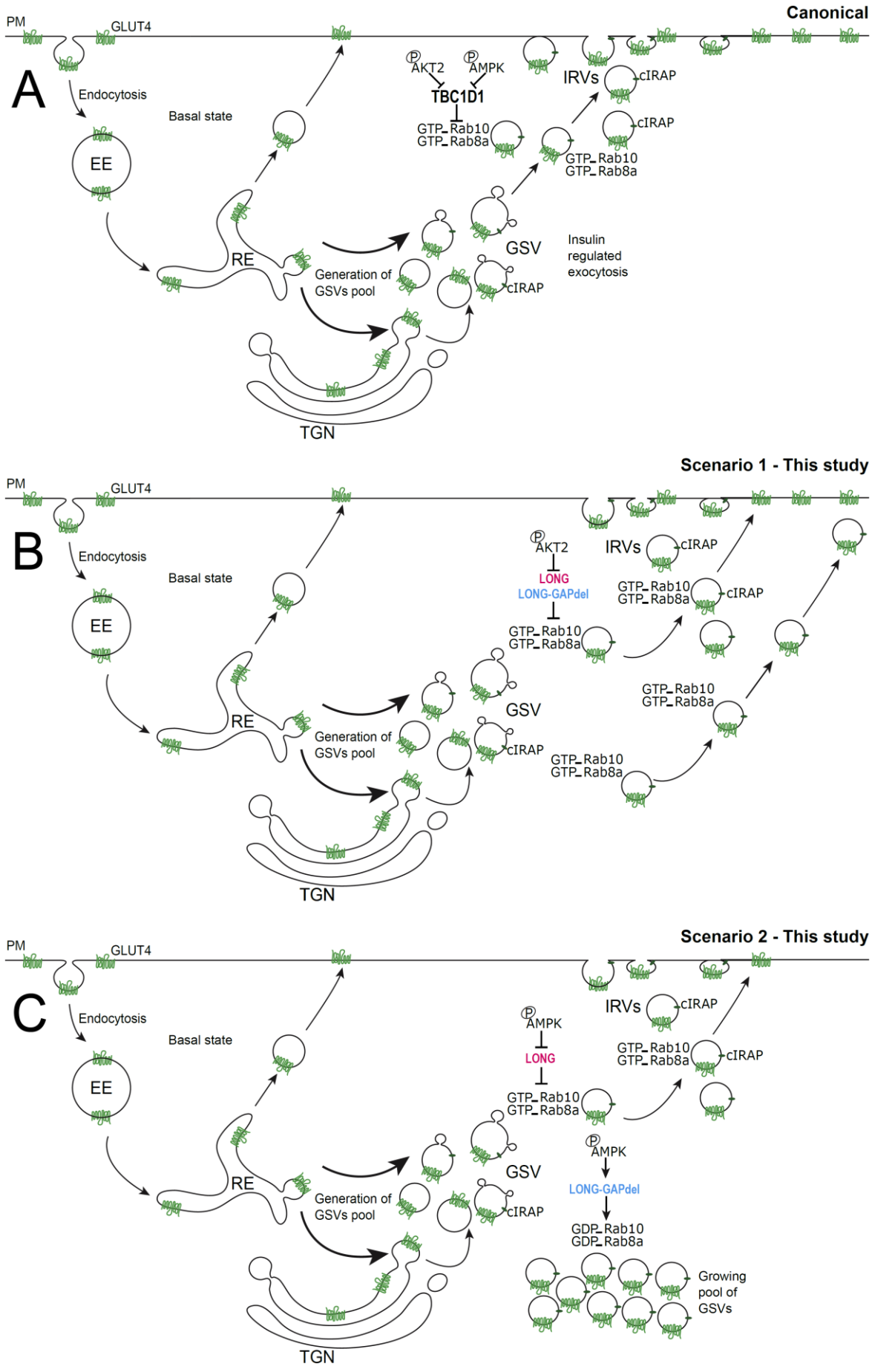
Canonical
A
PM
GLUT4
Endocytosis
Basal state
EE
RE
Generation of
GSVs pool
GSV
cIRAP
Insulin
regulated
exocytosis
AKT2
AMPK
TBC1D1
GTP_Rab10
GTP_Rab8a
IRVs
cIRAP
TGN
Scenario 1 - This study
B
LONG
LONG-GAPdel
Scenario 2 - This study
C
Growing
pool of
GSVs
GDP_Rab10
GDP_Rab8a

<u>Figure 26</u>: Effect of TBC1D1 splicing on the distribution of glucose transporters from intracellular storage vesicles to the plasma membrane of skeletal muscle (Source: adapted from Jaldin-Fincati, 2017)

(A) Illustration of the canonical signal events in a basal state and insulin-regulated GLUT4 translocation. At basal state, GLUT4 is constitutively recycled to and from the plasma membrane (PM), passing by the early endosomes (EE) to the recycled endosomes (RE). This dynamic sorting under insulin stimuli activates the generation of the glucose storage vesicles (GSV) and insulin-responsive vesicles (IRVs) from the RE and the trans-Golgi network (TGN). TBC1D1, responsible for vesicle sorting and mobilisation, has its GAP function inhibited under AKT2 and AMPK. Consequently, Rab8a and Rab10 bind to GTP, their active form, which mobilised the distribution of GSVs and IRVs to the PM via the insertion of GLUT4 into the membrane to allow glucose uptake. (B) Illustration of hypothetical new signal events in GLUT4 distribution at the PM under AKT2 and AMPK cues derived from this study. Under AKT2 stimuli, the GAP function of LONG and LONG-GAPdel isoforms are inhibited with no difference of apparent affinity. Subsequently, both Rabs studied remained active and mobilised the distribution of GSVs and IRVs to the PM via the insertion of GLUT4 into the membrane to allow glucose uptake (scenario 1). (C) Under AMPK stimuli, LONG isoform GAP function inhibition is enhanced, promoting a pool of active Rab8a and Rab10, which assists in distributing GSVs and IRVs at the PM. Subsequently, the absence of the GAP function of the LONG-GAPdel isoform likely contributes to promoting the inactive form of the Rab8a and Rab10, consequently maintaining a growing pool of GSVs in the intracellular membrane with a low rate of distribution of IRV at the PM of the cell (scenario 2). Abbreviations: PM, plasma membrane; EE, early endosomes; RE, recycling endosomes; IRV, insulin-responsive vesicles; GSV, glucose storage vesicles; TGN, trans-Golgi network.

Future research building on these findings could employ advanced RNA sequencing techniques, such as Isoform- or single-cell RNA --sequencing, to span the entire transcripts from 5´to 3´ends without the need for assembly or the provision of unambiguous evidence of the composition of individual transcript isoforms. These methods could provide a complete understanding of the dynamics of TBC1D1 AS and may reveal other low-abundance isoforms that conventional techniques might miss. Understanding the altered patterns of AS in *TBC1D1* pre-mRNAs might reveal how these changes may subtly but measurably affect drug efficacy and disease severity (Lipscombe et al., 2013). These insights can contribute to shaping and refining therapeutic strategies and interventions, offering targeted approaches to address specific splicing variations.

Moreover, research might explore the interaction partners, such as 14-3-3 and APPL2, of these two muscle-specific isoforms, which are known to influence cellular signaling pathways (Wu & Lu, 2021). An *in vivo* validation of *LONG-GAPdel* as a potential pathogenic variant in the context of genetics and molecular biology may also provide insights into the

genetic mechanisms underlying glucose uptake into cells, offering potential diagnostic and therapeutic possibilities for T2DM (Highland et al., 2023; Lee et al., 2023; Wu & Lu, 2021).

The function of the muscle-specific variant LONG-GAPdel, especially its unique regulatory features, remains a promising area for study in cells because knocking down and/or overexpressing this isoform in the cells may provide insightful perspectives on the glucose uptake mechanism *in vitro*. Likewise, an integrated approach that combines *in vitro* and *in vivo* studies using in-tissue validations may help confirm if the *TBC1D1* expression patterns observed in this study are mirrored in T2DM patients.

Quantifying *TBC1D1* expression in tissue samples from affected populations could become the basis for developing personalised treatments. Techniques such as in situ hybridisation, immunohistochemistry, and RNA fluorescence in situ hybridisation might be instrumental, offering direct in situ visualisation of the isoform distributions identified in this thesis.

Finally, future research may benefit from focusing on omics-based methods to achieve precise spatial and temporal mapping of TBC1D1 isoforms. This could reveal the structural and functional plasticity of TBC1D1 regulation in insulin-, contraction-responsive skeletal muscle. Such mapping may enable the development of interventions targeting specific subgroups within the T2DM population, potentially resulting in new therapeutic options tailored to the distinct molecular profiles of these patients.

6. References

Aguayo-Mazzucato, C., & Bonner-Weir, S. (2018). Pancreatic beta Cell Regeneration as a Possible Therapy for Diabetes. *Cell Metab*, *27*(1), 57-67. https://doi.org/10.1016/j.cmet.2017.08.007

Akizawa, Y., Kanno, H., Kawamichi, Y., Matsuda, Y., Ohta, H., Fujii, H., Matsui, H., & Saito, K. (2013). Enhanced expression of myogenic differentiation factors and skeletal muscle proteins in human amnion-derived cells via the forced expression of MYOD1. *Brain Dev*, *35*(4), 349-355. https://doi.org/10.1016/j.braindev.2012.05.012

Albers, P. H., Pedersen, A. J., Birk, J. B., Kristensen, D. E., Vind, B. F., Baba, O., Nohr, J., Hojlund, K., & Wojtaszewski, J. F. (2015). Human muscle fiber type-specific insulin signaling: impact of obesity and type 2 diabetes. *Diabetes*, *64*(2), 485-497. https://doi.org/10.2337/db14-0590

Ali, M. K., Pearson-Stuttard, J., Selvin, E., & Gregg, E. W. (2022). Interpreting global trends in type 2 diabetes complications and mortality. *Diabetologia*, *65*(1), 3-13. https://doi.org/10.1007/s00125-021-05585-2

Alvelos, M. I., Juan-Mateu, J., Colli, M. L., Turatsinze, J. V., & Eizirik, D. L. (2018). When one becomes many-Alternative splicing in beta-cell function and failure. *Diabetes Obes Metab*, *20 Suppl 2*(Suppl 2), 77-87. https://doi.org/10.1111/dom.13388

An, D., Toyoda, T., Taylor, E. B., Yu, H., Fujii, N., Hirshman, M. F., & Goodyear, L. J. (2010). TBC1D1 regulates insulin- and contraction-induced glucose transport in mouse skeletal muscle. *Diabetes*, *59*(6), 1358-1365. https://doi.org/10.2337/db09-1266

Asfour, H. A., Allouh, M. Z., & Said, R. S. (2018). Myogenic regulatory factors: The orchestrators of myogenesis after 30 years of discovery. *Exp Biol Med (Maywood)*, *243*(2), 118-128. https://doi.org/10.1177/1535370217749494

Baer, K., Lisinski, I., Gompert, M., Stuhlmann, D., Schmolz, K., Klein, H. W., & Al-Hasani, H. (2005). Activation of a GST-tagged AKT2/PKBbeta. *Biochim Biophys Acta*, *1725*(3), 340-347. https://doi.org/10.1016/j.bbagen.2005.04.002

Baharlou Houreh, M., Ghorbani Kalkhajeh, P., Niazi, A., Ebrahimi, F., & Ebrahimie, E. (2018). SpliceDetector: a software for detection of alternative splicing events in human and model organisms directly from transcript IDs. *Sci Rep*, *8*(1), 5063. https://doi.org/10.1038/s41598-018-23245-1

Balakrishnan, R., & Thurmond, D. C. (2022). Mechanisms by Which Skeletal Muscle Myokines Ameliorate Insulin Resistance. *Int J Mol Sci*, *23*(9). https://doi.org/10.3390/ijms23094636

Bano, G. (2013). Glucose homeostasis, obesity and diabetes. *Best Pract Res Clin Obstet Gynaecol*, *27*(5), 715-726. https://doi.org/10.1016/j.bpobgyn.2013.02.007

Baralle, M., & Baralle, F. E. (2021). Alternative splicing and liver disease. *Ann Hepatol*, *26*, 100534. https://doi.org/10.1016/j.aohep.2021.100534

Baus, D., Heermeier, K., De Hoop, M., Metz-Weidmann, C., Gassenhuber, J., Dittrich, W., Welte, S., & Tennagels, N. (2008). Identification of a novel AS160 splice variant that regulates GLUT4 translocation and glucose-uptake in rat muscle cells. *Cell Signal*, *20*(12), 2237-2246. https://doi.org/10.1016/j.cellsig.2008.08.010

Belfiore, A., Malaguarnera, R., Vella, V., Lawrence, M. C., Sciacca, L., Frasca, F., Morrione, A., & Vigneri, R. (2017). Insulin Receptor Isoforms in Physiology and Disease: An Updated View. *Endocr Rev*, *38*(5), 379-431. https://doi.org/10.1210/er.2017-00073

Bennett, C. F., Krainer, A. R., & Cleveland, D. W. (2019). Antisense Oligonucleotide Therapies for Neurodegenerative Diseases. *Annu Rev Neurosci*, *42*, 385-406. https://doi.org/10.1146/annurev-neuro-070918-050501

Bennett, C. F., & Swayze, E. E. (2010). RNA targeting therapeutics: molecular mechanisms of antisense oligonucleotides as a therapeutic platform. *Annu Rev Pharmacol Toxicol*, *50*, 259-293. https://doi.org/10.1146/annurev.pharmtox.010909.105654

Benninghoff, T., Espelage, L., Eickelschulte, S., Zeinert, I., Sinowenka, I., Muller, F., Schondeling, C., Batchelor, H., Cames, S., Zhou, Z., Kotzka, J., Chadt, A., & Al-Hasani, H. (2020). The RabGAPs TBC1D1 and TBC1D4 Control Uptake of Long-Chain Fatty Acids Into Skeletal Muscle via Fatty Acid Transporter SLC27A4/FATP4. *Diabetes*, *69*(11), 2281-2293. https://doi.org/10.2337/db20-0180

Beye, M., Hasselmann, M., Fondrk, M. K., Page, R. E., & Omholt, S. W. (2003). The gene csd is the primary signal for sexual development in the honeybee and encodes an SR-type protein. *Cell*, *114*(4), 419-429. https://doi.org/10.1016/s0092-8674(03)00606-8

Binsch, C., Barbosa, D. M., Hansen-Dille, G., Hubert, M., Hodge, S. M., Kolasa, M., Jeruschke, K., Weiss, J., Springer, C., Gorressen, S., Fischer, J. W., Lienhard, M., Herwig, R., Borno, S., Timmermann, B., Cremer, A. L., Backes, H., Chadt, A., & Al-Hasani, H. (2023). Deletion of Tbc1d4/As160 abrogates cardiac glucose uptake and increases myocardial damage after ischemia/reperfusion. *Cardiovasc Diabetol*, *22*(1), 17. https://doi.org/10.1186/s12933-023-01746-2

Black, D. L. (2003). Mechanisms of alternative pre-messenger RNA splicing. *Annu Rev Biochem*, *72*, 291-336. https://doi.org/10.1146/annurev.biochem.72.121801.161720

Bogan, J. S., & Kandror, K. V. (2010). Biogenesis and regulation of insulin-responsive vesicles containing GLUT4. *Curr Opin Cell Biol*, *22*(4), 506-512. https://doi.org/10.1016/j.ceb.2010.03.012

Boucher, J., Kleinridders, A., & Kahn, C. R. (2014). Insulin receptor signaling in normal and insulin-resistant states. *Cold Spring Harb Perspect Biol*, *6*(1). https://doi.org/10.1101/cshperspect.a009191

Brahma, M. K., Xiao, P., Popa, M., Negueruela, J., Vandenbempt, V., Demine, S., Cardozo, A. K., & Gurzov, E. N. (2022). Nova1 or Bim Deficiency in Pancreatic beta-Cells Does Not Alter Multiple Low-Dose Streptozotocin-Induced Diabetes and Diet-Induced Obesity in Mice. *Nutrients*, *14*(18). https://doi.org/10.3390/nu14183866

Bryant, N. J., & Gould, G. W. (2011). SNARE proteins underpin insulin-regulated GLUT4 traffic. *Traffic*, *12*(6), 657-664. https://doi.org/10.1111/j.1600-0854.2011.01163.x

Calarco, J. A., Xing, Y., Caceres, M., Calarco, J. P., Xiao, X., Pan, Q., Lee, C., Preuss, T. M., & Blencowe, B. J. (2007). Global analysis of alternative splicing differences between humans and chimpanzees. *Genes Dev*, *21*(22), 2963-2975. https://doi.org/10.1101/gad.1606907

Calixto, A. R., Moreira, C., & Kamerlin, S. C. L. (2020). Recent Advances in Understanding Biological GTP Hydrolysis through Molecular Simulation. *ACS Omega*, *5*(9), 4380-4385. https://doi.org/10.1021/acsomega.0c00240

Campbell, I. M., Shaw, C. A., Stankiewicz, P., & Lupski, J. R. (2015). Somatic mosaicism: implications for disease and transmission genetics. *Trends Genet*, *31*(7), 382-392. https://doi.org/10.1016/j.tig.2015.03.013

Cao, H., & Shockey, J. M. (2012). Comparison of TaqMan and SYBR Green qPCR methods for quantitative gene expression in tung tree tissues. *J Agric Food Chem*, *60*(50), 12296-12303. https://doi.org/10.1021/jf304690e

Carling, D. (2017). AMPK signalling in health and disease. *Curr Opin Cell Biol*, *45*, 31-37. https://doi.org/10.1016/j.ceb.2017.01.005

Cartee, G. D. (2015). Roles of TBC1D1 and TBC1D4 in insulin- and exercise-stimulated glucose transport of skeletal muscle. *Diabetologia*, *58*(1), 19-30. https://doi.org/10.1007/s00125-014-3395-5

Cartegni, L., Chew, S. L., & Krainer, A. R. (2002). Listening to silence and understanding nonsense: exonic mutations that affect splicing. *Nat Rev Genet*, *3*(4), 285-298. https://doi.org/10.1038/nrg775

Chadt, A., Immisch, A., de Wendt, C., Springer, C., Zhou, Z., Stermann, T., Holman, G. D., Loffing-Cueni, D., Loffing, J., Joost, H. G., & Al-Hasani, H. (2015). "Deletion of both Rab-GTPase-activating proteins TBC1D1 and TBC1D4 in mice eliminates insulin- and AICAR-stimulated glucose transport [corrected]. *Diabetes*, *64*(3), 746-759. https://doi.org/10.2337/db14-0368

Chadt, A., Leicht, K., Deshmukh, A., Jiang, L. Q., Scherneck, S., Bernhardt, U., Dreja, T., Vogel, H., Schmolz, K., Kluge, R., Zierath, J. R., Hultschig, C., Hoeben, R. C., Schurmann, A., Joost, H. G., &

Al-Hasani, H. (2008). Tbc1d1 mutation in lean mouse strain confers leanness and protects from diet-induced obesity. *Nat Genet*, *40*(11), 1354-1359. https://doi.org/10.1038/ng.244

Chavez, J. A., Roach, W. G., Keller, S. R., Lane, W. S., & Lienhard, G. E. (2008). Inhibition of GLUT4 translocation by Tbc1d1, a Rab GTPase-activating protein abundant in skeletal muscle, is partially relieved by AMP-activated protein kinase activation. *J Biol Chem*, *283*(14), 9187-9195. https://doi.org/10.1074/jbc.M708934200

Chen, M., & Manley, J. L. (2009). Mechanisms of alternative splicing regulation: insights from molecular and genomics approaches. *Nat Rev Mol Cell Biol*, *10*(11), 741-754. https://doi.org/10.1038/nrm2777

Chen, S., Murphy, J., Toth, R., Campbell, D. G., Morrice, N. A., & Mackintosh, C. (2008). Complementary regulation of TBC1D1 and AS160 by growth factors, insulin and AMPK activators. *Biochem J*, *409*(2), 449-459. https://doi.org/10.1042/BJ20071114

Cheng, K. C., Burdine, R. D., Dickinson, M. E., Ekker, S. C., Lin, A. Y., Lloyd, K. C. K., Lutz, C. M., MacRae, C. A., Morrison, J. H., O'Connor, D. H., Postlethwait, J. H., Rogers, C. D., Sanchez, S., Simpson, J. H., Talbot, W. S., Wallace, D. C., Weimer, J. M., & Bellen, H. J. (2022). Promoting validation and cross-phylogenetic integration in model organism research. *Dis Model Mech*, *15*(9). https://doi.org/10.1242/dmm.049600

Cheng, K. K., Zhu, W., Chen, B., Wang, Y., Wu, D., Sweeney, G., Wang, B., Lam, K. S., & Xu, A. (2014). The adaptor protein APPL2 inhibits insulin-stimulated glucose uptake by interacting with TBC1D1 in skeletal muscle. *Diabetes*, *63*(11), 3748-3758. https://doi.org/10.2337/db14-0337

Chew, Y. H., Shia, Y. L., Lee, C. T., Majid, F. A., Chua, L. S., Sarmidi, M. R., & Aziz, R. A. (2009). Modeling of glucose regulation and insulin-signaling pathways. *Mol Cell Endocrinol*, *303*(1-2), 13-24. https://doi.org/10.1016/j.mce.2009.01.018

Chua, C. E., & Tang, B. L. (2015). Role of Rab GTPases and their interacting proteins in mediating metabolic signalling and regulation. *Cell Mol Life Sci*, *72*(12), 2289-2304. https://doi.org/10.1007/s00018-015-1862-x

Clamp, M., Fry, B., Kamal, M., Xie, X., Cuff, J., Lin, M. F., Kellis, M., Lindblad-Toh, K., & Lander, E. S. (2007). Distinguishing protein-coding and noncoding genes in the human genome. *Proc Natl Acad Sci U S A*, *104*(49), 19428-19433. https://doi.org/10.1073/pnas.0709013104

Collins, C. A., Gnocchi, V. F., White, R. B., Boldrin, L., Perez-Ruiz, A., Relaix, F., Morgan, J. E., & Zammit, P. S. (2009). Integrated functions of Pax3 and Pax7 in the regulation of proliferation, cell size and myogenic differentiation. *PLoS One*, *4*(2), e4475. https://doi.org/10.1371/journal.pone.0004475

Corbeel, L., & Freson, K. (2008). Rab proteins and Rab-associated proteins: major actors in the mechanism of protein-trafficking disorders. *Eur J Pediatr*, *167*(7), 723-729. https://doi.org/10.1007/s00431-008-0740-z

Czech, M. P. (2017). Insulin action and resistance in obesity and type 2 diabetes. *Nat Med*, *23*(7), 804-814. https://doi.org/10.1038/nm.4350

Dash, S., Langenberg, C., Fawcett, K. A., Semple, R. K., Romeo, S., Sharp, S., Sano, H., Lienhard, G. E., Rochford, J. J., Howlett, T., Massoud, A. F., Hindmarsh, P., Howell, S. J., Wilkinson, R. J., Lyssenko, V., Groop, L., Baroni, M. G., Barroso, I., Wareham, N. J.,…Savage, D. B. (2010). Analysis of TBC1D4 in patients with severe insulin resistance. *Diabetologia*, *53*(6), 1239-1242. https://doi.org/10.1007/s00125-010-1724-x

Dash, S., Sano, H., Rochford, J. J., Semple, R. K., Yeo, G., Hyden, C. S., Soos, M. A., Clark, J., Rodin, A., Langenberg, C., Druet, C., Fawcett, K. A., Tung, Y. C., Wareham, N. J., Barroso, I., Lienhard, G. E., O'Rahilly, S., & Savage, D. B. (2009). A truncation mutation in TBC1D4 in a family with acanthosis nigricans and postprandial hyperinsulinemia. *Proc Natl Acad Sci U S A*, *106*(23), 9350-9355. https://doi.org/10.1073/pnas.0900909106

de Wendt, C., Espelage, L., Eickelschulte, S., Springer, C., Toska, L., Scheel, A., Bedou, A. D., Benninghoff, T., Cames, S., Stermann, T., Chadt, A., & Al-Hasani, H. (2021). Contraction-Mediated Glucose Transport in Skeletal Muscle Is Regulated by a Framework of AMPK, TBC1D1/4, and Rac1. *Diabetes*, *70*(12), 2796-2809. https://doi.org/10.2337/db21-0587

DeFronzo, R. A., & Tripathy, D. (2009). Skeletal muscle insulin resistance is the primary defect in type 2 diabetes. *Diabetes Care*, *32 Suppl 2*(Suppl 2), S157-163. https://doi.org/10.2337/dc09-S302

Deng, D., & Yan, N. (2016). GLUT, SGLT, and SWEET: Structural and mechanistic investigations of the glucose transporters. *Protein Sci*, *25*(3), 546-558. https://doi.org/10.1002/pro.2858

Descamps, D., Evnouchidou, I., Caillens, V., Drajac, C., Riffault, S., van Endert, P., & Saveanu, L. (2020). The Role of Insulin Regulated Aminopeptidase in Endocytic Trafficking and Receptor Signaling in Immune Cells. *Front Mol Biosci*, *7*, 583556. https://doi.org/10.3389/fmolb.2020.583556

Di Tommaso, P., Moretti, S., Xenarios, I., Orobitg, M., Montanyola, A., Chang, J. M., Taly, J. F., & Notredame, C. (2011). T-Coffee: a web server for the multiple sequence alignment of protein and RNA sequences using structural information and homology extension. *Nucleic Acids Res*, *39*(Web Server issue), W13-17. https://doi.org/10.1093/nar/gkr245

Dlamini, Z., Mokoena, F., & Hull, R. (2017). Abnormalities in alternative splicing in diabetes: therapeutic targets. *J Mol Endocrinol*, *59*(2), R93-R107. https://doi.org/10.1530/JME-17-0049

Eickelschulte, S., Hartwig, S., Leiser, B., Lehr, S., Joschko, V., Chokkalingam, M., Chadt, A., & Al-Hasani, H. (2021). AKT/AMPK-mediated phosphorylation of TBC1D4 disrupts the interaction with insulin-regulated aminopeptidase. *J Biol Chem*, *296*, 100637. https://doi.org/10.1016/j.jbc.2021.100637

ElSayed, N. A., Aleppo, G., Aroda, V. R., Bannuru, R. R., Brown, F. M., Bruemmer, D., Collins, B. S., Hilliard, M. E., Isaacs, D., Johnson, E. L., Kahan, S., Khunti, K., Leon, J., Lyons, S. K., Perry, M. L.,

Prahalad, P., Pratley, R. E., Seley, J. J., Stanton, R. C.,…on behalf of the American Diabetes, A. (2023). 2. Classification and Diagnosis of Diabetes: Standards of Care in Diabetes-2023. *Diabetes Care*, *46*(Suppl 1), S19-S40. https://doi.org/10.2337/dc23-S002

Engquist, E. N., & Zammit, P. S. (2021). The Satellite Cell at 60: The Foundation Years. *J Neuromuscul Dis*, *8*(s2), S183-S203. https://doi.org/10.3233/JND-210705

Esser, N., Utzschneider, K. M., & Kahn, S. E. (2020). Early beta cell dysfunction vs insulin hypersecretion as the primary event in the pathogenesis of dysglycaemia. *Diabetologia*, *63*(10), 2007-2021. https://doi.org/10.1007/s00125-020-05245-x

Evans, P. L., McMillin, S. L., Weyrauch, L. A., & Witczak, C. A. (2019). Regulation of Skeletal Muscle Glucose Transport and Glucose Metabolism by Exercise Training. *Nutrients*, *11*(10). https://doi.org/10.3390/nu11102432

Ferrari, F., Bock, P. M., Motta, M. T., & Helal, L. (2019). Biochemical and Molecular Mechanisms of Glucose Uptake Stimulated by Physical Exercise in Insulin Resistance State: Role of Inflammation. *Arq Bras Cardiol*, *113*(6), 1139-1148. https://doi.org/10.5935/abc.20190224

Flores-Opazo, M., McGee, S. L., & Hargreaves, M. (2020). Exercise and GLUT4. *Exerc Sport Sci Rev*, *48*(3), 110-118. https://doi.org/10.1249/JES.0000000000000224

Foley, K., Boguslavsky, S., & Klip, A. (2011). Endocytosis, recycling, and regulated exocytosis of glucose transporter 4. *Biochemistry*, *50*(15), 3048-3061. https://doi.org/10.1021/bi2000356

Fontanesi, L., & Bertolini, F. (2013). The TBC1D1 gene: structure, function, and association with obesity and related traits. *Vitam Horm*, *91*, 77-95. https://doi.org/10.1016/B978-0-12-407766-9.00004-3

Fontanesi, L., Colombo, M., Tognazzi, L., Scotti, E., Buttazzoni, L., Dall'Olio, S., Davoli, R., & Russo, V. (2011). The porcine TBC1D1 gene: mapping, SNP identification, and association study with meat, carcass and production traits in Italian heavy pigs. *Mol Biol Rep*, *38*(2), 1425-1431. https://doi.org/10.1007/s11033-010-0247-3

Fontanesi, L., Galimberti, G., Calo, D. G., Fronza, R., Martelli, P. L., Scotti, E., Colombo, M., Schiavo, G., Casadio, R., Buttazzoni, L., & Russo, V. (2012). Identification and association analysis of several hundred single nucleotide polymorphisms within candidate genes for back fat thickness in Italian Large White pigs using a selective genotyping approach. *J Anim Sci*, *90*(8), 2450-2464. https://doi.org/10.2527/jas.2011-4797

Francetic, T., & Li, Q. (2011). Skeletal myogenesis and Myf5 activation. *Transcription*, *2*(3), 109-114. https://doi.org/10.4161/trns.2.3.15829

Freed, D., Stevens, E. L., & Pevsner, J. (2014). Somatic mosaicism in the human genome. *Genes (Basel)*, *5*(4), 1064-1094. https://doi.org/10.3390/genes5041064

Fritzen, A. M., Madsen, A. B., Kleinert, M., Treebak, J. T., Lundsgaard, A. M., Jensen, T. E., Richter, E. A., Wojtaszewski, J., Kiens, B., & Frosig, C. (2016). Regulation of autophagy in human skeletal muscle: effects of exercise, exercise training and insulin stimulation. *J Physiol*, *594*(3), 745-761. https://doi.org/10.1113/JP271405

Frontera, W. R., & Ochala, J. (2015). Skeletal muscle: a brief review of structure and function. *Calcif Tissue Int*, *96*(3), 183-195. https://doi.org/10.1007/s00223-014-9915-y

Frosig, C., Pehmoller, C., Birk, J. B., Richter, E. A., & Wojtaszewski, J. F. (2010). Exercise-induced TBC1D1 Ser237 phosphorylation and 14-3-3 protein binding capacity in human skeletal muscle. *J Physiol*, *588*(Pt 22), 4539-4548. https://doi.org/10.1113/jphysiol.2010.194811

Fukuda, M. (2011). TBC proteins: GAPs for mammalian small GTPase Rab? *Biosci Rep*, *31*(3), 159-168. https://doi.org/10.1042/BSR20100112

Fukuda, N., Emoto, M., Nakamori, Y., Taguchi, A., Miyamoto, S., Uraki, S., Oka, Y., & Tanizawa, Y. (2009). DOC2B: a novel syntaxin-4 binding protein mediating insulin-regulated GLUT4 vesicle fusion in adipocytes. *Diabetes*, *58*(2), 377-384. https://doi.org/10.2337/db08-0303

Galicia-Garcia, U., Benito-Vicente, A., Jebari, S., Larrea-Sebal, A., Siddiqi, H., Uribe, K. B., Ostolaza, H., & Martin, C. (2020). Pathophysiology of Type 2 Diabetes Mellitus. *Int J Mol Sci*, *21*(17). https://doi.org/10.3390/ijms21176275

Gavriljuk, K., Gazdag, E. M., Itzen, A., Kotting, C., Goody, R. S., & Gerwert, K. (2012). Catalytic mechanism of a mammalian Rab.RabGAP complex in atomic detail. *Proc Natl Acad Sci U S A*, *109*(52), 21348-21353. https://doi.org/10.1073/pnas.1214431110

Goldtzvik, Y., Sen, N., Lam, S. D., & Orengo, C. (2023). Protein diversification through post-translational modifications, alternative splicing, and gene duplication. *Curr Opin Struct Biol*, *81*, 102640. https://doi.org/10.1016/j.sbi.2023.102640

Gonzalez, E., & McGraw, T. E. (2006). Insulin signaling diverges into Akt-dependent and -independent signals to regulate the recruitment/docking and the fusion of GLUT4 vesicles to the plasma membrane. *Mol Biol Cell*, *17*(10), 4484-4493. https://doi.org/10.1091/mbc.e06-07-0585

Graveley, B. R. (2008). The haplo-spliceo-transcriptome: common variations in alternative splicing in the human population. *Trends Genet*, *24*(1), 5-7. https://doi.org/10.1016/j.tig.2007.10.004

Haeusler, R. A., McGraw, T. E., & Accili, D. (2018). Biochemical and cellular properties of insulin receptor signalling. *Nat Rev Mol Cell Biol*, *19*(1), 31-44. https://doi.org/10.1038/nrm.2017.89

Hargreaves, M., & Spriet, L. L. (2020). Skeletal muscle energy metabolism during exercise. *Nat Metab*, *2*(9), 817-828. https://doi.org/10.1038/s42255-020-0251-4

Hasselmann, M., Gempe, T., Schiott, M., Nunes-Silva, C. G., Otte, M., & Beye, M. (2008). Evidence for the evolutionary nascence of a novel sex determination pathway in honeybees. *Nature*, *454*(7203), 519-522. https://doi.org/10.1038/nature07052

Hatakeyama, H., & Kanzaki, M. (2013). Regulatory mode shift of Tbc1d1 is required for acquisition of insulin-responsive GLUT4-trafficking activity. *Mol Biol Cell*, *24*(6), 809-817. https://doi.org/10.1091/mbc.E12-10-0725

Hatakeyama, H., Morino, T., Ishii, T., & Kanzaki, M. (2019). Cooperative actions of Tbc1d1 and AS160/Tbc1d4 in GLUT4-trafficking activities. *J Biol Chem*, *294*(4), 1161-1172. https://doi.org/10.1074/jbc.RA118.004614

Hayashi, T., Wojtaszewski, J. F., & Goodyear, L. J. (1997). Exercise regulation of glucose transport in skeletal muscle. *Am J Physiol*, *273*(6), E1039-1051. https://doi.org/10.1152/ajpendo.1997.273.6.E1039

He, S., Yan, L., Zhu, R., Wei, H., Wang, J., Zheng, L., & Zhang, Y. (2022). Skeletal-Muscle-Specific Overexpression of Chrono Leads to Disruption of Glucose Metabolism and Exercise Capacity. *Life (Basel)*, *12*(8). https://doi.org/10.3390/life12081233

Hernandez-Hernandez, J. M., Garcia-Gonzalez, E. G., Brun, C. E., & Rudnicki, M. A. (2017). The myogenic regulatory factors, determinants of muscle development, cell identity and regeneration. *Semin Cell Dev Biol*, *72*, 10-18. https://doi.org/10.1016/j.semcdb.2017.11.010

Highland, C. M., Thomas, L. L., & Fromme, J. C. (2023). Methods for Studying Membrane-Proximal GAP Activity on Prenylated Rab GTPase Substrates. *Methods Mol Biol*, *2557*, 507-518. https://doi.org/10.1007/978-1-0716-2639-9_29

Hoffman, N. J., & Elmendorf, J. S. (2011). Signaling, cytoskeletal and membrane mechanisms regulating GLUT4 exocytosis. *Trends Endocrinol Metab*, *22*(3), 110-116. https://doi.org/10.1016/j.tem.2010.12.001

Holman, G. D. (2020). Structure, function and regulation of mammalian glucose transporters of the SLC2 family. *Pflugers Arch*, *472*(9), 1155-1175. https://doi.org/10.1007/s00424-020-02411-3

Homma, Y., Hiragi, S., & Fukuda, M. (2021). Rab family of small GTPases: an updated view on their regulation and functions. *FEBS J*, *288*(1), 36-55. https://doi.org/10.1111/febs.15453

Hossain, M. J., Al-Mamun, M., & Islam, M. R. (2024). Diabetes mellitus, the fastest growing global public health concern: Early detection should be focused. *Health Sci Rep*, *7*(3), e2004. https://doi.org/10.1002/hsr2.2004

Howlett, K. F., Sakamoto, K., Garnham, A., Cameron-Smith, D., & Hargreaves, M. (2007). Resistance exercise and insulin regulate AS160 and interaction with 14-3-3 in human skeletal muscle. *Diabetes*, *56*(6), 1608-1614. https://doi.org/10.2337/db06-1398

Hutagalung, A. H., & Novick, P. J. (2011). Role of Rab GTPases in membrane traffic and cell physiology. *Physiol Rev*, *91*(1), 119-149. https://doi.org/10.1152/physrev.00059.2009

Iberite, F., Gruppioni, E., & Ricotti, L. (2022). Skeletal muscle differentiation of human iPSCs meets bioengineering strategies: perspectives and challenges. *NPJ Regen Med*, *7*(1), 23. https://doi.org/10.1038/s41536-022-00216-9

Ishikura, S., & Klip, A. (2008). Muscle cells engage Rab8A and myosin Vb in insulin-dependent GLUT4 translocation. *Am J Physiol Cell Physiol*, *295*(4), C1016-1025. https://doi.org/10.1152/ajpcell.00277.2008

Ismail, A., & Tanasova, M. (2022). Importance of GLUT Transporters in Disease Diagnosis and Treatment. *Int J Mol Sci*, *23*(15). https://doi.org/10.3390/ijms23158698

Jaiswal, N., Gavin, M. G., Quinn, W. J., 3rd, Luongo, T. S., Gelfer, R. G., Baur, J. A., & Titchenell, P. M. (2019). The role of skeletal muscle Akt in the regulation of muscle mass and glucose homeostasis. *Mol Metab*, *28*, 1-13. https://doi.org/10.1016/j.molmet.2019.08.001

Jaldin-Fincati, J. R., Pavarotti, M., Frendo-Cumbo, S., Bilan, P. J., & Klip, A. (2017). Update on GLUT4 Vesicle Traffic: A Cornerstone of Insulin Action. *Trends Endocrinol Metab*, *28*(8), 597-611. https://doi.org/10.1016/j.tem.2017.05.002

Jessen, N., An, D., Lihn, A. S., Nygren, J., Hirshman, M. F., Thorell, A., & Goodyear, L. J. (2011). Exercise increases TBC1D1 phosphorylation in human skeletal muscle. *Am J Physiol Endocrinol Metab*, *301*(1), E164-171. https://doi.org/10.1152/ajpendo.00042.2011

Jewell, J. L., Oh, E., Ramalingam, L., Kalwat, M. A., Tagliabracci, V. S., Tackett, L., Elmendorf, J. S., & Thurmond, D. C. (2011). Munc18c phosphorylation by the insulin receptor links cell signaling directly to SNARE exocytosis. *J Cell Biol*, *193*(1), 185-199. https://doi.org/10.1083/jcb.201007176

Jobbins, A. M., Yu, S., Paterson, H. A. B., Maude, H., Kefala-Stavridi, A., Speck, C., Cebola, I., & Vernia, S. (2023). Pre-RNA splicing in metabolic homeostasis and liver disease. *Trends Endocrinol Metab*, *34*(12), 823-837. https://doi.org/10.1016/j.tem.2023.08.007

Jordens, I., Molle, D., Xiong, W., Keller, S. R., & McGraw, T. E. (2010). Insulin-regulated aminopeptidase is a key regulator of GLUT4 trafficking by controlling the sorting of GLUT4 from endosomes to specialized insulin-regulated vesicles. *Mol Biol Cell*, *21*(12), 2034-2044. https://doi.org/10.1091/mbc.e10-02-0158

Juan-Mateu, J., Villate, O., & Eizirik, D. L. (2016). MECHANISMS IN ENDOCRINOLOGY: Alternative splicing: the new frontier in diabetes research. *Eur J Endocrinol*, *174*(5), R225-238. https://doi.org/10.1530/EJE-15-0916

Karlsson, H. K., Chibalin, A. V., Koistinen, H. A., Yang, J., Koumanov, F., Wallberg-Henriksson, H., Zierath, J. R., & Holman, G. D. (2009). Kinetics of GLUT4 trafficking in rat and human skeletal muscle. *Diabetes*, *58*(4), 847-854. https://doi.org/10.2337/db08-1539

Keller, S. R., Scott, H. M., Mastick, C. C., Aebersold, R., & Lienhard, G. E. (1995). Cloning and characterization of a novel insulin-regulated membrane aminopeptidase from Glut4 vesicles. *J Biol Chem*, *270*(40), 23612-23618. https://doi.org/10.1074/jbc.270.40.23612

Kerner, W., Bruckel, J., & German Diabetes, A. (2014). Definition, classification and diagnosis of diabetes mellitus. *Exp Clin Endocrinol Diabetes*, *122*(7), 384-386. https://doi.org/10.1055/s-0034-1366278

Kerwin, A. J., Jr., Lop, A. L., Vicente, K., Weiler, T., & Kana, S. L. (2023). Testing With Intent in Mosaic Conditions: A Case-Based Review. *Cureus*, *15*(11), e49644. https://doi.org/10.7759/cureus.49644

Kim, B. H., Woo, T. G., Kang, S. M., Park, S., & Park, B. J. (2022). Splicing Variants, Protein-Protein Interactions, and Drug Targeting in Hutchinson-Gilford Progeria Syndrome and Small Cell Lung Cancer. *Genes (Basel)*, *13*(2). https://doi.org/10.3390/genes13020165

Kim, H. K., Pham, M. H. C., Ko, K. S., Rhee, B. D., & Han, J. (2018). Alternative splicing isoforms in health and disease. *Pflugers Arch*, *470*(7), 995-1016. https://doi.org/10.1007/s00424-018-2136-x

Kioumourtzoglou, D., Gould, G. W., & Bryant, N. J. (2014). Insulin stimulates syntaxin4 SNARE complex assembly via a novel regulatory mechanism. *Mol Cell Biol*, *34*(7), 1271-1279. https://doi.org/10.1128/MCB.01203-13

Kjobsted, R., Roll, J. L. W., Jorgensen, N. O., Birk, J. B., Foretz, M., Viollet, B., Chadt, A., Al-Hasani, H., & Wojtaszewski, J. F. P. (2019). AMPK and TBC1D1 Regulate Muscle Glucose Uptake After, but Not During, Exercise and Contraction. *Diabetes*, *68*(7), 1427-1440. https://doi.org/10.2337/db19-0050

Klinck, R., Laberge, G., Bisson, M., McManus, S., Michou, L., Brown, J. P., & Roux, S. (2014). Alternative splicing in osteoclasts and Paget's disease of bone. *BMC Med Genet*, *15*, 98. https://doi.org/10.1186/s12881-014-0098-1

Knudsen, J. R., Steenberg, D. E., Hingst, J. R., Hodgson, L. R., Henriquez-Olguin, C., Li, Z., Kiens, B., Richter, E. A., Wojtaszewski, J. F. P., Verkade, P., & Jensen, T. E. (2020). Prior exercise in humans redistributes intramuscular GLUT4 and enhances insulin-stimulated sarcolemmal and endosomal GLUT4 translocation. *Mol Metab*, *39*, 100998. https://doi.org/10.1016/j.molmet.2020.100998

Kosfeld, A., Kreuzer, M., Daniel, C., Brand, F., Schafer, A. K., Chadt, A., Weiss, A. C., Riehmer, V., Jeanpierre, C., Klintschar, M., Brasen, J. H., Amann, K., Pape, L., Kispert, A., Al-Hasani, H., Haffner, D., & Weber, R. G. (2016). Whole-exome sequencing identifies mutations of TBC1D1 encoding a Rab-GTPase-activating protein in patients with congenital anomalies of the kidneys and urinary tract (CAKUT). *Hum Genet*, *135*(1), 69-87. https://doi.org/10.1007/s00439-015-1610-1

Koumanov, F., Richardson, J. D., Murrow, B. A., & Holman, G. D. (2011). AS160 phosphotyrosine-binding domain constructs inhibit insulin-stimulated GLUT4 vesicle fusion with the plasma membrane. *J Biol Chem*, *286*(19), 16574-16582. https://doi.org/10.1074/jbc.M111.226092

Kowalski, G. M., & Bruce, C. R. (2014). The regulation of glucose metabolism: implications and considerations for the assessment of glucose homeostasis in rodents. *Am J Physiol Endocrinol Metab*, *307*(10), E859-871. https://doi.org/10.1152/ajpendo.00165.2014

Kyrou, I., Tsigos, C., Mavrogianni, C., Cardon, G., Van Stappen, V., Latomme, J., Kivela, J., Wikstrom, K., Tsochev, K., Nanasi, A., Semanova, C., Mateo-Gallego, R., Lamiquiz-Moneo, I., Dafoulas, G., Timpel, P., Schwarz, P. E. H., Iotova, V., Tankova, T., Makrilakis, K.,…Feel4Diabetes-study, G. (2020). Sociodemographic and lifestyle-related risk factors for identifying vulnerable groups for type 2 diabetes: a narrative review with emphasis on data from Europe. *BMC Endocr Disord*, *20*(Suppl 1), 134. https://doi.org/10.1186/s12902-019-0463-3

Lamber, E. P., Siedenburg, A. C., & Barr, F. A. (2019). Rab regulation by GEFs and GAPs during membrane traffic. *Curr Opin Cell Biol*, *59*, 34-39. https://doi.org/10.1016/j.ceb.2019.03.004

Larance, M., Ramm, G., Stockli, J., van Dam, E. M., Winata, S., Wasinger, V., Simpson, F., Graham, M., Junutula, J. R., Guilhaus, M., & James, D. E. (2005). Characterization of the role of the Rab GTPase-activating protein AS160 in insulin-regulated GLUT4 trafficking. *J Biol Chem*, *280*(45), 37803-37813. https://doi.org/10.1074/jbc.M503897200

Larsen, J. K., Larsen, M. R., Birk, J. B., Steenberg, D. E., Hingst, J. R., Hojlund, K., Chadt, A., Al-Hasani, H., Deshmukh, A. S., Wojtaszewski, J. F. P., & Kjobsted, R. (2022). Illumination of the Endogenous Insulin-Regulated TBC1D4 Interactome in Human Skeletal Muscle. *Diabetes*, *71*(5), 906-920. https://doi.org/10.2337/db21-0855

Lee, E. J., Noh, S. J., Choi, H., Kim, M. W., Kim, S. J., Seo, Y. A., Jeong, J. E., Shin, I., Kim, J. S., Choi, J. K., Cho, D. Y., & Chang, S. (2023). Comparative RNA-Seq Analysis Revealed Tissue-Specific Splicing Variations during the Generation of the PDX Model. *Int J Mol Sci*, *24*(23). https://doi.org/10.3390/ijms242317001

Leney, S. E., & Tavare, J. M. (2009). The molecular basis of insulin-stimulated glucose uptake: signalling, trafficking and potential drug targets. *J Endocrinol*, *203*(1), 1-18. https://doi.org/10.1677/JOE-09-0037

Leto, D., & Saltiel, A. R. (2012). Regulation of glucose transport by insulin: traffic control of GLUT4. *Nat Rev Mol Cell Biol*, *13*(6), 383-396. https://doi.org/10.1038/nrm3351

Lipscombe, D., Andrade, A., & Allen, S. E. (2013). Alternative splicing: functional diversity among voltage-gated calcium channels and behavioral consequences. *Biochim Biophys Acta*, *1828*(7), 1522-1529. https://doi.org/10.1016/j.bbamem.2012.09.018

Livak, K. J., & Schmittgen, T. D. (2001). Analysis of relative gene expression data using real-time quantitative PCR and the 2(-Delta Delta C(T)) Method. *Methods*, *25*(4), 402-408. https://doi.org/10.1006/meth.2001.1262

Love, S. L., Emerson, J. D., Koide, K., & Hoskins, A. A. (2023). Pre-mRNA splicing-associated diseases and therapies. *RNA Biol*, *20*(1), 525-538. https://doi.org/10.1080/15476286.2023.2239601

Lui, A., Sparks, R., Patel, R., & Patel, N. A. (2021). Identification of Sortilin Alternatively Spliced Variants in Mouse 3T3L1 Adipocytes. *Int J Mol Sci*, *22*(3). https://doi.org/10.3390/ijms22030983

Mafakheri, S., Chadt, A., & Al-Hasani, H. (2018). Regulation of RabGAPs involved in insulin action. *Biochem Soc Trans*, *46*(3), 683-690. https://doi.org/10.1042/BST20170479

Mafakheri, S., Florke, R. R., Kanngiesser, S., Hartwig, S., Espelage, L., De Wendt, C., Schonberger, T., Hamker, N., Lehr, S., Chadt, A., & Al-Hasani, H. (2018). AKT and AMP-activated protein kinase regulate TBC1D1 through phosphorylation and its interaction with the cytosolic tail of insulin-regulated aminopeptidase IRAP. *J Biol Chem*, *293*(46), 17853-17862. https://doi.org/10.1074/jbc.RA118.005040

Majumdar, S., Acharya, A., & Prakash, B. (2017). Structural plasticity mediates distinct GAP-dependent GTP hydrolysis mechanisms in Rab33 and Rab5. *FEBS J*, *284*(24), 4358-4375. https://doi.org/10.1111/febs.14314

Makeyev, E. V., Zhang, J., Carrasco, M. A., & Maniatis, T. (2007). The MicroRNA miR-124 promotes neuronal differentiation by triggering brain-specific alternative pre-mRNA splicing. *Mol Cell*, *27*(3), 435-448. https://doi.org/10.1016/j.molcel.2007.07.015

Malakar, P., Chartarifsky, L., Hija, A., Leibowitz, G., Glaser, B., Dor, Y., & Karni, R. (2016). Insulin receptor alternative splicing is regulated by insulin signaling and modulates beta cell survival. *Sci Rep*, *6*, 31222. https://doi.org/10.1038/srep31222

Manning, B. D., & Toker, A. (2017). AKT/PKB Signaling: Navigating the Network. *Cell*, *169*(3), 381-405. https://doi.org/10.1016/j.cell.2017.04.001

Marasco, L. E., & Kornblihtt, A. R. (2023). The physiology of alternative splicing. *Nat Rev Mol Cell Biol*, *24*(4), 242-254. https://doi.org/10.1038/s41580-022-00545-z

Marcheva, B., Perelis, M., Weidemann, B. J., Taguchi, A., Lin, H., Omura, C., Kobayashi, Y., Newman, M. V., Wyatt, E. J., McNally, E. M., Fox, J. E. M., Hong, H., Shankar, A., Wheeler, E. C., Ramsey, K. M., MacDonald, P. E., Yeo, G. W., & Bass, J. (2020). A role for alternative splicing in circadian control of exocytosis and glucose homeostasis. *Genes Dev*, *34*(15-16), 1089-1105. https://doi.org/10.1101/gad.338178.120

Mesinovic, J., Fyfe, J. J., Talevski, J., Wheeler, M. J., Leung, G. K. W., George, E. S., Hunegnaw, M. T., Glavas, C., Jansons, P., Daly, R. M., & Scott, D. (2023). Type 2 Diabetes Mellitus and Sarcopenia as Comorbid Chronic Diseases in Older Adults: Established and Emerging Treatments and Therapies. *Diabetes Metab J*, *47*(6), 719-742. https://doi.org/10.4093/dmj.2023.0112

Meyre, D., Farge, M., Lecoeur, C., Proenca, C., Durand, E., Allegaert, F., Tichet, J., Marre, M., Balkau, B., Weill, J., Delplanque, J., & Froguel, P. (2008). R125W coding variant in TBC1D1 confers risk for familial obesity and contributes to linkage on chromosome 4p14 in the French population. *Hum Mol Genet*, *17*(12), 1798-1802. https://doi.org/10.1093/hmg/ddn070

Miinea, C. P., Sano, H., Kane, S., Sano, E., Fukuda, M., Peranen, J., Lane, W. S., & Lienhard, G. E. (2005). AS160, the Akt substrate regulating GLUT4 translocation, has a functional Rab GTPase-activating protein domain. *Biochem J*, *391*(Pt 1), 87-93. https://doi.org/10.1042/BJ20050887

Miklos, G. L., & Rubin, G. M. (1996). The role of the genome project in determining gene function: insights from model organisms. *Cell*, *86*(4), 521-529. https://doi.org/10.1016/s0092-8674(00)80126-9

Mizgier, M. L., Casas, M., Contreras-Ferrat, A., Llanos, P., & Galgani, J. E. (2014). Potential role of skeletal muscle glucose metabolism on the regulation of insulin secretion. *Obes Rev*, *15*(7), 587-597. https://doi.org/10.1111/obr.12166

Modrek, B., & Lee, C. J. (2003). Alternative splicing in the human, mouse and rat genomes is associated with an increased frequency of exon creation and/or loss. *Nat Genet*, *34*(2), 177-180. https://doi.org/10.1038/ng1159

Mohan, S., Sheena, A., Poulose, N., & Anilkumar, G. (2010). Molecular dynamics simulation studies of GLUT4: substrate-free and substrate-induced dynamics and ATP-mediated glucose transport inhibition. *PLoS One*, *5*(12), e14217. https://doi.org/10.1371/journal.pone.0014217

Moltke, I., Grarup, N., Jorgensen, M. E., Bjerregaard, P., Treebak, J. T., Fumagalli, M., Korneliussen, T. S., Andersen, M. A., Nielsen, T. S., Krarup, N. T., Gjesing, A. P., Zierath, J. R., Linneberg, A., Wu, X., Sun, G., Jin, X., Al-Aama, J., Wang, J., Borch-Johnsen, K.,…Hansen, T. (2014). A common Greenlandic TBC1D4 variant confers muscle insulin resistance and type 2 diabetes. *Nature*, *512*(7513), 190-193. https://doi.org/10.1038/nature13425

Morais, P., Adachi, H., & Yu, Y. T. (2021). Spliceosomal snRNA Epitranscriptomics. *Front Genet*, *12*, 652129. https://doi.org/10.3389/fgene.2021.652129

Mukund, K., & Subramaniam, S. (2020). Skeletal muscle: A review of molecular structure and function, in health and disease. *Wiley Interdiscip Rev Syst Biol Med*, *12*(1), e1462. https://doi.org/10.1002/wsbm.1462

Nagasawa, C. K., & Garcia-Blanco, M. A. (2023). Early Splicing Complexes and Human Disease. *Int J Mol Sci*, *24*(14). https://doi.org/10.3390/ijms241411412

Nilsen, T. W., & Graveley, B. R. (2010). Expansion of the eukaryotic proteome by alternative splicing. *Nature*, *463*(7280), 457-463. https://doi.org/10.1038/nature08909

Nolan, C. J., Ruderman, N. B., Kahn, S. E., Pedersen, O., & Prentki, M. (2015). Insulin resistance as a physiological defense against metabolic stress: implications for the management of subsets of type 2 diabetes. *Diabetes*, *64*(3), 673-686. https://doi.org/10.2337/db14-0694

Norgren, S., Zierath, J., Wedell, A., Wallberg-Henriksson, H., & Luthman, H. (1994). Regulation of human insulin receptor RNA splicing in vivo. *Proc Natl Acad Sci U S A*, *91*(4), 1465-1469. https://doi.org/10.1073/pnas.91.4.1465

Pan, Q., Shai, O., Lee, L. J., Frey, B. J., & Blencowe, B. J. (2008). Deep surveying of alternative splicing complexity in the human transcriptome by high-throughput sequencing. *Nat Genet*, *40*(12), 1413-1415. https://doi.org/10.1038/ng.259

Pan, X., Eathiraj, S., Munson, M., & Lambright, D. G. (2006). TBC-domain GAPs for Rab GTPases accelerate GTP hydrolysis by a dual-finger mechanism. *Nature*, *442*(7100), 303-306. https://doi.org/10.1038/nature04847

Park, S. Y., Jin, W., Woo, J. R., & Shoelson, S. E. (2011). Crystal structures of human TBC1D1 and TBC1D4 (AS160) RabGTPase-activating protein (RabGAP) domains reveal critical elements for GLUT4 translocation. *J Biol Chem*, *286*(20), 18130-18138. https://doi.org/10.1074/jbc.M110.217323

Parolin, M. L., Chesley, A., Matsos, M. P., Spriet, L. L., Jones, N. L., & Heigenhauser, G. J. (1999). Regulation of skeletal muscle glycogen phosphorylase and PDH during maximal intermittent exercise. *Am J Physiol*, *277*(5), E890-900. https://doi.org/10.1152/ajpendo.1999.277.5.E890

Paronetto, M. P., Passacantilli, I., & Sette, C. (2016). Alternative splicing and cell survival: from tissue homeostasis to disease. *Cell Death Differ*, *23*(12), 1919-1929. https://doi.org/10.1038/cdd.2016.91

Pehmoller, C., Treebak, J. T., Birk, J. B., Chen, S., Mackintosh, C., Hardie, D. G., Richter, E. A., & Wojtaszewski, J. F. (2009). Genetic disruption of AMPK signaling abolishes both contraction- and insulin-stimulated TBC1D1 phosphorylation and 14-3-3 binding in mouse skeletal muscle. *Am J Physiol Endocrinol Metab*, *297*(3), E665-675. https://doi.org/10.1152/ajpendo.00115.2009

Peng, Y. D., Xu, H. Y., Ye, F., Lan, X., Peng, X., Rustempasic, A., Yin, H. D., Zhao, X. L., Liu, Y. P., Zhu, Q., & Wang, Y. (2015). Effects of sex and age on chicken TBC1D1 gene mRNA expression. *Genet Mol Res*, *14*(3), 7704-7714. https://doi.org/10.4238/2015.July.13.16

Petersen, M. C., & Shulman, G. I. (2018). Mechanisms of Insulin Action and Insulin Resistance. *Physiol Rev*, *98*(4), 2133-2223. https://doi.org/10.1152/physrev.00063.2017

Pfeffer, S. R. (2017). Rab GTPases: master regulators that establish the secretory and endocytic pathways. *Mol Biol Cell*, *28*(6), 712-715. https://doi.org/10.1091/mbc.E16-10-0737

Powers, A. C. (2021). Type 1 diabetes mellitus: much progress, many opportunities. *J Clin Invest*, *131*(8). https://doi.org/10.1172/JCI142242

Prokunina-Olsson, L., Kaplan, L. M., Schadt, E. E., & Collins, F. S. (2009). Alternative splicing of TCF7L2 gene in omental and subcutaneous adipose tissue and risk of type 2 diabetes. *PLoS One*, *4*(9), e7231. https://doi.org/10.1371/journal.pone.0007231

Qiao, A., Zhou, J., Xu, S., Ma, W., Boriboun, C., Kim, T., Yan, B., Deng, J., Yang, L., Zhang, E., Song, Y., Ma, Y. C., Richard, S., Zhang, C., Qiu, H., Habegger, K. M., Zhang, J., & Qin, G. (2021). Sam68 promotes hepatic gluconeogenesis via CRTC2. *Nat Commun*, *12*(1), 3340. https://doi.org/10.1038/s41467-021-23624-9

Rajan, S., Jagatheesan, G., Karam, C. N., Alves, M. L., Bodi, I., Schwartz, A., Bulcao, C. F., D'Souza, K. M., Akhter, S. A., Boivin, G. P., Dube, D. K., Petrashevskaya, N., Herr, A. B., Hullin, R., Liggett, S. B., Wolska, B. M., Solaro, R. J., & Wieczorek, D. F. (2010). Molecular and functional characterization of a novel cardiac-specific human tropomyosin isoform. *Circulation*, *121*(3), 410-418. https://doi.org/10.1161/CIRCULATIONAHA.109.889725

Ramalingam, L., Oh, E., Yoder, S. M., Brozinick, J. T., Kalwat, M. A., Groffen, A. J., Verhage, M., & Thurmond, D. C. (2012). Doc2b is a key effector of insulin secretion and skeletal muscle insulin sensitivity. *Diabetes*, *61*(10), 2424-2432. https://doi.org/10.2337/db11-1525

Richter, E. A., Derave, W., & Wojtaszewski, J. F. (2001). Glucose, exercise and insulin: emerging concepts. *J Physiol*, *535*(Pt 2), 313-322. https://doi.org/10.1111/j.1469-7793.2001.t01-2-00313.x

Roach, W. G., Chavez, J. A., Miinea, C. P., & Lienhard, G. E. (2007). Substrate specificity and effect on GLUT4 translocation of the Rab GTPase-activating protein Tbc1d1. *Biochem J*, *403*(2), 353-358. https://doi.org/10.1042/BJ20061798

Roberts, T. C., Langer, R., & Wood, M. J. A. (2020). Advances in oligonucleotide drug delivery. *Nat Rev Drug Discov*, *19*(10), 673-694. https://doi.org/10.1038/s41573-020-0075-7

Romero, I. G., Ruvinsky, I., & Gilad, Y. (2012). Comparative studies of gene expression and the evolution of gene regulation. *Nat Rev Genet*, *13*(7), 505-516. https://doi.org/10.1038/nrg3229

Romijn, J. A., Coyle, E. F., Sidossis, L. S., Gastaldelli, A., Horowitz, J. F., Endert, E., & Wolfe, R. R. (1993). Regulation of endogenous fat and carbohydrate metabolism in relation to exercise intensity and duration. *Am J Physiol*, *265*(3 Pt 1), E380-391. https://doi.org/10.1152/ajpendo.1993.265.3.E380

Ross, S. A., Scott, H. M., Morris, N. J., Leung, W. Y., Mao, F., Lienhard, G. E., & Keller, S. R. (1996). Characterization of the insulin-regulated membrane aminopeptidase in 3T3-L1 adipocytes. *J Biol Chem*, *271*(6), 3328-3332. https://doi.org/10.1074/jbc.271.6.3328

Rubin, C. J., Zody, M. C., Eriksson, J., Meadows, J. R., Sherwood, E., Webster, M. T., Jiang, L., Ingman, M., Sharpe, T., Ka, S., Hallbook, F., Besnier, F., Carlborg, O., Bed'hom, B., Tixier-Boichard, M., Jensen, P., Siegel, P., Lindblad-Toh, K., & Andersson, L. (2010). Whole-genome resequencing reveals loci under selection during chicken domestication. *Nature*, *464*(7288), 587-591. https://doi.org/10.1038/nature08832

Ruijter, J. M., Barnewall, R. J., Marsh, I. B., Szentirmay, A. N., Quinn, J. C., van Houdt, R., Gunst, Q. D., & van den Hoff, M. J. B. (2021). Efficiency Correction Is Required for Accurate Quantitative PCR Analysis and Reporting. *Clin Chem*, *67*(6), 829-842. https://doi.org/10.1093/clinchem/hvab052

Rutti, S., Arous, C., Nica, A. C., Kanzaki, M., Halban, P. A., & Bouzakri, K. (2014). Expression, phosphorylation and function of the Rab-GTPase activating protein TBC1D1 in pancreatic beta-cells. *FEBS Lett*, *588*(1), 15-20. https://doi.org/10.1016/j.febslet.2013.10.050

Sahlin, K., Tonkonogi, M., & Soderlund, K. (1998). Energy supply and muscle fatigue in humans. *Acta Physiol Scand*, *162*(3), 261-266. https://doi.org/10.1046/j.1365-201X.1998.0298f.x

Sahm, A., Bens, M., Szafranski, K., Holtze, S., Groth, M., Gorlach, M., Calkhoven, C., Muller, C., Schwab, M., Kraus, J., Kestler, H. A., Cellerino, A., Burda, H., Hildebrandt, T., Dammann, P., & Platzer, M. (2018). Long-lived rodents reveal signatures of positive selection in genes associated with lifespan. *PLoS Genet*, *14*(3), e1007272. https://doi.org/10.1371/journal.pgen.1007272

Sakamoto, K., & Holman, G. D. (2008). Emerging role for AS160/TBC1D4 and TBC1D1 in the regulation of GLUT4 traffic. *Am J Physiol Endocrinol Metab*, *295*(1), E29-37. https://doi.org/10.1152/ajpendo.90331.2008

Saltiel, A. R. (2021). Insulin signaling in health and disease. *J Clin Invest*, *131*(1). https://doi.org/10.1172/JCI142241

Sano, H., Kane, S., Sano, E., Miinea, C. P., Asara, J. M., Lane, W. S., Garner, C. W., & Lienhard, G. E. (2003). Insulin-stimulated phosphorylation of a Rab GTPase-activating protein regulates GLUT4 translocation. *J Biol Chem*, *278*(17), 14599-14602. https://doi.org/10.1074/jbc.C300063200

Sargeant, A. J. (2007). Structural and functional determinants of human muscle power. *Exp Physiol*, *92*(2), 323-331. https://doi.org/10.1113/expphysiol.2006.034322

Savkur, R. S., Philips, A. V., Cooper, T. A., Dalton, J. C., Moseley, M. L., Ranum, L. P., & Day, J. W. (2004). Insulin receptor splicing alteration in myotonic dystrophy type 2. *Am J Hum Genet*, *74*(6), 1309-1313. https://doi.org/10.1086/421528

Scheepers, A., Joost, H. G., & Schurmann, A. (2004). The glucose transporter families SGLT and GLUT: molecular basis of normal and aberrant function. *JPEN J Parenter Enteral Nutr*, *28*(5), 364-371. https://doi.org/10.1177/0148607104028005364

Shepard, P. J., & Hertel, K. J. (2008). Conserved RNA secondary structures promote alternative splicing. *RNA*, *14*(8), 1463-1469. https://doi.org/10.1261/rna.1069408

Smith, J. A. B., Murach, K. A., Dyar, K. A., & Zierath, J. R. (2023). Exercise metabolism and adaptation in skeletal muscle. *Nat Rev Mol Cell Biol*, *24*(9), 607-632. https://doi.org/10.1038/s41580-023-00606-x

Song, J., & Richard, S. (2015). Sam68 Regulates S6K1 Alternative Splicing during Adipogenesis. *Mol Cell Biol*, *35*(11), 1926-1939. https://doi.org/10.1128/MCB.01488-14

Song, Y., Parada, G., Lee, J. T. H., & Hemberg, M. (2024). Mining alternative splicing patterns in scRNA-seq data using scASfind. *Genome Biol*, *25*(1), 197. https://doi.org/10.1186/s13059-024-03323-6

Sorek, R., & Ast, G. (2003). Intronic sequences flanking alternatively spliced exons are conserved between human and mouse. *Genome Res*, *13*(7), 1631-1637. https://doi.org/10.1101/gr.1208803

Spaulding, H. R., & Yan, Z. (2022). AMPK and the Adaptation to Exercise. *Annu Rev Physiol*, *84*, 209-227. https://doi.org/10.1146/annurev-physiol-060721-095517

Spinner, N. B., & Conlin, L. K. (2014). Mosaicism and clinical genetics. *Am J Med Genet C Semin Med Genet*, *166C*(4), 397-405. https://doi.org/10.1002/ajmg.c.31421

Springer, C., Binsch, C., Weide, D., Toska, L., Cremer, A. L., Backes, H., Scheel, A. K., Espelage, L., Kotzka, J., Sill, S., Kurowski, A., Kim, D., Karpinski, S., Schnurr, T. M., Hansen, T., Hartwig, S., Lehr, S., Cames, S., Bruning, J.,…Chadt, A. (2024). Depletion of TBC1D4 improves the metabolic exercise response by overcoming genetically induced peripheral insulin resistance. *Diabetes*. https://doi.org/10.2337/db23-0463

Stenmark, H. (2009). Rab GTPases as coordinators of vesicle traffic. *Nat Rev Mol Cell Biol*, *10*(8), 513-525. https://doi.org/10.1038/nrm2728

Stockli, J., Meoli, C. C., Hoffman, N. J., Fazakerley, D. J., Pant, H., Cleasby, M. E., Ma, X., Kleinert, M., Brandon, A. E., Lopez, J. A., Cooney, G. J., & James, D. E. (2015). The RabGAP TBC1D1 plays a central role in exercise-regulated glucose metabolism in skeletal muscle. *Diabetes*, *64*(6), 1914-1922. https://doi.org/10.2337/db13-1489

Stone, S., Abkevich, V., Russell, D. L., Riley, R., Timms, K., Tran, T., Trem, D., Frank, D., Jammulapati, S., Neff, C. D., Iliev, D., Gress, R., He, G., Frech, G. C., Adams, T. D., Skolnick, M. H., Lanchbury, J. S., Gutin, A., Hunt, S. C., & Shattuck, D. (2006). TBC1D1 is a candidate for a severe obesity gene and evidence for a gene/gene interaction in obesity predisposition. *Hum Mol Genet*, *15*(18), 2709-2720. https://doi.org/10.1093/hmg/ddl204

Su, T., Hollas, M. A. R., Fellers, R. T., & Kelleher, N. L. (2023). Identification of Splice Variants and Isoforms in Transcriptomics and Proteomics. *Annu Rev Biomed Data Sci*, *6*, 357-376. https://doi.org/10.1146/annurev-biodatasci-020722-044021

Sugnet, C. W., Kent, W. J., Ares, M., Jr., & Haussler, D. (2004). Transcriptome and genome conservation of alternative splicing events in humans and mice. *Pac Symp Biocomput*, 66-77. https://doi.org/10.1142/9789812704856_0007

Sun, Y., Bilan, P. J., Liu, Z., & Klip, A. (2010). Rab8A and Rab13 are activated by insulin and regulate GLUT4 translocation in muscle cells. *Proc Natl Acad Sci U S A*, *107*(46), 19909-19914. https://doi.org/10.1073/pnas.1009523107

Sun, Y., Chiu, T. T., Foley, K. P., Bilan, P. J., & Klip, A. (2014). Myosin Va mediates Rab8A-regulated GLUT4 vesicle exocytosis in insulin-stimulated muscle cells. *Mol Biol Cell*, *25*(7), 1159-1170. https://doi.org/10.1091/mbc.E13-08-0493

Sylow, L., Kleinert, M., Richter, E. A., & Jensen, T. E. (2017). Exercise-stimulated glucose uptake - regulation and implications for glycaemic control. *Nat Rev Endocrinol*, *13*(3), 133-148. https://doi.org/10.1038/nrendo.2016.162

Sylow, L., Tokarz, V. L., Richter, E. A., & Klip, A. (2021). The many actions of insulin in skeletal muscle, the paramount tissue determining glycemia. *Cell Metab*, *33*(4), 758-780. https://doi.org/10.1016/j.cmet.2021.03.020

Szekeres, F., Chadt, A., Tom, R. Z., Deshmukh, A. S., Chibalin, A. V., Bjornholm, M., Al-Hasani, H., & Zierath, J. R. (2012). The Rab-GTPase-activating protein TBC1D1 regulates skeletal muscle glucose metabolism. *Am J Physiol Endocrinol Metab*, *303*(4), E524-533. https://doi.org/10.1152/ajpendo.00605.2011

Szukiewicz, D. (2023). Molecular Mechanisms for the Vicious Cycle between Insulin Resistance and the Inflammatory Response in Obesity. *Int J Mol Sci*, *24*(12). https://doi.org/10.3390/ijms24129818

Taniguchi, C. M., Emanuelli, B., & Kahn, C. R. (2006). Critical nodes in signalling pathways: insights into insulin action. *Nat Rev Mol Cell Biol*, *7*(2), 85-96. https://doi.org/10.1038/nrm1837

Taylor, E. B., An, D., Kramer, H. F., Yu, H., Fujii, N. L., Roeckl, K. S., Bowles, N., Hirshman, M. F., Xie, J., Feener, E. P., & Goodyear, L. J. (2008). Discovery of TBC1D1 as an insulin-, AICAR-, and contraction-stimulated signaling nexus in mouse skeletal muscle. *J Biol Chem*, *283*(15), 9787-9796. https://doi.org/10.1074/jbc.M708839200

Tazi, J., Bakkour, N., & Stamm, S. (2009). Alternative splicing and disease. *Biochim Biophys Acta*, *1792*(1), 14-26. https://doi.org/10.1016/j.bbadis.2008.09.017

Thompson, D., Regev, A., & Roy, S. (2015). Comparative analysis of gene regulatory networks: from network reconstruction to evolution. *Annu Rev Cell Dev Biol*, *31*, 399-428. https://doi.org/10.1146/annurev-cellbio-100913-012908

Thyfault, J. P., & Bergouignan, A. (2020). Exercise and metabolic health: beyond skeletal muscle. *Diabetologia*, *63*(8), 1464-1474. https://doi.org/10.1007/s00125-020-05177-6

Tigano, A., Colella, J. P., & MacManes, M. D. (2020). Comparative and population genomics approaches reveal the basis of adaptation to deserts in a small rodent. *Mol Ecol*, *29*(7), 1300-1314. https://doi.org/10.1111/mec.15401

Tomic, D., Shaw, J. E., & Magliano, D. J. (2022). The burden and risks of emerging complications of diabetes mellitus. *Nat Rev Endocrinol*, *18*(9), 525-539. https://doi.org/10.1038/s41574-022-00690-7

Treebak, J. T., Pehmoller, C., Kristensen, J. M., Kjobsted, R., Birk, J. B., Schjerling, P., Richter, E. A., Goodyear, L. J., & Wojtaszewski, J. F. (2014). Acute exercise and physiological insulin induce distinct phosphorylation signatures on TBC1D1 and TBC1D4 proteins in human skeletal muscle. *J Physiol*, *592*(2), 351-375. https://doi.org/10.1113/jphysiol.2013.266338

van Gerwen, J., Shun-Shion, A. S., & Fazakerley, D. J. (2023). Insulin signalling and GLUT4 trafficking in insulin resistance. *Biochem Soc Trans*, *51*(3), 1057-1069. https://doi.org/10.1042/BST20221066

van Loon, L. J., Greenhaff, P. L., Constantin-Teodosiu, D., Saris, W. H., & Wagenmakers, A. J. (2001). The effects of increasing exercise intensity on muscle fuel utilisation in humans. *J Physiol*, *536*(Pt 1), 295-304. https://doi.org/10.1111/j.1469-7793.2001.00295.x

Vichaiwong, K., Purohit, S., An, D., Toyoda, T., Jessen, N., Hirshman, M. F., & Goodyear, L. J. (2010). Contraction regulates site-specific phosphorylation of TBC1D1 in skeletal muscle. *Biochem J*, *431*(2), 311-320. https://doi.org/10.1042/BJ20101100

Vitting-Seerup, K. (2023). Most protein domains exist as variants with distinct functions across cells, tissues and diseases. *NAR Genom Bioinform*, *5*(3), lqad084. https://doi.org/10.1093/nargab/lqad084

Volckmar, A. L., Han, C. T., Putter, C., Haas, S., Vogel, C. I., Knoll, N., Struve, C., Gobel, M., Haas, K., Herrfurth, N., Jarick, I., Grallert, H., Schurmann, A., Al-Hasani, H., Hebebrand, J., Sauer, S., & Hinney, A. (2016). Analysis of Genes Involved in Body Weight Regulation by Targeted Re-Sequencing. *PLoS One*, *11*(2), e0147904. https://doi.org/10.1371/journal.pone.0147904

Vuong, C. K., Black, D. L., & Zheng, S. (2016). The neurogenetics of alternative splicing. *Nat Rev Neurosci*, *17*(5), 265-281. https://doi.org/10.1038/nrn.2016.27

Wahl, M. C., Will, C. L., & Luhrmann, R. (2009). The spliceosome: design principles of a dynamic RNP machine. *Cell*, *136*(4), 701-718. https://doi.org/10.1016/j.cell.2009.02.009

Wang, E. T., Sandberg, R., Luo, S., Khrebtukova, I., Zhang, L., Mayr, C., Kingsmore, S. F., Schroth, G. P., & Burge, C. B. (2008). Alternative isoform regulation in human tissue transcriptomes. *Nature*, *456*(7221), 470-476. https://doi.org/10.1038/nature07509

Wang, T., Wang, J., Hu, X., Huang, X. J., & Chen, G. X. (2020). Current understanding of glucose transporter 4 expression and functional mechanisms. *World J Biol Chem*, *11*(3), 76-98. https://doi.org/10.4331/wjbc.v11.i3.76

Wang, Y., Xu, H. Y., Gilbert, E. R., Peng, X., Zhao, X. L., Liu, Y. P., & Zhu, Q. (2014). Detection of SNPs in the TBC1D1 gene and their association with carcass traits in chicken. *Gene*, *547*(2), 288-294. https://doi.org/10.1016/j.gene.2014.06.061

Waterhouse, A. M., Procter, J. B., Martin, D. M., Clamp, M., & Barton, G. J. (2009). Jalview Version 2--a multiple sequence alignment editor and analysis workbench. *Bioinformatics*, *25*(9), 1189-1191. https://doi.org/10.1093/bioinformatics/btp033

Waters, S. B., D'Auria, M., Martin, S. S., Nguyen, C., Kozma, L. M., & Luskey, K. L. (1997). The amino terminus of insulin-responsive aminopeptidase causes Glut4 translocation in 3T3-L1 adipocytes. *J Biol Chem*, *272*(37), 23323-23327. https://doi.org/10.1074/jbc.272.37.23323

White, M. F., & Kahn, C. R. (2021). Insulin action at a molecular level - 100 years of progress. *Mol Metab*, *52*, 101304. https://doi.org/10.1016/j.molmet.2021.101304

Whiteman, E. L., Cho, H., & Birnbaum, M. J. (2002). Role of Akt/protein kinase B in metabolism. *Trends Endocrinol Metab*, *13*(10), 444-451. https://doi.org/10.1016/s1043-2760(02)00662-8

Wilhelmi, I., Neumann, A., Jahnert, M., Ouni, M., & Schurmann, A. (2021). Enriched Alternative Splicing in Islets of Diabetes-Susceptible Mice. *Int J Mol Sci*, *22*(16). https://doi.org/10.3390/ijms22168597

Will, E., & Gallwitz, D. (2001). Biochemical characterization of Gyp6p, a Ypt/Rab-specific GTPase-activating protein from yeast. *J Biol Chem*, *276*(15), 12135-12139. https://doi.org/10.1074/jbc.M011451200

Williams, D., Hicks, S. W., Machamer, C. E., & Pessin, J. E. (2006). Golgin-160 is required for the Golgi membrane sorting of the insulin-responsive glucose transporter GLUT4 in adipocytes. *Mol Biol Cell*, *17*(12), 5346-5355. https://doi.org/10.1091/mbc.e06-05-0386

Wilmes, S., & Kummel, D. (2023). Insights into the role of the membranes in Rab GTPase regulation. *Curr Opin Cell Biol*, *83*, 102177. https://doi.org/10.1016/j.ceb.2023.102177

Winder, W. W., & Thomson, D. M. (2007). Cellular energy sensing and signaling by AMP-activated protein kinase. *Cell Biochem Biophys*, *47*(3), 332-347. https://doi.org/10.1007/s12013-007-0008-7

Woo, J. R., Kim, S. J., Kim, K. Y., Jang, H., Shoelson, S. E., & Park, S. (2017). The carboxy-terminal region of the TBC1D4 (AS160) RabGAP mediates protein homodimerization. *Int J Biol Macromol*, *103*, 965-971. https://doi.org/10.1016/j.ijbiomac.2017.05.119

Wu, J., & Lu, G. (2021). Multiple functions of TBCK protein in neurodevelopment disorders and tumors. *Oncol Lett*, *21*(1), 17. https://doi.org/10.3892/ol.2020.12278

Wu, W., Syed, F., Simpson, E., Lee, C. C., Liu, J., Chang, G., Dong, C., Seitz, C., Eizirik, D. L., Mirmira, R. G., Liu, Y., & Evans-Molina, C. (2021). The Impact of Pro-Inflammatory Cytokines on Alternative Splicing Patterns in Human Islets. *Diabetes*. https://doi.org/10.2337/db20-0847

Yin, H., Price, F., & Rudnicki, M. A. (2013). Satellite cells and the muscle stem cell niche. *Physiol Rev*, *93*(1), 23-67. https://doi.org/10.1152/physrev.00043.2011

Yu, H., Rathore, S. S., Davis, E. M., Ouyang, Y., & Shen, J. (2013). Doc2b promotes GLUT4 exocytosis by activating the SNARE-mediated fusion reaction in a calcium- and membrane bending-dependent manner. *Mol Biol Cell*, *24*(8), 1176-1184. https://doi.org/10.1091/mbc.E12-11-0810

Zammit, P. S. (2017). Function of the myogenic regulatory factors Myf5, MyoD, Myogenin and MRF4 in skeletal muscle, satellite cells and regenerative myogenesis. *Semin Cell Dev Biol*, *72*, 19-32. https://doi.org/10.1016/j.semcdb.2017.11.011

Zhang, J., Jiang, Z., & Shi, A. (2022). Rab GTPases: The principal players in crafting the regulatory landscape of endosomal trafficking. *Comput Struct Biotechnol J*, *20*, 4464-4472. https://doi.org/10.1016/j.csbj.2022.08.016

Zhang, X. H., & Chasin, L. A. (2006). Comparison of multiple vertebrate genomes reveals the birth and evolution of human exons. *Proc Natl Acad Sci U S A*, *103*(36), 13427-13432. https://doi.org/10.1073/pnas.0603042103

Zhong, Q., Xiao, X., Qiu, Y., Xu, Z., Chen, C., Chong, B., Zhao, X., Hai, S., Li, S., An, Z., & Dai, L. (2023). Protein posttranslational modifications in health and diseases: Functions, regulatory

mechanisms, and therapeutic implications. *MedComm (2020)*, *4*(3), e261. https://doi.org/10.1002/mco2.261

Zhou, Z., Menzel, F., Benninghoff, T., Chadt, A., Du, C., Holman, G. D., & Al-Hasani, H. (2017). Rab28 is a TBC1D1/TBC1D4 substrate involved in GLUT4 trafficking. *FEBS Lett*, *591*(1), 88-96. https://doi.org/10.1002/1873-3468.12509

7. Supplement

7.1 Contribution to manuscripts

De Wendt C, Espelage L, Eickelschulte S, Springer C, Toska L, Scheel A, **Bedou Awovi Didi**, Benninghoff T, Cames S, Stermann T, Chadt A, Al-Hasani H (2021). Contraction-Mediated Glucose Transport in Skeletal Muscle Is Regulated by a Framework of AMPK, TBC1D1/4, and Rac1. Diabetes. doi: 10.2337/db21-0587

Contribution: I was involved in the interpretation of the data.

Pia Marlene Förster, Moira Fee Pottgießer, Christian Binsch, **Awovi Didi Humpert**, Carolin Brügge, Michelle Isabel Deatc, Regina Ensenauer, Alexandra Chadt, Hege Thoresen, Margriet Ouwens, Sonja Hartwig, Stefan Lehr, Hadi Al-Hasani. High-resolution analyses of the secretomes from murine C2C12 cells and primary human skeletal muscle cells reveal distinct differences in contraction-regulated myokine secretion (in preparation)

Contribution: I contributed to the research through experimental work, comprehensive data analysis, and interpretation, helping to streamline the decision-making process within the team.

Parts of this thesis are planned to be published in a separate paper. The manuscript is currently in preparation.

Awovi Didi Humpert, T. Stermann, S. Eickelschulte, C. Springer, C. Binsch, S. Greve, L. Espelage, L. Peifer-Weiß, M. Suresh, T. Thambiaiyah, A. Chadt, H. Al-Hasani. RabGAP TBC1D1 displays skeletal muscle-specific splice transcript variants with comparable molecular characteristics (in preparation)

Contribution: I contributed as the primary author of the manuscript, framing the research and focusing on data analysis and interpretation. My role supported the research objectives through the study design, conducting the experiments, collecting the data and driving the subsequent analysis and interpretation in collaboration with the team.

7.2 Supplementary figures

A

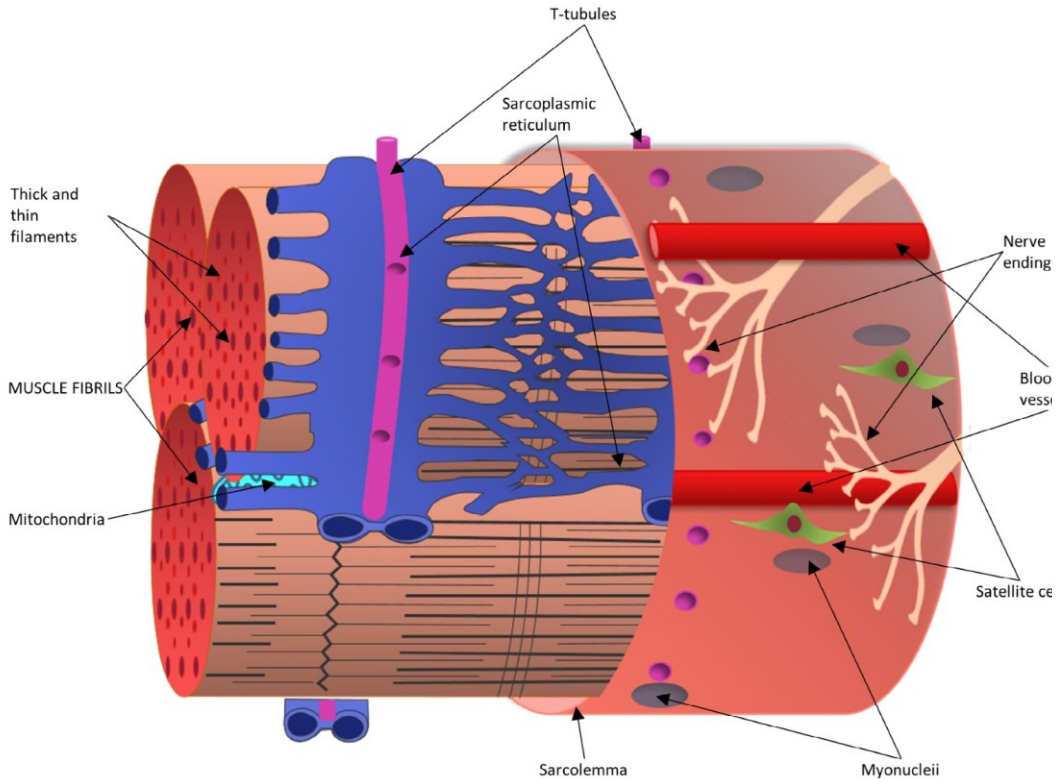

B

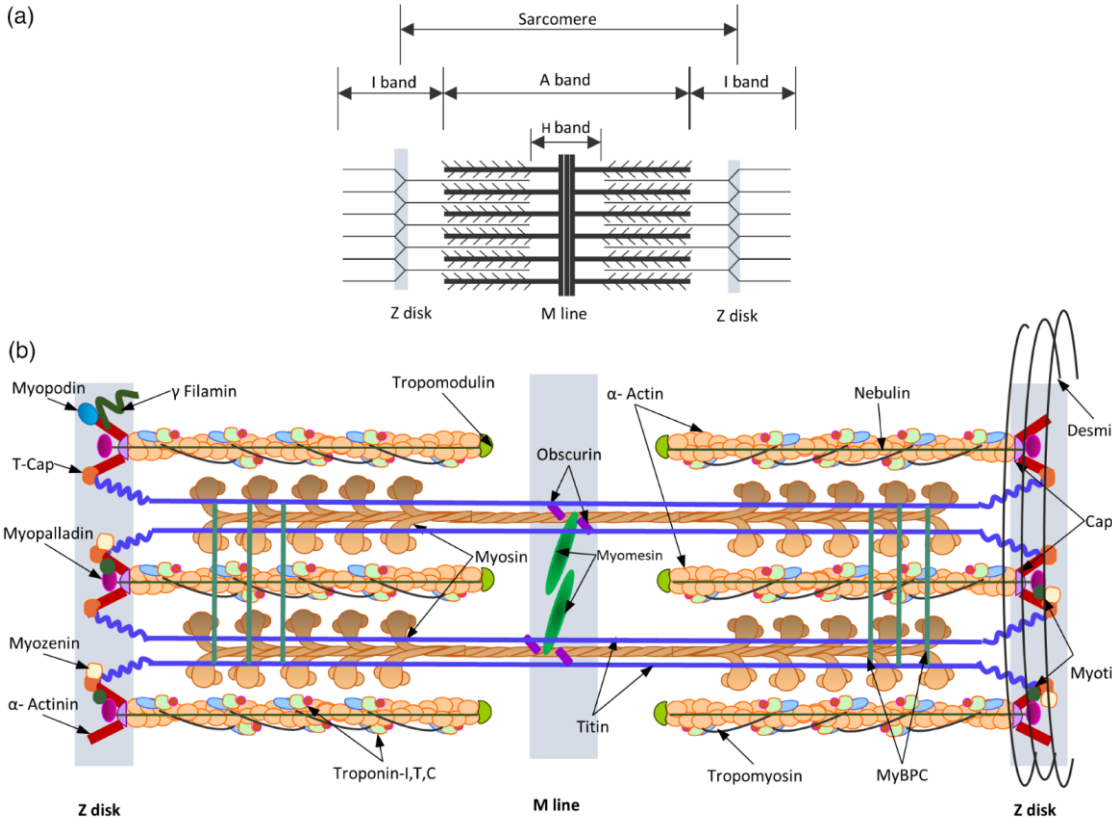

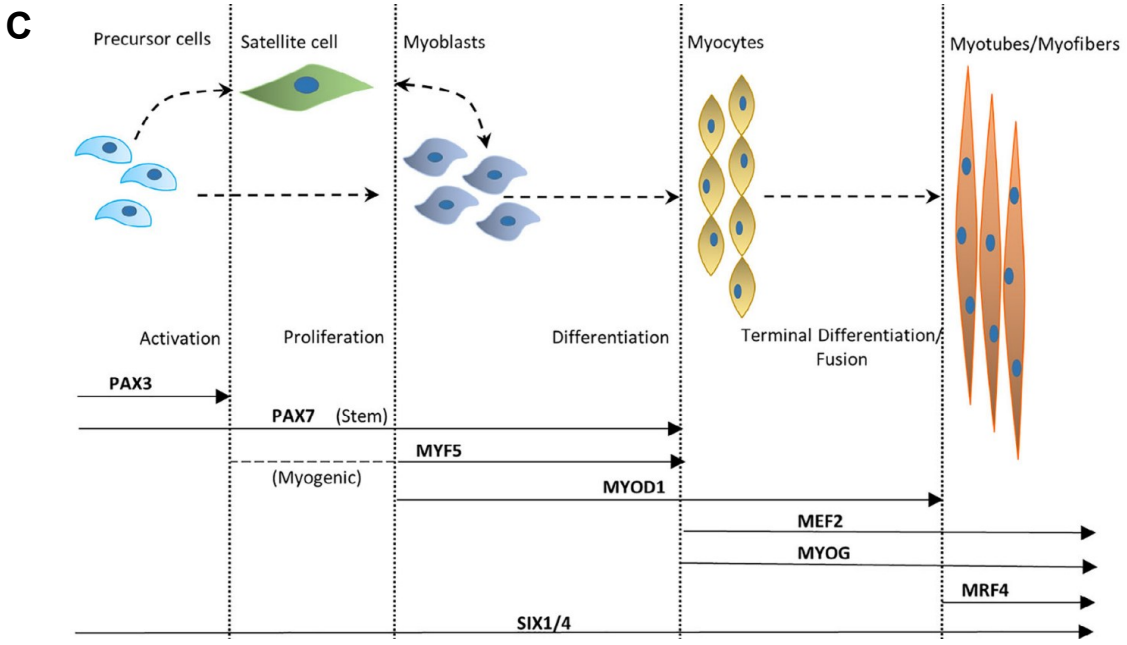

<u>Supplementary Figure 1</u>: Schematic overview of skeletal muscle myofiber structure, the sarcomere and the hierarchy of the transcription factors in myogenesis (Mukund & Subramaniam, 2020)

(A) a mature muscle fiber is depicted as a bundle of myofibrils within the sarcolemma, surrounded by the sarcoplasmic reticulum and intersected by T-tubules. Myofibers group into fascicles form the muscle tissue. Satellite cells are located beneath the basal lamina of muscle near myonuclei. Innervating nerves and capillaries are along the muscle fiber. (B) Part (a) depicts the arrangement of thick and thin filaments in striated skeletal muscle sarcomere, and part (b) illustrates the sarcomere organization and location of the significant sarcomeric proteins. The critical process involves cytosolic Ca^{2+}, which induces a conformational change in troponin C, exposing myosin binding sites on actin. Myosin heads bind to actin and move along it, driving sarcomeric contraction. Titin and nebulin assist as “molecular templates “ by maintaining the length of thick and thin filaments. Proteins in the M-line and the Z-disk ensure the structural integrity of these filaments, whereas Desmin intermediate filaments strengthen and integrate the muscle cell structure by linking adjacent myofibrils. (C) Hierarchical regulation of myogenic lineage transcription factor during muscle development. Satellite stem cells expressing *PAX7* emerge from *PAX3/PAX7*-positive progenitors, whereas satellite myogenic cells further activate *MYF5*. The stem cells activated and engaged in the cell cycle, express *MYF5* and *MYOD1*. Terminal differentiation starts with the activation of *MYOG* and *MEF2*, marked by the downregulation of *MYF5* and then later *MYOD1*. The expression of *MRF4* occurs several days after the differentiation starts, followed by the decline of *MYOG*.

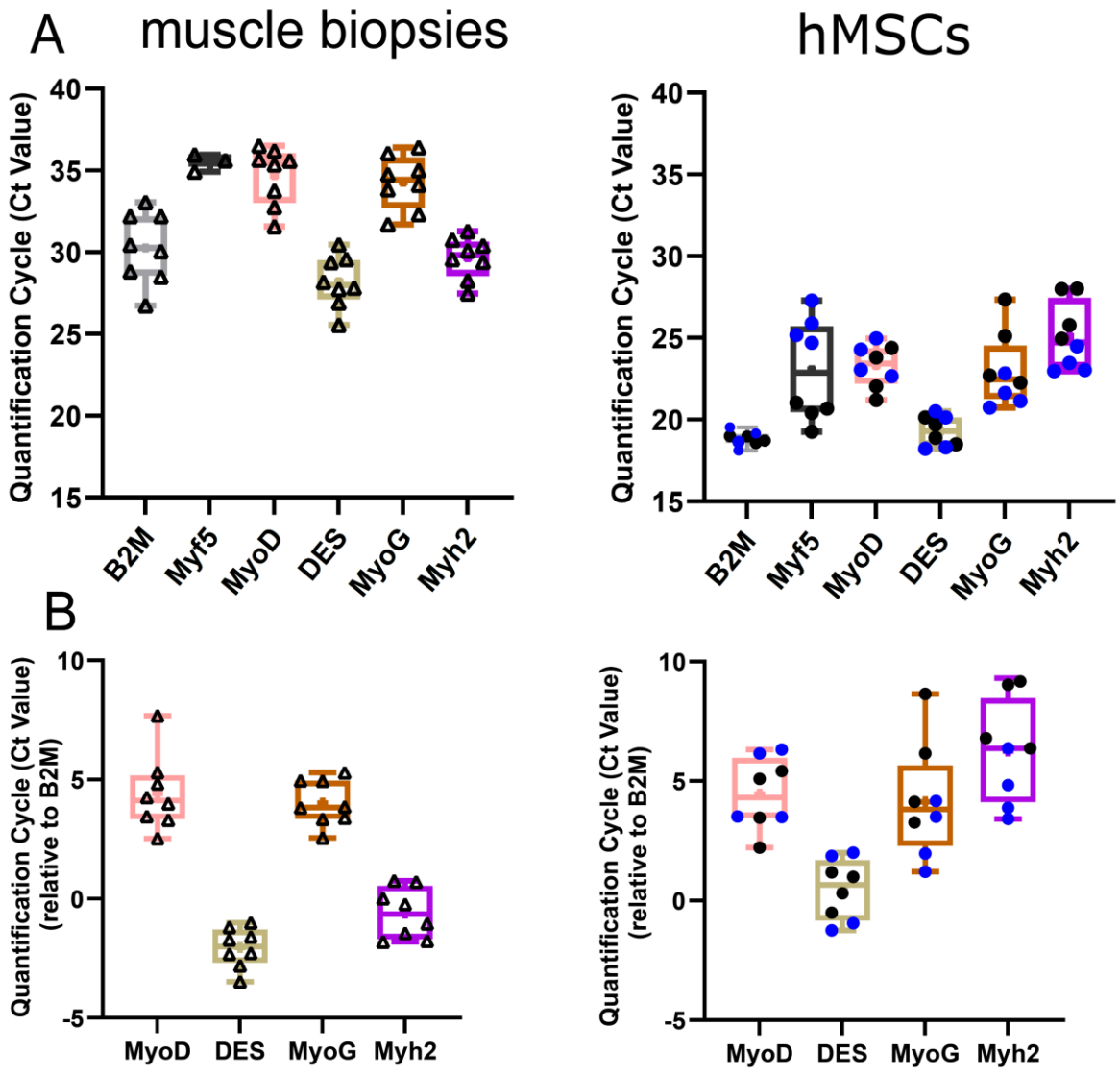

<u>Supplementary Figure 2</u>: Distribution of the Myogenic Regulatory Factors (MRFs) and the muscle Structural Proteins (MSPs) genes quantification cycle (Ct) values in muscle biopsies (left - n=8) and primary hMSCs (right - n=4)

(A) Ct values of MRFs and MSPs in muscle biopsies and primary hMSCs. (B) Relative distribution of the Ct values of the MRFs and the MSPs in muscle biopsies and primary hMSCs. Boxes represent 25 ~ 75% of data; whiskers indicate the minimum and the maximum values of Ct values; lines in each box indicate median values; triangle indicates the biopsies; dark circles indicate the myoblasts; blue circles indicate the myotubes. Data is presented as mean ± SEM.

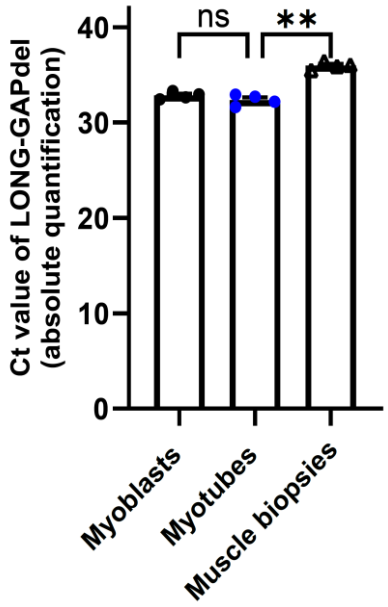

Supplementary Figure 3: CT value of *LONG-GAPdel* expression in primary human cells

LONG-GAPdel quantification cycle (CT) values in primary hMSCs (n=4) and muscle biopsies (n=4). Data are mean ± SEM, and one-way ANOVA was computed using myotubes versus all conditions. ns: non-significative, **, p<0.01 (Dunnett's multiple comparisons test).

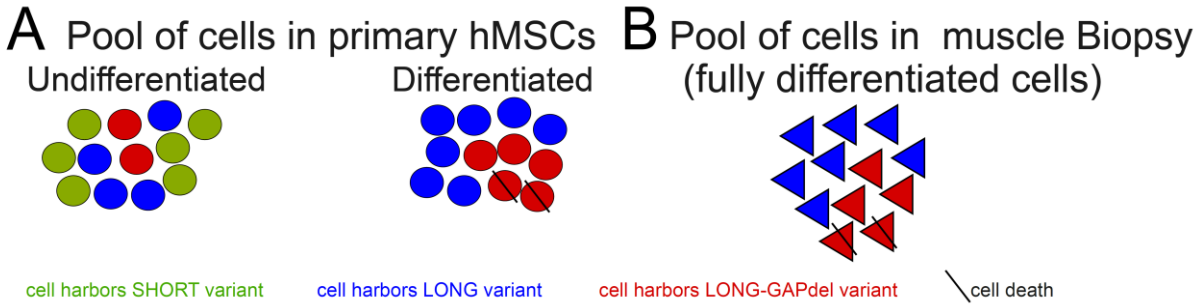

Supplementary Figure 4: Illustration of the concept of mosaicism

Mutation distribution among the cell-type (A) primary hMSCs and (B) muscle biopsy. Cell death may reduce the total number of cells harbouring somatic mutation.

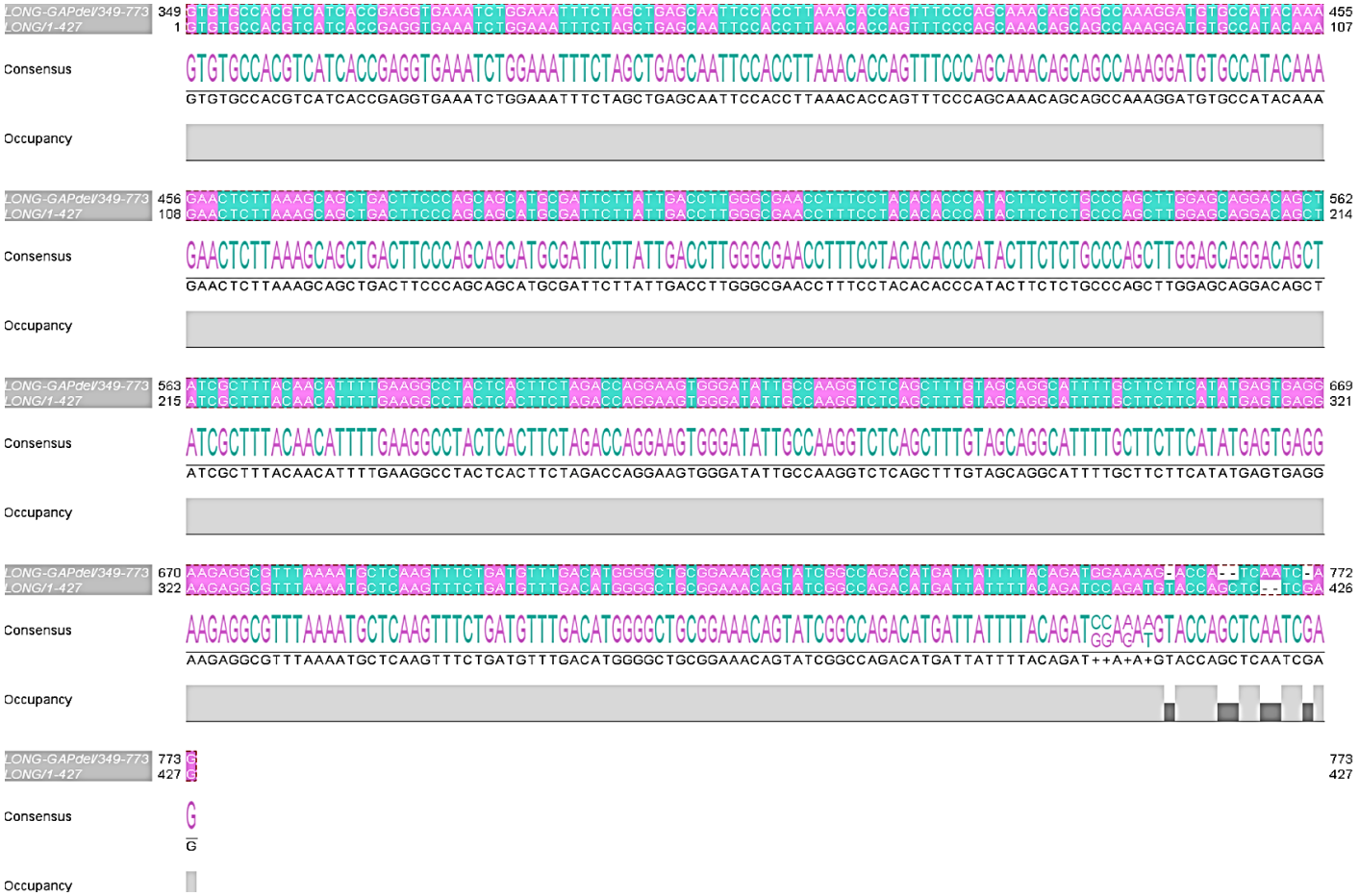

<u>Supplementary Figure 5</u>: Sequence alignment of LONG-GAPdel and LONG the purines and pyrimidines content of the RabGAP TBC domain structure

The Rab-GAP TBC domain genomic coordinates (Figure 12) span the exons 17 to 20 (Figure 11) within the coding sequence. Pairwise Alignment of the Rab-GAP TBC domain structure illustrating the purines (adenine and guanine) and pyrimidines (cytosine and thymine) content between the two splice transcript variants.

7.3 Index of figures

7.4 Index of tables

7.5 Abbreviations

	Meaning or Definition
°C	Degree Celsius
µg	Microgram
µl	Microliter
AA	Amino Acids
AKT	RAC-alpha serine/threonine-protein kinase, protein kinase B
AMP	Adenosine monophosphate
AMPK	5´-AMP-activated protein kinase
ANOVA	Analysis of variance
AP	Alternative promoter
APS	Ammonium persulfate
AS160	Akt substrate of 160 kDa
AS	Alternative splicing
A3´SS	Alternative acceptor 3´splice sites
A5´SS	Alternative donor 5´splice sites
AT	Alternative terminator
ATP	Adenosine triphosphate
BCA	Bicinchoninic acid assay
bp	Base pair
BSA	Bovine serum albumin
CaMKK	Calcium/calmodulin-dependent protein kinases
CBD	Ca+/calmodulin-binding domain
cDNA	Complementary DNA
cIRAP	Cytoplasmic tail of IRAP
Ct	Cycle threshold
DNA	Deoxyribonucleic acid
DMSO	Dimethyl Sulfoxide
dNTP	Dideoxy-nucleoside triphosphate
DTT	Dithiothreitol
ECL	Enhanced chemiluminescence
EDTA	Ethylene diamine tetraacetic acid
EE	Early endosomes
EGTA	Ethylene glycol tetraacetic acid

	Meaning or Definition
GAPDH	Glyceraldehyde 3-phosphate dehydrogenase
GDP	Guanosine diphosphate
GLUT4	Glucose transporter type 4
GSH-columns	Glutathione Sepharose columns
GST	Glutathione S-Transferase
GSVs	Glucose storage vesicles
GTP	Guanosine-5´-triphosphate
HCl	Hydrochloric acid
hMSCs	Human Skeletal Muscle Myoblast Cells
HRP	Horse radish peroxidase
IR	Insulin resistance
IRAP	Insulin-regulated aminopeptidase
IRS1/2	Insulin receptor substrate 1, 2
IRV	Insulin-responsive vesicles
KCl	Potassium chloride
kDa	Kilodalton
Km	Michaelis constant
LKB1	Liver kinase B1
MOI	Multiplicity of infection
mg	Milligram
ml	Millilitre
MEF2	Myocyte enhancer factor 2
MRFs	Myogenic regulatory factors
MRF4	Myogenic regulatory factor 4
mRNA	Messenger RNA
MSPs	Muscle structural proteins
mTORC2	Mechanistic Target of Rapamycin Complex 2
MUSCLE	Multiple Sequence Comparison by Log-Expectation
MYH2	Myosin heavy chain 2
MYOD	Myoblast determination protein 1
MYOG	Myogenin
NaCl	Sodium chloride
NCBI	National center for biotechnology information
nmol	Nanomole

	Meaning or Definition
NM	Nucleotide mRNA
NP	Nucleotide protein
PAGE	Polyacrylamide gel electrophoresis
PBS	Phosphate-buffered saline
PCR	Polymerase chain reaction
PDK1	3-phosphoinositide-dependent protein kinase 1
PI3K	Phosphatidylinositol-3-kinase
PM	Plasma membrane
PTB-domain	Phosphotyrosine-binding domain
PVDF	Polyvinylidene fluoride
RT-qPCR	Reverse transcription quantitative real-time PCR
Rab	Ras-related in brain
RE	Recycling endosomes
RI	Retained intron
RNA	Ribonucleic acid
RT	Room temperature
SDS	Sodium dodecyl sulfate
SEM	Standard error of the mean
siRNA	Small interfering RNA
T2DM	Type 2 diabetes mellitus
TBC1D1	TBC1 domain family member 1
TBC1D4	TBC1 domain family member 2
TBS-T	Tri-buffered saline with tween 20
TEMED	Tetramethylethylenediamine
TGN	Trans Golgi network
UCSC genome browser	University of California, Santa Cruz genome browser
Virus stock P0	Virus stock at Passage 0
Vmax	Maximum reaction velocity
WT	Wild type

7.6 Acknowledgements

First of all, I would like to express my deepest gratitude to my supervisors, Prof. Dr. Hadi Al-Hassani and Dr. Alexandra Chadt, for giving me the opportunity to undertake research in their research group for pathobiochemistry at the esteemed German Diabetes Center (DDZ). I am thankful to Prof. Dr. Hadi Al-Hassani for his guidance, insightful discussions, and constructive feedback throughout the development of this project. Your support, including the chance to participate in the iGRAD graduate school courses, has been invaluable. In particular, I am grateful for providing me the opportunities to present my findings at seminars and international conferences. I also very much appreciate Dr. Alexandra Chadt for all the support, fresh perspectives, and readiness to assist with ideas and solutions for this “unique” project within the research group.

I thank Prof. Dr. Axel Gödecke for his willingness to be the second reviewer of my dissertation and for his valuable time and input.

A special thank you goes to all of my colleagues for the encouraging exchanges, discussions and laughs. A thank you goes to my students Tharsha Thambiaiyah and Megha Suresh, whom I had the pleasure of supervising and teaching during their theses, which in turn helped me reflect on certain aspects of my project.

I am grateful to Dr. Samaneh Eickelshulte and Dr. Delsi Altenhofen for your guidance and encouragement, the precious support in- and outside the lab and the incredible moments together, especially during, but – of course – also after COVID-19. Thanks to Dr. Christian Binsch for always welcoming me into his office and finding the time to answer questions, particularly those involving bioinformatics. Thanks to Dr. Christian Springer for the fruitful exchanges in our office and your great support. A thank you goes to Dr. Birgit Knebel and Dr. Pia Fahlbusch for your attentive listening when I presented during our lab meetings and the spontaneous help I received whenever I reached out. Also, a warm thanks to Dr. Lena Espelage, Dr. Sarah Greve, Dr. Sarah Görigk, Dr. Anna Scheel, Dr. Aleksandra Nikolic, Dr. Pia Marlene Förster, Jenny Khuong, Katharina Kaiser, Leon Peifer-Weiß, Sebastian Sill, Marina Tautz for the excellent team spirit and the moments we shared together. A big thank you to the technical crew, especially Dagmar Grittner, Carina Heitmann, Angelika Horrighs, Annette Kurowski and Antonia Osmers, for supporting at the lab.

I want to thank my family and friends for their love, patience, and support during this journey far from home. The distance and the lack of seeing each other, first due to COVID-19 and second due to my lack of time, did not diminish your love for me. That love was invaluable and carried me throughout my journey. A thank you is not enough to express my deepest gratitude for your spiritual support and all our regular calls. I cherished them all. Especially those from my mother Gertrude Elom Gu-Konu, who was by my side every step of the way, always standing by me with all her love, prayers and good advice. Without you, I would not be who I am and where I am today. You are my hero for your silent bravery and endurance. Finally, I am grateful for the mentoring I received from Dr. Christelle Njiki Noufele, I am glad to have met you.

Above all, I want to express my heartfelt gratitude and love to my husband, who has been patient and supportive along the way. Your love has carried me daily throughout this challenging journey. Your presence and efforts to understand the challenges helped me stay on the narrow road. Thank you for standing by my side every step of the way.

Eidesstattliche Erklärung

Hiermit erkläre ich, dass ich die vorliegende Dissertation selbstständig und ohne fremde Hilfe unter Beachtung der „Grundsätze zur Sicherung guter wissenschaftlicher Praxis an der Heinrich-Heine-Universität Düsseldorf“ verfasst habe. Es wurden nur die angegebenen Quellen und Hilfsmittel benutzt. Wörtlich und inhaltlich übernommene Gedanken wurden als solche kenntlich gemacht.

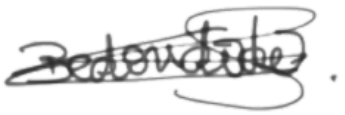

Düsseldorf, den 21.01.2025

Awovi Didi Tolo Humpert (geb. Bedou)